CHARACTERIZATION OF PHOTOSYNTHETIC STRESS ENDPOINTS TO HEAVY METALS, CRUDE OIL COMPONENTS, AND DISPERSANTS

By

SOPHIA JOHNSON-WORRELL

A dissertation submitted to the

Graduate School-New Brunswick

Rutgers, The State University of New Jersey

In partial fulfillment of the requirements

For the degree of

Doctor of Philosophy

Graduate Program in Environmental Science

Written under the direction of

Maxim Gorbunov

And approved by

_____

_____

_____

_____

New Brunswick, New Jersey

May, 2013

ABSTRACT OF THE DISSERTATION

CHARACTERIZATION OF PHOTOSYNTHETIC STRESS ENDPOINTS TO HEAVY METALS, CRUDE OIL COMPONENTS, AND DISPERSANTS

By

SOPHIA JOHNSON-WORRELL

Dissertation Director:

Maxim Gorbunov

Due to their persistence, abiotic factors such as industrial waste waters, heavy metals, petrochemicals, and oil dispersants have become a global concern. Effects of such toxicants on aquatic ecosystem health were investigated using photosynthetic characteristics of marine microalgae as an endpoint. Despite progress in understanding the biophysics of the photosystem of marine photoautotrophs, there is a lack of consensus of which photosynthetic reactions are the target of heavy metal and oil pollution.

The objective of this work used the model organisms *Thalassiosira wessiflogii* (diatom) and *Symbiodinum spp.* (coral symbionts) to: (1) evaluate the toxic effects of metals (Cu, Zn, Pb, and Sn), petrochemicals, and chemically dispersed petrochemicals on photosynthetic light-harvesting processes, photochemistry, and photosynthetic electron transport under different growth irradiance; (2) determine the primary target(s), (3) elucidate the sequence of physiological alterations, and (4) characterize the unique fluorescence signatures of aforementioned compounds on the photosynthetic apparatus using the fluorescence induction and relaxation technique.

Parameters reflecting the secondary photosynthetic reactions (P_{max}) were influenced first under both growth irradiance when cells were exposed to metals. The

exception to this statement is for Pb, which had measurable effects to cell growth rates prior to P_{max} under high irradiance. P_{max} diverged from the control at the same time except under low irradiance for Cu and Pb. Effects to cell growth rates were the only measured response under low irradiance Zn exposure. I concluded that the primary target for the test metals were sites affecting the secondary photosynthetic reactions.

Exposure to petrochemicals and dispersed petrochemicals under both growth irradiances inhibited the same photosynthetic parameters (P_{max}, and the connectivity parameter). Corexit alleviated some measurable effects when cells were exposed to benzene and dispersed crude oil under low irradiance. I concluded that the primary targets of petrochemical were to the primary and secondary photosynthetic reactions. Effects to the secondary photosynthetic reactions are assumed to lower the amount of sugar produced, which would lower the organism's growth rate. Thus, a bottom-up effect on the food web could occur. The unique fluorescence signatures identified between metals and petrochemicals can be utilized as a diagnostic tool for rapid pollution detection.

ACKNOWLEDGEMENTS

The pages of my dissertation reflected the culmination of years of study and the inspiring relationships developed along the way. I have received support and encouragement from many individuals. The list is long but I cherish each contribution to my development as a scholar.

My husband, Maurice, for his personal support, being my drill sergeant, and spiritual up lifter. Because of you, I have re-defined and re-designed my role and contribution to the world. To my parents (Chad and Gean Johnson) for being the voice of reason, cheerleaders, and spiritual counselor. Thank you for being a source of encouragement and inspiration to me throughout my life. Thank you for helping me find and realize my potential. To my grandparents (Inell Perry, Pearlie Nixon, and Willie Nixon), brother (Isaac Johnson), in-laws (Bridget and Learch Matthews), family, and friends for their support and prayers.

To my advisor Dr. Maxim Gorbunov for allowing me to exercise my spirit of adventure in regards to research, continually helping me improve my written communication skills, and providing platforms for me to enhance my verbal communication skills. To Dr. Reinfelder whose guidance and insight has made this a rewarding journey. I would like to thank the rest of my dissertation committee of Liping Wei and Keith Cooper for their support over the past two years as I completed my study. Thank you Ms. Lora, Nora, Carrie, Jeana, Benjamin, and Orly for listening to me talk about my research, providing constructive criticism, and encouragement.

Thank you to SEBS for providing me with a teaching assistantship.

Table of Contents

LIST OF TABLES

LIST OF FIGURES

ABBREVIATIONS

PSII	photosystem two
PSI	photosystem one
Q_a	primary electron acceptor
PQ	plastoquinone
Fv/Fm	quantum efficiency of photochemistry of PSII of dark adapted sample
F_m	maximum fluorescence of dark adapted sample
F_o	minimum fluorescence of dark adapted sample
Fv	variable fluorescence = Fm - Fo
α	initial slope parameter of the photosynthesis versus irradiance curve
PAR	photosynthetically available radiation ($\mu mol/m^{-2}/s^{-1}$)
E_k	light saturation coefficient ($\mu mol/m^{-2}/s^{-1}$)
P_{max}	maximum photosynthetic rate (relative units)
STF	single turnover flash
MTF	multiple turnover flash

CHAPTER 1

1.0 INTRODUCTION TO PHOTOSYNTHESIS

Ecosystems are maintained through the cycling of energy and nutrients. Energy enters the ecosystem as solar energy and is transformed to chemical energy by photosynthesis. Hence, photosynthesizers control the biological flow of energy. Photosynthesis produces carbohydrate and oxygen using carbon dioxide and water as the reactants. This process is catalyzed by light and termed photochemistry. Photochemistry includes four stages: absorption of light resulting in the formation of oxygen, electron transport yielding the reduction of nicotinamide-adenine-dinucleotide-phosphate ($NADP^+$) to its reduced form NADPH, adenosine triphosphate (ATP) generation, and carbon fixation. It is within the thylakoid membrane of chloroplast that photochemistry occurs. The chloroplast is housed within the thylakoid membrane (where light reactions occur) surrounded by an aqueous matrix called the stroma (where dark reactions occur) Figure 1.1. The stacked membrane regions of the thylakoid membrane are the grana. The interconnecting single membrane region is stroma lamellae of the thylakoid membrane Figure 1.1. Photosystem II (PSII) and cytochrome b6f are located in the stacked granal regions and Photosystem I (PSI) is located in the unstacked stromal and peripheral regions (Simpson and Von Wettstin, 1989). Also located in the unstacked regions of the thylakoid are ATP synthase (Simpson and Von Wettstin, 1989).

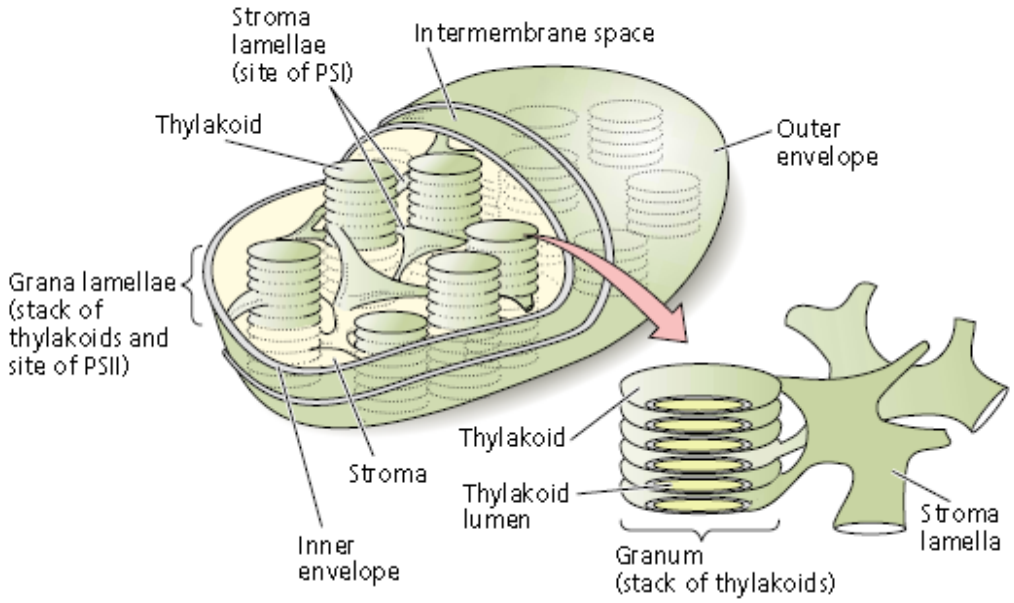

Fig. 1.1 Structure of photosynthetic apparatus. Photosynthesis occurs within the chloroplast located within the thylakoid. Stacks of thylakoids are collectively called grana and each stack is termed granum. Areas where membranes are not stacked are termed stroma lamella. (Taiz and Zeiger, 167)

PSII, PSI, cytochrome b6f, and ATP-synthase are the four major transmembrane complexes embedded within the thylakoid membrane necessary to carry out the primary photosynthetic reactions. Both photosystems carry out light driven electron transfer and are surrounded by light harvesting complexes. The light harvesting complexes increase the cross-sectional area utilized for light absorption by increasing the total number of chlorophyll around the reaction center and broadening the absorption bands (Morishige and Dreyfuss, 1998). There are different types of chlorophylls within the light harvesting complex that differ by the wavelength of light it can absorb. Therefore, chlorophyll molecules are arranged to funnel energy towards the reaction center. Light absorbed by chlorophyll molecules raise its energetic level above its ground state. To return to its ground state, the chlorophyll may emit the absorbed energy as heat, fluorescence, and utilize the energy in the photochemical process. These three processes (fluorescence, heat dissipation, and photochemistry) are in direct competition with each other.

1.1 PRIMARY REACTIONS OF PHOTOSYNTHESIS, PHOTOCHEMISTRY

Kautsky and Hirsch (1931) noted upon transferring a leaf from darkness to light that the photosystem were progressively closed and the fluorescence yield increased. The rise in fluorescence relates to the reduction of the primary plastoquinone. When the primary plastoquinone is fully reduced, PSII cannot result in a stable charge separation thus the de-excitation pathways favor fluorescence or heat and the reaction center is closed. It is at this time that the maximum fluorescence yield is obtained. Energy transfer through the antennae may be rerouted to other reaction centers yielding an increase in σ_{PSII} as PSII reaction center becomes inactive (Falkowski and Kolber, 1995). The σ_{PSII} will decrease if the energy transfer is removed through heat dissipation (Babin et al., 1996; Olaizola et al., 1994). σ_{PSII} is the functional absorption cross-section of PSII and describes the probability that a photon is used for photochemical reaction (Falkowski and Raven, 2007).

To achieve photochemistry, there is coordination between light absorption by chlorophyll, electron transport, and ATP generation. This coordination is achieved through a series of oxidation-reduction reactions. Evaluation of time-dependent oxidation-reduction changes of chlorophyll fluorescence is analyzed using variable fluorescence techniques including the Fluorescence Induction and Relaxation Fluorometer. Fluorescence kinetics are measured in four phases. Phase 1 consists of a strong short pulse of 100 µs yielding F_o to F_m and Fv/Fm (Gorbunov and Falkowski, 2004). Next, a weak modulated light is applied to record the relaxation kinetics of the Q_A acceptor. The Multiple Turnover Flash consists of a strong long pulse of 50 ms in duration saturating PSII and the PQ pool (Gorbunov and Falkowski, 2004). Phase 4

records the kinetics of the PQ pool re-oxidation on the timescale of 1s. An example of a recorded fluorescence yield is noted in Figure 1.2 below. The phases are notated on the Figure 1.2.

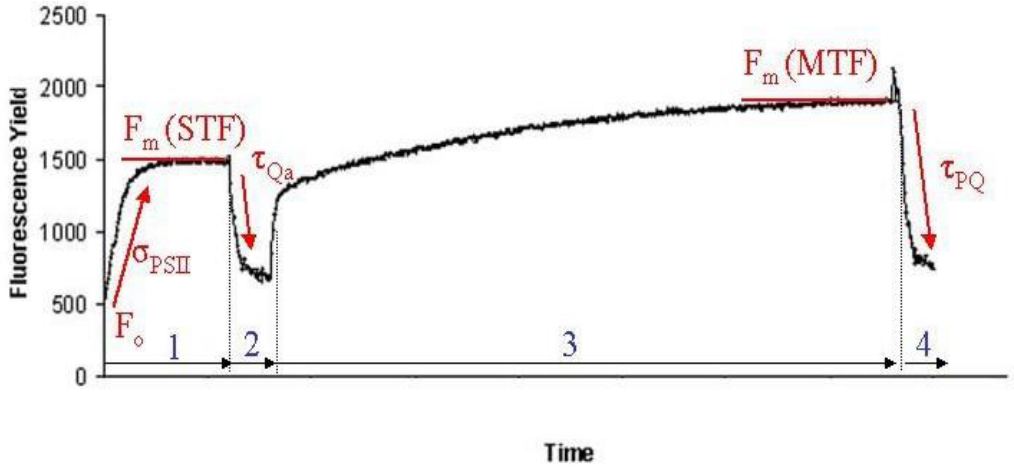

Fig. 1.2 Fluoresence Induction Curve. The fast phase noted as 1 estimates the quantum yield. Here the minimum fluoresence (F_o) is yielded when all reaction centers are open. The rate of rise is proportional to the functional cross-section, σ_{PSII}. The magnitude of rise is proportional to the number of open reaction centers. The peak of the rise is the maximum fluorescence yield, F_m. Next is phase 2, which follows the rise. The time constant recorded for the process of Q_A re-oxidization which concludes the single turnover flash (STF). Phase 3 is the start of the multiple turnover flash (MTF). Here the plastoquinone (PQ) pool is being fully reduced and re-oxidized (phase 4). (Gorbunov and Falkowski, 2004)

The transfer of electrons and protons are carried out in the thylakoid membrane through four stages. Electrons are transferred to $NADP^+$ in the first stage. Next, water is split and oxygen is released. Then, protons are pumped across the stroma. Finally, ATP is produced. After absorbing light, the excited PSII reduces pheophytin creating a cation radical PSII (Klimov and Krasnovsky, 1981). Electrons from pheophytin are transferred to cytochrome b6f by mobile electron carriers called plastoquinone. There are different types of plastoquinones within this system with different redox states. Electrons from the primary plastoquinone, Q_A, are transferred to the secondary plastoquinone, Q_B. Q_A can only transfer one electron at a time. After receiving two electrons, Q_B is fully reduced. So, two photochemical events at PSII are required to fully reduce Q_B. The reduction of

Q_B also requires protons from the stroma side of the membrane (Kolber and Falkowski, 1993).

Upon Q_B oxidation by cytochrome b6f, four hydrogen ions are released into the thylakoid lumen. The release of four hydrogen ions is a result of water splitting and oxygen production. PSII is oxidized by the tyrosine residue on the D1 protein. Cytochrome b6f couples the oxidation of the plastoquinone with the reduction of plastocyanin (the next mobile electron carrier) to translocate the protons across the thylakoid membrane. Using ferredoxin-NADP oxidoreductase, ferredoxin transfers electrons to $NADP^+$. The final products include NADPH and an electrochemical potential yielding ATP production. A model depicting the primary reaction steps is below in Figure 1.3.

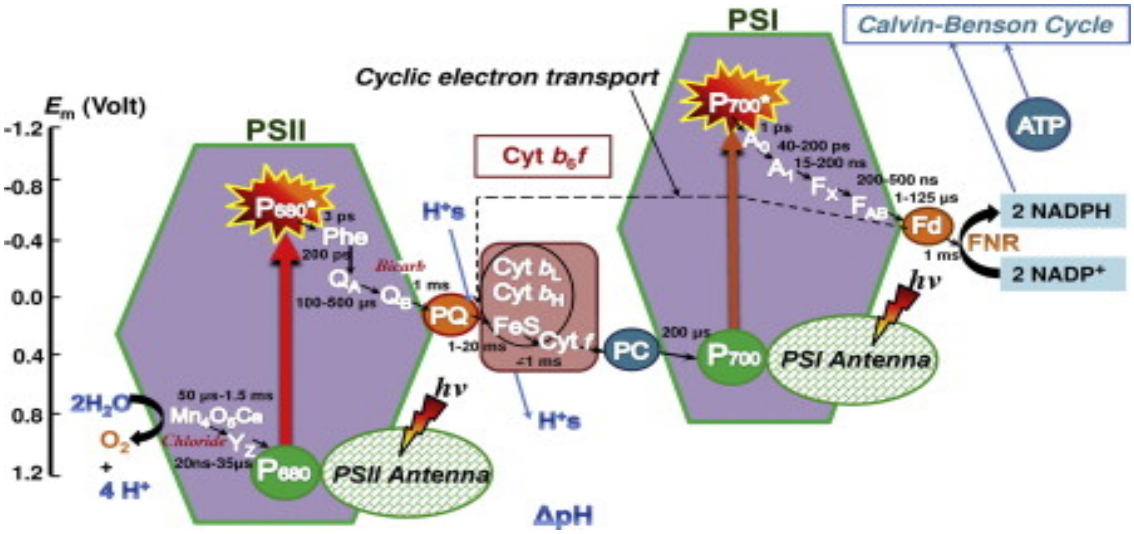

Fig. 1.3 Z-scheme of electron transport. This diagram shows the light-driven redox process from water to Q_B within PSII and the light-driven redox process from plastocyanin to ferredoxin within PSI using a mid-point potential scheme. Each biochemical's tendency to donate electrons increases as its electrical potential becomes more negative. Thus, P680* will readily give and electron to pheophytin (Phe) because its electrical potential is less than P680*. P700* will readily give an electron to Ao whose electrical potential is less than P700*. The oxidized PSII is reduced by the oxygen evolving complex. (Stribert and Govindjee, 2011)

1.2 SECONDARY PHOTOSYNTHETIC REACTION, CALVIN CYCLE

Reduced carbon is an energy source and the building block for organic compounds that originates from the Calvin cycle. When carbon dioxide concentrations are high, the carboxylase activity of ribulose-1,5-bisphosphate carboxylase/oxygenase (Rubisco) is favored and the Calvin cycle proceeds (Yeoh et al., 1981). The major stages that occur in the Calvin cycle are: the attachment of carbon dioxide to Rubisco (carboxylation), the formation of Glyceraldehyde-3-Phosphate (G3P) (reduction), and the regeneration of Rubisco's carbamate group from G3P. Stage one, carboxylation by Rubisco proceeds in five steps. First, an enolization reaction occurs where hydrogen is removed (reviewed by Sharkey, 1998). Second, carbon dioxide is added to the enediolate intermediate (reviewed by Sharkey, 1998). The third and fourth steps are hydration and carbon bond cleavage (reviewed by Sharkey, 1998). The final step is the protonation of a 3-phosphoglycerate (PGA) (reviewed by Sharkey, 1998). Decarbamylation of Rubisco during the carboxylation step rendering the enzyme inactive.

In the second stage, each PGA is phosphorylated using ATP and reduced by NADPH produced during the primary photosynthetic reactions to G3P. Three turns of the Calvin cycle are required to produce one G3P. Using triose phosphate isomerase, G3P is isomerized to dihydroxyacetone phosphate (DHAP) (reviewed by Taiz and Zeiger, 2005). The last stage of carbon fixation requires the reshuffling of five G3P carbon molecules to regenerate Rubisco. Adolase catalyzes the condensation reaction using the reactants DHAP and a G3P to yield fructose-1,6-bisphosphate (FBP) (reviewed by Taiz and Zeiger, 2005). FBP is hydrolyzed to Fructose-6-phosphate and reacts with transketolase (reviewed by Taiz and Zeiger, 2005). Two carbons are transferred by

transketolase to a third molecule of G3P yielding erythrose-4-phosphate and xylulose-5-phosphate (reviewed by Taiz and Zeiger, 2005). Catalyzed by aldolase, another DHAP combines with erythrose-4-phosphate to yield sedoheptulose-1,7-bishphosphate (SBP) (reviewed by Taiz and Zeiger, 2005). SBP donates two carbons to the last G3P via transketolase yielding ribose-5-phosphate and xylulose-5-phosphate (reviewed by Taiz and Zeiger, 2005). The two molecules of xylulose-5-phosphate and ribose-5-phosophate are converted to ribulose-5-phosphate by ribulose-5-phosphate epimerase and

1.3 PHOTOACCLIMATION

The photosynthetic apparatus balances light absorption and utilization despite the varying light quantity. Molecular modifications to the light harvesting antenna size ensure that the absorbed energy does not exceed the utilization capacity, which can result in the production of reactive oxygen species. The variations noted in the light harvesting antenna in different light quantities are described as sun-type and shade-type chloroplast. The morphological differences between chloroplast adapted to sun versus shade environments are listed in Table 1.1. Sun-type chloroplasts have greater photosynthetic capacities and saturate at higher irradiance than shade-type chloroplast (Boardman, 1977; Wild, 1979). Because of the higher chlorophyll a/b ration and higher chlorophyll a and b content per leaf area, sun-type chloroplast has a lower stacking of thylakoid appressed region (Anderson and Andersson, 1988). Shade-type chloroplasts use low irradiance more effectively than sun-type chloroplast due to an increase in the number and size of chloroplast. Without alterations to its light absorbing components, in low irradiance conditions sun-type chloroplast would not have enough organelle structure (thylakoid, PSII, chloroplast) to efficiently harvest light energy.

Sun-type	Shade-type	Reference
Smaller area of thylakoid membrane and less thylakoid per granum	Larger area of thylakoid membrane and more thylakoid per granum	Lichtenthaler et al., 1984; Goodchild et al.,1972
No change in chloroplast size	Chloroplast size are large	Anderson et al., 1988
Lower chlorophyll per chloroplast	More chlorophyll per chloroplast	Goryshina, 1980; Anderson et al., 1973
	Larger apparent PSII photosynthetic unit	Chu and Anderson, 1984;Wild et al., 1986
High stromal/thylakoid volume	Low stromal/thylakoid volume	Anderson et al., 1988
Lower stacking degree of granum	High granum stacks	Lichtenthaler and Burkart, 1999
Higher chlorophyll/b ratio	Lower chlorophyll a/b ratio	Lichtenthaler et al., 1984; Lichtenthaler and Burkart, 1999

Table 1.1 Sun/Shade adaptation of thylakoid membrane and chloroplast structure and composition

1.4 METAL TOXICITY

Water is one of the essential resources for life to thrive. Urbanization, industrialization, and improper disposal of waste material provide a source for various contents to leach into water bodies. The leaching of compounds influences the suitability of water to support life. One class of anthropogenic material of concern is heavy metals. Metals are involved in various biological reactions. Any element above its physiological concentration yields toxicity. Other issues related to metals are its interchangeability. Although its physical nature is similar between certain metals, its chemical activity is dissimilar. Different influences of heavy metals on the photosynthetic functions have been described in the literature throughout the decades. As with any stress, the sequence and scale of changes described are relative to the dose, species, and other physiological factors such as temperature, light quality, and light duration. Accumulation of some metals in general retarded growth, reduced chlorophyll content and biosynthesis, inhibited the photosynthetic electron transport, inhibited the enzymes involved in the

photosynthetic carbon reduction, and inhibition of the oxygen evolution (Mysliwa-Kurdziel et al., 2004).

1.5 COPPER TOXICITY

Copper, Cu, is an essential metal found in cellular compartments and organelles. Typical coastal concentrations of Cu are estimated in the low ng/L concentration (Bruland and Logan, 2004). Apparent toxic effects noted in phytoplankton occurred at Cu concentration around 64 ng/L (Sunda and Guillard, 1976; Anderson and Morel, 1978). It is the free ionic form of Cu that's assumed to cause toxicity. Physiological changes induced by Cu depend on the growth stage, temperature, and pH (reviewed by Yruela, 2005). The primary photosynthetic reactions documented as the site of action under Cu exposure include: PSII, oxygen-evolving complex, plastoquinone pool, cytochrome b6f, plastocyanin, PSI, ferredoxin, and ferredoxin $NADP^+$ oxidoreductase (Krupa and Baszynski, 1995; Shio et al., 1978; Clijsters and van Assche, 1985; Yruela et al., 1993b; Prasad et al., 2001; Burda et al., 2002; Lidon and Henriques, 1993). Cu exposure resulted in the decline in the abundance of plastocyanin which could alter the electron transport between the two photosystems (Droppa et al., 1984). Other complexes within the electron transport chain have been inhibited by Cu exposure. Cytochrome b6f inhibition from quinol competition is attributed to Cu exposure (Rao et al., 2000). Inhibition of the electron transport can result in a decrease in quantum efficiency of photochemistry of PSII. Alterations in the content and number of chlorophyll are another way to decrease the maximum quantum yield of photochemistry. Kupper et al. (1998) showed that the substituted the central atom of chlorophyll, Mg, yielding an unstable first excitation state that result in a lower fluorescence quantum yield. Reduced chlorophyll

biosynthesis noted by the decline in chlorophyll accumulation and the slowed chlorophyll incorporation into PSII (Prasad et al., 2001; Caspi et al., 1999). Accumulation of copper was also found to inhibit the oxygen evolution, interrupt Rubisco activity, react with free thiol enzyme groups, inhibits cell division, and inhibits mitochondrial electron transport (Ouzounidou, 1996; Lanaras et al., 1993; Stauber and Florence, 1985; Cedeno-Maldonado and Swader, 1972).

1.6 LEAD TOXICITY

As a non-essential metal, lead (Pb) pollution is still a concern despite efforts taken to limit its input into the environment. Pb inhibits the activity of sulfhydryl containing enzymes, cell division, Rubisco carboxylase activity, and chlorophyll biosynthesis enzyme (van Assche and Clijsters, 1990; Prassad and Prassad, 1987; Vallee and Ulmer, 1972). Other enzymes involved in carbon fixation, phosphoenol pyruvate carboxylase and glyceraldehydes 3-phosphate dehydrogenase, also display inhibition under Pb stress (Vojtechova and Leblova, 1991; Vallee and Ulmer, 1972). The major transmembrane protein complexes within the thylakoid are also affected through lipid composition alteration of the thylakoid membrane (Stefanov et al., 1995). One phytotoxic effect of Pb is the reduction in chlorophylls ability to capture photons and funnel the energy to the reaction center. This result is achieved through changes in chloroplast structure and synthesis, and an increase in the chlorophyll degradation enzyme, chlorophyllase (Rebechini and Hanzely, 1974; Burzynski, 1987; Drazkiewica, 1994). Exposure to Pb has been reported to displace the entry and uptake of cations such as Ca into the cell, and decreases the concentration of cations within the cell (Rashid et al., 1991; Godbold and Kettner, 1991; Walker et al., 1977).

1.7 TIN TOXICITY

Presently, tin (Sn) is utilized in the production of textiles, sponge, and biocides (Kannan and Lee, 1996; Hoch, 2001). Inorganic tin is less toxic than organic tin. The difference in toxicity between inorganic and organic tin corresponds to its absorption ability. The lipophilic nature of organic tin yields to its increase toxicity over inorganic tin.

Of the organic types of tin, the order of toxicity increases as the number of tin atoms increases (Hoch, 2001). Mono- and di-butyltins are of environmental concern due to its leaching from PVC material (Quevauviller et al., 1991). Dibutultin has been used in industrial products to stabilize PVC material against decomposition by heat and light (Hoch, 2001). In addition to the release of organic tin, inorganic tin is also leached from PVC material. Another aquatic input source of tin is antifouling paint. Sn based biocide paints are designed to release at a rate of 1.6 $\mu g/cm^2$ (Batley, 141). Organotin bind to suspended particles including algae and dissolved organic matter (Gadd, 2000). Concentrations as high as 200 µM tributyltin chloride did not effect Fv/Fm values but the electron transport within PSI was hindered at concentrations greater than 20 µM tributyltin chloride in the mung bean plant (Krugh and Miles, 1996). Components of Cytochrome b6f, cytochrome b563, and re-oxidation were slowed by exposure to 100 µM of triphenyltin chloride and 40 µM tributyltin chloride (Klughammer et al., 1998). Inorganic Sn (II) was more toxic than Sn (IV) when *Synechocystis aquatilis* was exposed (Pawlik-Skowronska et al., 1997). The chlorophyll-a concentration decreased at 10 mg/L of Sn (II). Primary production was completely inhibited at 30 mg/L of di- or tri-butyltin

(Wong et al., 1982). Sn (II) was more toxic on primary productivity whereas Sn (IV) was more toxic to reproduction (Wong et al., 1982).

1.8 ZINC TOXICITY

The type and extent of effects observed under zinc (Zn) stress was concentration dependent. The arrest in the cell division, decline in nutrient uptake, and elemental concentration has been reported by several investigators (Bonnet et al., 2000; Sagardoy et al., 2009; Mateo-Naranjo et al., 2008). However, changes in the photochemical efficiency under Zn stress are inconsistent. This is attributed to the species, its tolerance to Zn, and Zn accumulation. Mateos-Naranjo et al. (2008) noted a decline in the photochemical efficiency during high light exposure when cordgrass was exposed to Zn concentrations up to 100 mmol. Thus, the effects of Zn were only experienced at higher light intensities for cordgrass (Mateos-Naranjo et al., 2008). The specific mechanism of action for the disturbance of the photochemical efficiency was attributed to an increase in the nonphotochemical quenching, de-epoxidation of the xanthophyll cycle pigment, and minimal fluorescence (Ralph and Burchett, 1998; Chaloub et al., 2005; Sagardoy et al., 2009). Sugar beet shoots treated with 50µM had less iron and nitrogen but more phosphorus and calcium (Sagardoy et al., 2009). As the treatment concentration increased to 300 µM, other nutrients (potassium, magnesium, and manganese) were negatively affected (Sagardoy et al., 2009). At low Zn concentrations, there is a slight increase in the content of photosynthetic pigments chlorophyll-a, chlorophyll-b, and carotene. As the treatment concentration increased, the pigments listed previously decrease (Sagardoy et al., 2009; Ralph and Burchett, 1998). Alterations in the ratio of chlorophyll content can infer if the size of light harvesting antenna is increasing or

decreasing. If the abundance of chlorophyll increases, the size of the light harvesting antenna will increase. This situation was observed in *Amphora coffeaeformis* and *Entomoneis paludosa* at 20 µM the scientific world journal.

1.9 CRUDE OIL COMPOSITION, DISTRIBUTION, & SPILLS

Crude oils are composites of different hydrocarbon classifications (naphthenic, paraffinic, and aromatics), resin, sulfur, ash, and asphaltenes (Simanzhenkov and Idem, 2003). Variations in the percentage of hydrocarbon classifications, resins and asphaltenes exist between light and heavy crude oil. Heavier crude oils have a higher percentage of aromatics, and heteroatom containing molecules. However, minimal variation occurs between the carbon, hydrogen, nitrogen, oxygen, sulfur, and metal elements concentration between light and heavy crude oil. Upon release into a water body, a percentage of oil enters the water column as oil droplet. Typically water and oil are not miscible. However, there is a small portion of crude oil that dissolves in water. The soluble portion of crude oil is termed the water accommodated fraction (WAF).

Oil spills are inevitable. Spills are caused by natural seepage, accidents or failure in oil operations. Within the depths of the oceans, there are frequent small releases of oil. Natural seepage of oil accounts for more than 60% of oil spills at sea yielding approximately 47 million gallons of oil input into the sea (U.S. Congressional Research Service, 2010). The rate of release from the natural seeps is slow allowing the surrounding ecosystem to adapt. Oil exploration, extraction and transportation are the other source of oil release into the ocean.

Due to its used in various products, crude oil extraction does not seem to lessen. The movement of crude oil from a reservoir to its final destination involves multiple

modes of transportation. Most of the imported oil comes in from the Gulf of Mexico region of the United States, Figure 1.4. Approximately, 50% of oil incidents and spills occur in the Gulf of Mexico (U.S. Congressional Research Service, 2010). The number and volume of spills occurring in those multiple transfer steps are noted below in Table 1.2 for the years 2000 and 2009. The number and volume of spills by various sources occurring between 2000 and 2009 has decreased. The size of spills has also decreased from 2000 to 2009 as noted in Table 1.3.

	2000			2009	
source	number	volume (millions gallons)		number	volume (millions gallons)
tankship	111	608,176		34	14,415
tankbarge	229	133,540		166	5,678
all other vessels	5,220	291,927		1,585	92,388
facilities	1,054	311,604		963	38,299
pipelines	25	17,021		17	1,739
all other nonvessels	566	45,136		312	27,557
unknown	1,149	23,966		415	15,113

Table 1.2 Statistical summary of oil and petroleum discharge via transportation sources and categorized by number and volume per source (Recreated from Congressional Research Service: Oil Spills in US Coastal Waters: Background, Governance, and Issues for Congress)

	2000			2009	
size of spill (gallons)	number	volume(millions gallons)		number	volume (millions gallons)
1 to 100	8,058	39,355		3,351	24,428
101 to 1,000	219	78,779		123	46,062
1,001 to 3,000	37	67,529		9	20,907
3,001 to 5,000	12	45,512		2	6,872
5,001 to 10,000	16	112,415		3	21,400
10,001 to 50,000	6	108,400		4	75,520
50,001 to 100,000	4	266,380			
100,001 to 1,000,000	2	713,000			

Table 1.3 Statistical summary of oil and petroleum volumes discharged into US waters separated by spill size (Recreated from Congressional Research Service: Oil Spills in US Coastal Waters: Background, Governance, and Issues for Congress)

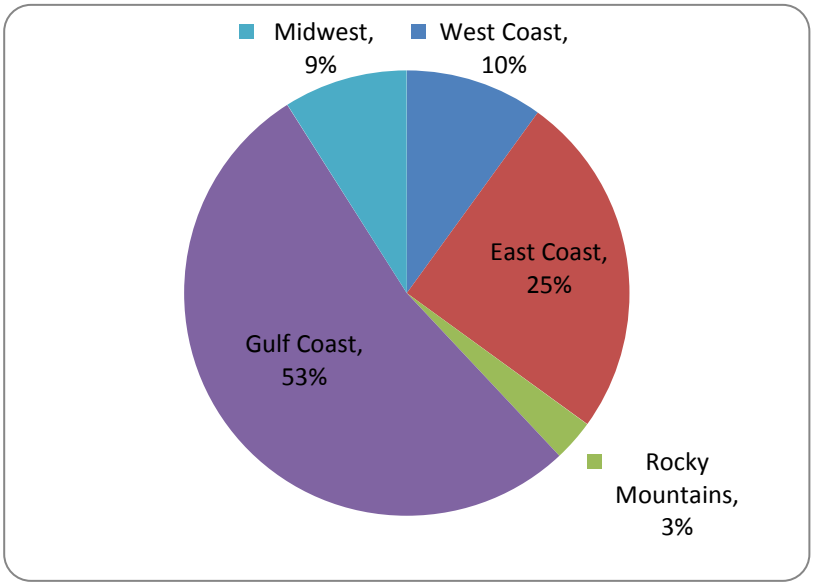

Fig. 1.4 Average Annual Distribution of US Oil Imports by Geographic Region. Recreated from Congressional Research Service: Oil Spills in US Coastal Waters: Background, Governance, and Issues for Congress

1.10 WATER ACCOMODATED FRACTION/CHEMICALLY ENHANCED WATER ACCOMODATED FRACTION

Each spill scenario has different characteristics: oil type, spill size, environmental conditions, and release rate. These factors influence the response method and the

dispersant used. For a dispersant to be considered usable on oil spills, it must be on the National Oil and Hazardous Substance Pollution Contingency Plan (NCP). There is no specified level of toxicity deemed ineligible for listing on NCP. Listing Criteria includes the dispersant application and storage methods, demonstration of 50% efficacy plus or minus 5% on the average of two crude oils using a swirling flask test, and efficacy and toxicity testing information (EPA, 2011). When dispersants are used to enhance biodegradation, the chemically enhanced water accommodated fraction (CEWAF) is termed to include the percentage mixture of oil-dispersant-water that enters the water column. Of the spills occurring yearly, spills between 12 and 1,200 billion barrels (bbl) are remediated with dispersants sometimes but dispersants are always used on spills greater than 1,200 bbl in the open ocean (Committee on Effectives of Oil et al., 1989).

It is apparent from the literature that the WAF is a non-specific metabolic inhibitor. Metabolic inhibitions by oil include: transpiration, photosynthesis, respiration, ATP yield, mortality, swimming behavior, and germination. Few studies using photosynthesis as an endpoint were explored past 1976. Exposure to oil reduced the photosynthetic rate in seagrass, apple plant, kelp, and citrus plant (Riehl and Wedding, 1959; Clendenning, 1959; Hoffman, 1935; Ralph and Burchett, 1998). For example, Perez et al. (2010) noted that the acute effects of Prestige WAF showed growth as a more sensitive endpoint than fluorescence. The authors concluded that the decline in growth reflected the volatile WAF fraction and fluorescence better reflected petrochemical toxicity. Supporting this finding, Piehler et al. (2003) noted an effect to the primary production after long-term exposure to diesel fuel.

Reversible responses were observed in *Halophila ovalis* after exposure to Corexit 9527 and CEWAF using Bass Strait crude oil (Ralph and Burchett, 1998). The quantum yield of photochemistry (ΔF`/Fm`) was more sensitive than the maximum quantum yield of photochemistry (Fv/Fm). Within an hour, Ralph and Burchett (1998) described a decline in ΔF`/Fm` in all treatments. This parameter recovered after 48 hours in all treatments except WAF. Toxicity of Bass Strait crude oil WAF was also reported in experiments conducted on green hydra by Mitchell and Holdway (2000). The lethal concentration of 50% (LC_{50}) for WAF of test specimens was ten times lower than any CEWAF. Dispersants alone had a LC_{50} of approximately twenty-five times higher than CEWAF. Acute responses to green hydra were more severe using Corexit 9500 than 9527. However, the chronic response was greater with Corexit 9527 than 9500 (Mitchell and Holdway, 2000). Contrary to the above studies where WAF had the most severe response, corals are more severely effected by CEWAF than WAF. CEWAF with Corexit 9527 yield the utilization of only 20% of the photochemical products produced by brain corals during photosynthesis (Cook and Knap, 1983). CEWAF is documented to reduce settlement rates of coral larvae, alterations in morphology, and an increase in the abortion of planula larvae at low concentrations (Epstein et al., 2000).

Since oil toxic components for marine biota are aromatic and asphaltic content, ecotoxicological evaluation of mostly polycyclic aromatic hydrocarbons (PAH) with up to five rings have been completed. It was found that when PAH is exposed to light photooxidized products are formed. Also under light, PAH undergoes a reaction called photosensitization which generates reactive oxygen species (ROS). Once PAHs enters the cell, toxicity is defined as the synergy between the photooxidized product and ROS.

Once photomodified products are formed, these compounds accumulate in the thylakoid, chloroplast, and microsome (Duxbury et al., 1997). Within the chloroplast, photooxidized PAH products cross-react with proteins and lipids yielding an interference with the electron transport chain (Mallakin et al., 2000). PAH photomodified products are able to accept and donate electrons within the electron transport chain, which decline the quantum efficiency. Inhibition to the electron transport chain was reported in studies conducted by Huang et al. (1997), Marwood et al. (1999), Babu et al. (2001), and Mallakin et al. (2002). Diminished chlorophyll was also noted by exposure to PAH. Chlorophyll content can diminish 95% that of the control that bleaching is recorded along with a decline in the quantum efficiency (Marwood et al., 2001).

Certain metals and PAHs, WAF, and CEWAF will penetrate into the cell despite the cell membrane's purpose as a diffusion barrier. Majority of enzymes can be inhibited by metals. Whereas, WAF and CEWAF alter cellular osmotic pressure. Thus, almost every metabolic pathway may exhibit sensitivity towards a metals, PAHs, WAF, or CEWAF. Investigators have documented the lethal or growth effects due to the hazards previously mentioned. This study aimed to examine the early onset toxicity related to select metals, WAF, CEWAF, and PAH on the metabolic process, photosynthesis.

CHAPTER 2

2.0 Effects of Sn on the Primary and Secondary Photosynthetic Reactions

Johnson-Worrell, S. and Gorbunov, M. 2011. Effects of Sn on the Primary and Secondary Photosynthetic Reactions. *International Journal of Sustainable Water and Environmental Systems* 2 (1/2): 97-102.

2.1 ABSTRACT

Waterways highly trafficked by vessels incorporate antifouling compounds into marine paints applied to the ship's hull. This paint prevents marine organism attachment. Although effective in controlling fouling attachment, compounds within antifouling paints inhibits numerous processes within the photosynthetic machinery, such as the re-oxidation of the quinones and the reduction in quantum efficiency of photosystem II. Tri-butylin (TBT) was the principal compound with this paint. TBT released into the waters became bioavailable and potent to non-targeted organisms. Using the Fluorescence Induction and Relaxation technology, we examined changes in photosynthetic and physiological characteristics of the model organism, *Thalassiosira weissflogii*, under sub-lethal exposure of Sn under high and low light conditions. Irrespective of light condition, the primary photosynthetic reaction kinetics of treated did not differ in response compared to the control. However, the analysis did reveal impairment of the secondary photosynthetic reaction.

2.2 INTRODUCTION

Photosynthetic organisms employ mechanisms to facilitate efficient use of absorbed light. Absorbed light is either re-emitted as fluorescence, dissipated as heat, or used for photochemistry. These pathways are in competition. Thus, the reduction of two processes is related to the increase in the third pathway. Photochemistry is the

conversion of carbon dioxide into organic carbon compounds utilizing solar energy. This conversion process begins with the extraction of electrons from water to form molecular oxygen. Electrons extracted from water are transferred within the photosynthetic apparatus to quinones, Cytochrome b6f complex, plastocyanin, and finally to photosystem I (PSI). There are two parts to photochemistry. The first part takes place within the thylakoid membrane of the chloroplast. Here light energy is directly utilized resulting in the process termed light dependent reaction. Next, the products produced during the light dependent reaction are utilized in the next process termed light independent reaction.

The photosynthetic performance and apparatus are regulated by light intensity. Changes in light quantity results in the adjustment of: the photosynthetic unit size, number of chloroplast within the thylakoid, the number of thylakoids within the grana, and the number of chlorophyll within the chloroplast (Leong and Anderson, 1984). Impacts on the photosynthetic apparatus results in maintaining an efficient quantum yield of photosystem II. Therefore, photosynthetic organisms grown under high light intensity have higher photosynthetic capabilities than organisms grown under lower light intensity. These changes alter the photosynthetic electron transport which can be represented by the photosynthetic irradiance (P-I) curve and monitored as the electron flow on the acceptor side of photosystem II (PSII) and between the two photosystems.

When photosynthetic organisms experience variation in light intensities in addition to other environmental stressors, there is an alteration in the conversion of energy. The impacts of different metals are based on its physiological role and chemical physical properties. The interactions of some metals with PSII and its inhibitory effects have been

well characterized. These studies observed a decline in quantum yield of photochemistry in PSII (Fv/Fm) (Baumann et al., 2009; Branquinho et al., 1997; Mallick and Mohn, 2003). The decrease in Fv/Fm is attributed to damaged PSII reaction centers incapable of absorbing light. In addition to reporting a decline in Fv/Fm, inhibition of various stages of the photosynthesis apparatus has also been reported for metal exposure. Other physiological effects due to PSII metal toxicity include disruption in disulfide links, substitution of Mg^{2+}, and decrease in chlorophyll content (Branquinho et al., 1997; Yruela et al., 1993a). The inhibitory concentration depends on whether the metal serves a metabolic function. Micronutrients such as Zn yield beneficial response at low concentration and toxic response at concentration exceeding the metabolic need.

Sn, which has no biological function, affects aquatic organisms in the concentration range of parts per trillion. Its pollutant relevance spawns from its incorporation as tributyltin in antifouling paint. Although, the half-life of tin in the water column is relatively short, its half-life is the sediment is long. This inhibition of biodegradation presents an issue for new coral settlement.

Prior to this study, the quantum yield of photochemistry in PSII, the electron transport chain, and the P-I curve were examined separately. Therefore, to identify the timeline of inhibitory effects to the metabolic and photosynthetic function, primary and secondary photosynthetic parameters were measured in tandem. This study aimed to examine the interactions between photosynthesis and light intensity under Sn stress.

2.3 MATERIALS & METHODS

2.3.1 ALGAL MATERIAL AND SAMPLE TREATMENT

Thalassiosira weissflogii were maintained in F/2 medium, incubated at 18°C and either 30 (low light) or 500 (high light) µmol/m^{-2}/s^{-1} of white fluorescent light on a 12-hr photoperiod. $SnCl_2$ was made in percent solution stocks with a tested metal concentration of 800 µM. *T. weissflogii* experimental cultures were made one hour prior to the first measurement.

2.3.2 FLUORESCENCE MEASUREMENTS

T. weissflogii were dark adapted prior to the start of the experiment. Chlorophyll a fluorescence was measured on *T. weissflogii* using Fluorescence Induction and Relaxation System (FIRe) (Gorbunov and Falkowski, 2004). After adjusting each culture to ambient light for 20 minutes, 2 mL was pipetted out of each flask and dark adapted for 10 minutes. The aliquots was transferred into a cuvette and placed inside the FIRe. The kinetic phases of fluorescence induction are describe here after and is illustrated in Fig. 1.2 (Falkowski and Raven, 1997). First, single turnover flash (STF) protocol was completed followed by the multiple turnover flash (MTF) protocol. Under the STF protocol, the minimal fluorescence level (F_o), the maximum fluorescence level (F_m), the variable fluorescence (Fv), and the electron transport rate to the primary electron acceptor was obtained. Equation 1 gives the formula to obtain parameter Fv. When the primary electron acceptor (Q_A) is oxidized, fluorescence is at a minimum, F_o. As Q_a becomes reduced, the fluorescence yield increases until the fluorescence maximum is reached, F_m. The length of the STF was 100 µs, the number of pulses in the relaxation sequence was 40, and the time interval between relaxation pulses was 60 µs. The plateau of F_m was

assured for each measurement. For the MTF, the electron transport between the two photosystems was obtained. The length of the MTF was 100 µs, the number of pulses in the relaxation sequence was 40, and the time interval between relaxation pulses was 60 µs. STF and MTF measurements were made in triplets. Please refer to Fig. 1.2 for the schematic showing kinetic phase of fluorescence induction.

$$Fv = F_m - F_o \quad (1)$$

The quantum efficiency of photochemistry of PSII was calculated as the ratio noted in equation 2.

$$F_m - F_o / F_m \quad (2)$$

Another 2mL aliquot was removed from the flask and dark-adapted for 10 minutes prior to the start of the continuous actinic illumination. The aliquot was transferred into a cuvette and placed inside the FIRe. Samples were exposed to 12 increasing photosynthetically available radiation (PAR) irradiance levels, from 0 up to 1500 $\mu mol/m^{-2}/s^{-1}$. Between each step, samples were acclimated to the next irradiance level for 30 seconds. 10 measurements were made at each irradiance level for control samples and 30 measurements were made for treatment samples with 500 ms between each measurement. From this data, the relative electron rate was calculated for every light level as illustrated in equation 3.

$$PAR^* \Delta F` / F_m` \quad (3)$$

This information was plotted and curve fitted in Sigma Plot with a hyperbolic equation resulting in the maximum photosynthetic rate (P_{max}) and the light saturation coefficient parameter (E_k) was obtained.

2.4 RESULTS

2.4.1 POPULATION GROWTH

The growth rate was measured to observe the effects of the whole organism. The growth rate for cells exposed to Sn was impaired (data not shown). Under low light growth conditions, cells exposed to Sn experienced an average decrease in growth rate that was greater than that experienced under high light growth conditions.

2.4.2 QUANTUM YIELD OF PSII (Fv/Fm)

Fig. 2.2 A and B represent the daily measurement of the photochemical efficiency of PSII, Fv/Fm. Fv/Fm began at an efficiency value of 0.552 and 0.568 for treated cells under LL and HL respectively. The quantum efficiency value for control cells under both light conditions was 0.557. The photosynthetic efficiency was influenced by Sn in a similar manner under both light conditions. Minor variations were observed throughout the five day study. The high light Sn Fv/Fm decreased 25% compared to the low light growth conditions Sn Fv/Fm on day three.

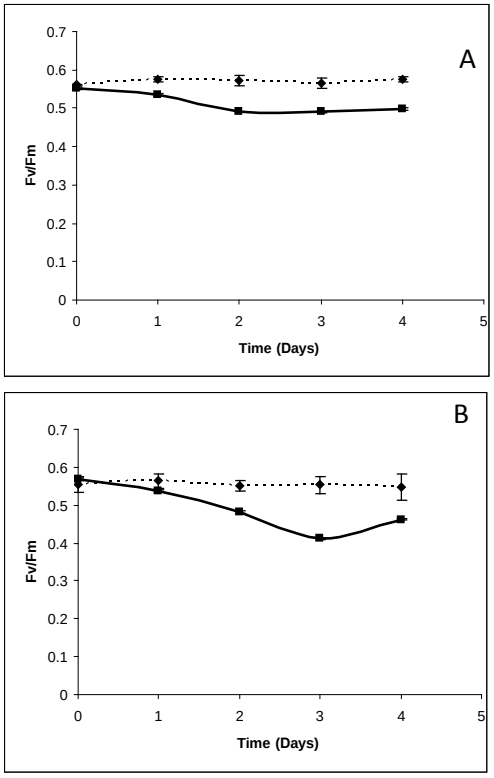

Fig. 2.1 Quantum Yield of photochemistry in PSII for cells grown under low light (A) and high light irradiance (B). The dotted line is the control and the solid line is Sn.

2.4.3 ELECTRON TRANSPORT RATE THROUGH PSII

Cultures exposed to 800 µM of Sn under high light growth irradiance displayed minor effects on the PSII acceptor side electron transport and the electron flow between the two photosystems (Fig. 2.4 A&B). Whereas no observed changes were noted in the electron transport between the photosystems under low light growth conditions (Fig. 2.3 A). The maximum increase of Q_A and PQ re-oxidation was 30%, which occurred on day two (Fig. 2.3 B). This same maximum increase was observed for Q_A re-oxidation under low light growth conditions on the last two days of the experiment. This minor effect on the PSII acceptor side electron transport was the only change noted under low light growth conditions (Fig. 2.3 A).

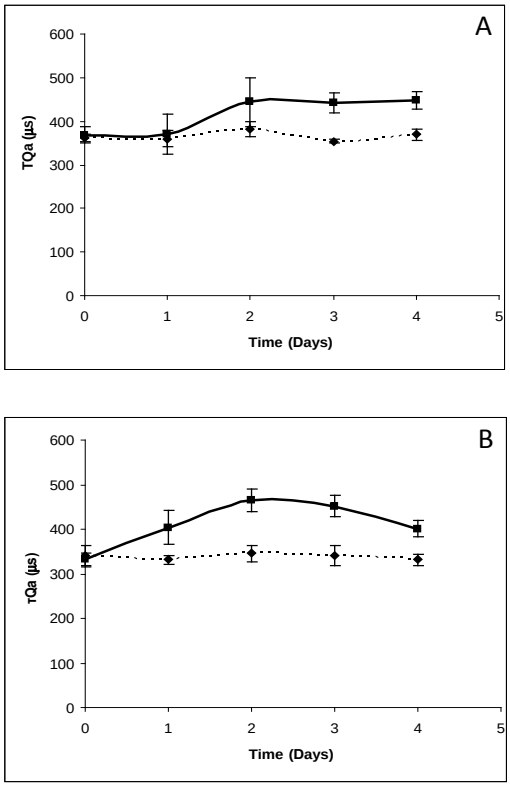

Fig. 2.2 Electron transport rates on the acceptor side of photosystem II for cells grown under low light (A) and high light irradiance (B). The dotted line is the control and the solid line is Sn. τ_{QA} is the re-oxidation of the primary electron acceptor.

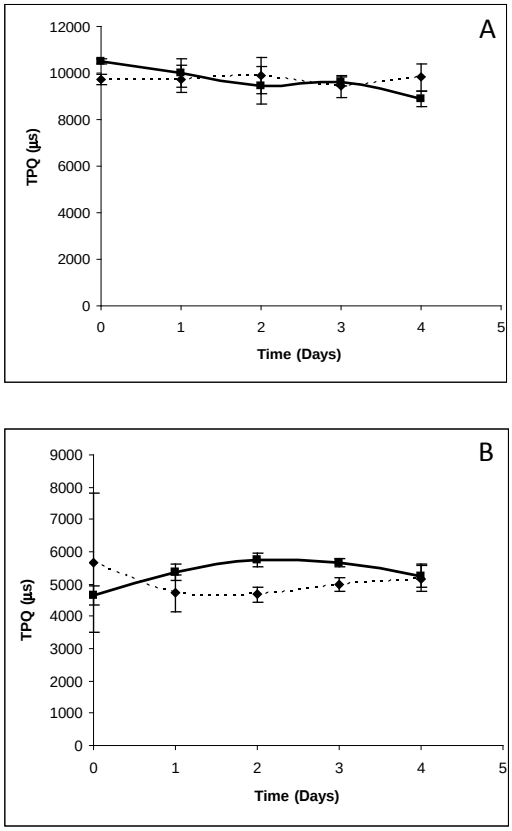

Fig. 2.3 Electron Transport Rates between photosystem II and I for cells grown under low light (A) and high light irradiance (B). The dotted line is the control and the solid line is Sn. τ_{PQ} is the re-oxidation of the plastoquinone.

2.3.4 P-I CURVE

Effects on the secondary photosynthetic reactions were analyzed using the maximum photosynthetic rate (P_{max}), and the light saturation (E_k) parameters. P-I curve provided information on the overall photosynthetic performance. There are three regions of the P-I curve, the light limited, light saturated, and the photoinhibition regions. The alpha (α) of the light limited region is analogous to Fv/Fm. Different patterns were observed for P_{max} and E_k when treated cells were compared to the control under different growth light irradiances.

After exposure to Sn, the P-I curve displayed a change in P_{max} and α for cells grown under both light levels. The initial rise corresponds to α which is analogous with Fv/Fm. The deviation of the treated high and low light growth irradiance cells' α from the control was also noted in Fv/Fm changes (Fig. 2.5 & 2.6 B). The light irradiance corresponding to the maximum rise represents the beginning of P_{max}. The initial rise of the P-I curve was restricted to a light irradiance no greater than 80 and 140 $\mu mol/m^{-2}/s^{-1}$ for cells grown under high and light growth conditions, respectively on the first day of the experiment (Fig. 2.5 & 2.6 A). This restriction decreased to 70 $\mu mol/m^{-2}/s^{-1}$ for treated cells grown under high light growth irradiance on day six and to 30 $\mu mol/m^{-2}/s^{-1}$ for light growth conditions treated cells on day five. P_{max} and E_k values declined on day one with a maximum deviation of 30% for cultures grown under light growth conditions (Fig. 2.5 A). This decline progressed exponentially for P_{max} concluding at 70% deviation and 60% for E_k on day five. Under high growth irradiance, the initial decline on day one was more dramatic than that observed under low growth irradiance but the concluding decline

was less severe under high light growth conditions. P_{max} and E_k declined 50% on day one and concluded with a deviation of 60% and 50% respectively (Fig. 2.6 A & B).

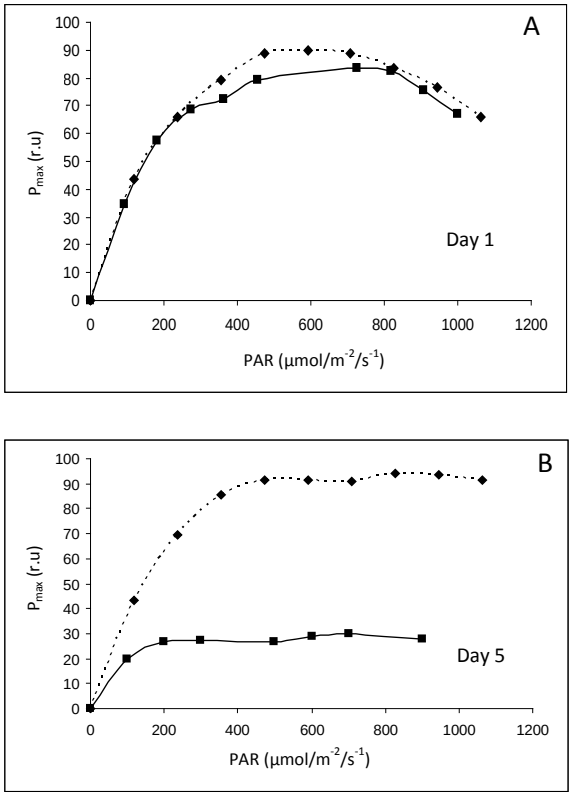

Fig. 2.4 Photosynthesis- Irradiance curves under low light irradiance on day one (A) and day five (B). The dotted line is the control and the solid line is Sn.

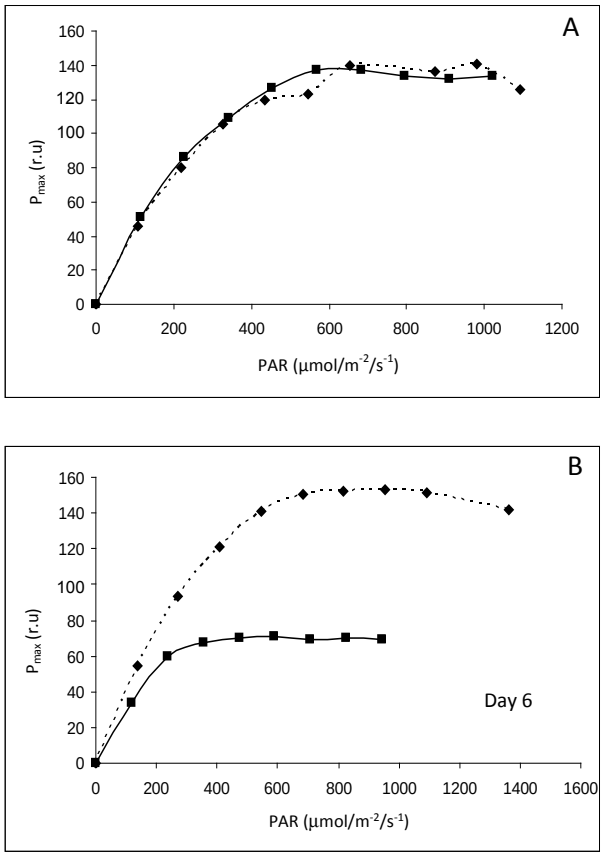

Fig. 2.5 Photosynthesis-Irradiance curves under high light irradiance on day one (A) and day six where the dotted line is the control and the solid line is Sn

2.5 DISCUSSION

Photosynthesis is the biochemical process where sunlight catalyzes the conversion of carbon dioxide to chemical energy. The conclusion of this process is the reduction of atmospheric carbon dioxide into glucose. Photochemistry involves many steps which are represented by many parameters. Different conclusions are arrived when each parameter is measured independently. Thus, this study evaluated the primary and secondary photosynthetic reactions in tandem for five day after exposing *T. weissflogii* to 800 µM of Sn.

In non-stressful conditions, photosynthesis and growth rate are coupled. Applying one or multiple stressors will result in the uncoupling of growth and photosynthesis.

Growth reduction and inhibition are typical responses of metal toxicity. Growth impairment was observed in *T. weissflogii* cultures under both light conditions when exposed to Sn. Our study observed this uncoupling under low light conditions only. On day three, no growth had occurred but Fv/Fm remained healthy. This period of no growth was also observed under high light conditions. However, Fv/Fm resulted in a quantum efficiency values that would be considered unhealthy. Once the stationary phase was over, Fv/Fm recovered and obtained a healthy quantum efficiency value. The population numbers did not affect the photomachinery in cultures exposed to Sn under both light conditions. For these cultures, cell division was uncoupled from Fv/Fm.

Based on the results in this study, it is our theory that Fv/Fm maintenance was due to the rate of PSII inactivation matching its repair rate. This claim is supported by an article written by Takahashi et al. (2008) on environmental stressors. The results presented in the Takahashi et al. (2008) article states that Fv/Fm decline resulted from the cell's inability to repair damaged PSII centers. Even though Fv/Fm for high light growth conditions Sn diminished, it recovered to a value comparable with the control. Out of the six parameters measured, Fv/Fm was the last parameter affected. Thus, Fv/Fm is not the primary target.

Because light is continuously absorbed, cultures grown under high light growth conditions have excess excitation. To avoid PSII inactivation or photoinhibition, the electron transport rate was increased between the photosystems (Behrenfeld et al., 1998). While under low light growth conditions, the electron transport rate is decreased to ensure that the light harvesting and excitation energy trapping are synchronized.

The electron transport rate between the photosystems was slowed down but no effect on Fv/Fm was observed indicating an affect after Q_A. However, this inhibition was not permanent. Back flow of electrons was not considered as a possible explanation since no alteration in the electron transport on the acceptor side was noted. Therefore, an alternative electron flow or the non-contribution to photochemistry by the damaged reaction centers is one explanation of the results observed.

The maximum rate of dark reaction is reflected in the rate measured under continuous light. Changes between the first and last day of the P-I curve high and low light growth conditions Sn in this study was attributed to direct interaction to Rubisco. P_{max} and alpha declined in high and low light growth irradiance Sn. A decrease in alpha and P_{max} indicates that the PSII inhibition exceeded its repair ability (Gordillo et al., 2001). The initial slope of P-I curve determines the light capturing efficiency. Prior to light saturation, the P-I cure is light limited and photochemical quenching dominates. The information here within explains the differences observed between cells grown under high versus low light growth irradiance. Under high light growth irradiance conditions, E_k was higher than the growth irradiance for cells grown under low light growth irradiance conditions. High light growth irradiance grown cells were also indicated by a low slope while cells grown under low irradiance have high slope. These observations were also noted in the results by Rosenqvist (2001) and Cruz and Serodio (2008). The differences are due to the development of the chloroplast under that light irradiance. The development of the chloroplast under high light growth irradiance is characterized by low amounts of thylakoids per chloroplast section, low stacking degree, more exposed chloroplast membranes, and higher rates of net CO_2 assimilation (Alves et al., 2002;

Lichtenthaler and Burkart, 1999; Ritz et al., 2000). Thus, the slope was lower for high light growth irradiance adapted cells since the light harvesting capacity was reduced. Low light growth conditions chloroplasts are characterized by having opposite attributes than that of high light growth irradiance chloroplast (Alves et al., 2002; Lichtenthaler and Burkart, 1999; Ritz et al., 2000).

2.6 CONCLUSION

The results of this investigation showed that Sn targeted the secondary photosynthetic reaction. This conclusion was made by analyzing the order at which measured parameters deviated from the control.

Light Irradiance	P_{max}	E_k	Fv/Fm	Electron transport rate between photosystems	PSII acceptor side electron transport	Growth rate
LL	1^{st} ++	1^{st} ++	2^{nd} +	No effect	No effect	2^{nd}
HL	1^{st} ++	1^{st} +++	3^{rd} +	No effect	No effect	2^{nd}

Table 2.1: Divergence timeline for each measured physiological parameter under Sn exposure. The statistical significance is notated at + marks. + indicates a $p < 0.05$, ++ is a $p < 0.01$, and +++ is a $p < 0.001$. P-values greater than 0.05 are not reported.

The timeline of the physiological parameters divergence from the control for Sn is detailed in Table 2.1. Sn effects were independent of growth irradiance. Minor changes to Fv/Fm were noted at the conclusion of the experiment under high growth irradiance. Irrespective of growth irradiance, P_{max} and E_k varied from the control prior to the other parameters measured. Changes in P_{max} and E_k were attributed to the direct interaction of the metal ion with Rubisco under low growth irradiance. The decline in Fv/Fm under high growth irradiance was the combination of the metal ion with the inability of PSII to repair itself faster than damaged occurred.

CHAPTER 3

3.0 Heavy Metal Inhibition of photosynthesis: targeting secondary photosynthetic reactions

3.1 ABSTRACT

Stressors to the photosynthetic apparatus appear as a decline in growth, ATP production, respiration, photosynthesis, change in chloroplast ultrastructure, or a change in the electron transport rate. My working hypothesis was that metal exposure differs from other stressors by targeting the secondary photosynthetic reactions. The toxic effect of two essential (Cu and Zn) and a non-essential (Pb) metals on the primary and secondary photosynthetic reactions were analyzed using fluorescence induction and relaxation kinetics. *Thalassiosira weissflogii* exposed to 25 µM Cu, 50 µM Zn and 450 µM Pb demonstrated the strongest sensitivity to parameters representing dark reactions (P_{max} and E_k). The photosensitivity of the photosynthetic apparatus increased under Cu exposure. The results suggest that the maximum photosynthetic rate and light saturation coefficient are the most sensitive parameters under all tested metal exposure and that the secondary photosynthetic reactions were the primary site of inhibition.

3.2 INTRODUCTION

Of the elements categorized as heavy metals, few have physiological importance. Examples of essential metals include Cu and Zn. Cu is a component of the protein plastocyanin, which is included in the photosynthetic electron transport system (Quigg et al., 2003). Copper is also required in protein synthesis, chloroplast and mitochondria reactions, and carbohydrate metabolism. Zn is included in the DNA binding protein, Zn fingers, alcohol dehydrogenase, and biosynthesis of plant growth hormones (Klug and

Rhodes, 1987; Wahbeh, 1984). All other metal ions not involved in metabolic processes are categorized as non-essential. When metals are present at concentrations greater than the physiological threshold, toxic effects are exerted. Many effects are associated with the interaction of heavy metals with molecules containing sulfur, nitrogen, and oxygen.

Predictions of the site of action for metals are based on their affinity for various ligands. Thus, metals have been classified according to their ligand binding affinity. Borderline class metals (e.g. Cu^{2+}, Sn^{2+}, Zn^{2+} and Fe^{2+}) show about the same preference of bonding to oxygen, sulfur, or nitrogen atoms (Nieboer and Richardson, 1980). Within the borderline class, copper resulted in the greatest toxicity followed by zinc (Lyngby and Brix, 1984; Malea, 1994; Afkar et al., 2010). Based on the understanding of metal affinity to ligands, investigations of metal affinity to the sulfhydryl groups within ribulose-1,5-bisphosphate carboxylase oxygenase (Rubisco) were undertaken (Stiborova et al., 1988; vanAssche and Clijsters, 1986a). Inhibition to Rubisco by Cu and Zn interactions occurs from destabilizing the sulfhydryl groups within Rubisco's catalytic site or substitution of the magnesium ion within Rubisco's active site (Mateos-Naranjo et al., 2008; review by Borkow and Gabbay, 2005). Displacement of essential metal ions of the Rubisco enzyme yields a different electronic configuration and improper functioning.

The physiological damage induced by heavy metals has been extensively monitored. Excess metals cause alterations in almost every physiological process within the cell which has attributed to a lack of agreement in the mechanism of action for heavy metals. Investigations of deleterious effects to chlorophyll biosynthesis, Calvin Cycle enzymes, and primary photochemical reactions have been reported (Arellano et al., 1995; Garcia-Ferris and Moreno, 1994; Mateos-Naranjo, 2008; Plekhanov and Chemeris,

2003). Evidence points to direct effects (electron transport flow within PSII or dark reactions), and indirect effects related to reactive oxygen species (ROS) interactions with biophysical processes as potential mechanism of action for heavy metals (Rashid et al., 1991, 1994; Mohanty et al., 1989; Yruela et al., 1993b; Arellano et al., 1995; Uribe and Stark, 1982). These studies have focused on select processes within the photosynthetic apparatus to understand abiotic stress response. However, the sequence of physiological alterations within the cell under metal exposure remains a topic of controversy.

This paper characterizes the temporal stress response of *Thalassiosira weissflogii* to Cu, Zn, and Pb using the Fluorescence Induction and Relaxation Fluorometer (FIRe). To my knowledge, this was the first time the FIRe has been used to assess metal toxicity. The main objectives of this research are therefore: to evaluate different metal effects under different growth irradiance, to determine the primary target of metal stress, to elucidate the sequence of physiological alterations within the photosynthetic apparatus under metal exposure, and to characterize the unique fluorescence signature specific to each metal. We focused the physiological study on metal stress because metal toxicity alters redox potentials, and enzymatic activity. Moreover, the problem of metal toxicity is expected to intensify with an increase in ocean acidification due to climate change, which could affect the carbon assimilation application employed by photosynthesizers.

3.3 MATERIALS & METHODS

3.3.1 TEST ORGANISM AND GROWTH CONDITIONS

T. weissflogii were grown in F/2 medium under 12-hr photoperiod in an 18°C incubator. Light intensity was either 100 or 700 μmol/m^{-2}/ s^{-1} of low or high light, respectively white fluorescent light for the five day growth period.

3.3.2 EXPOSURE DETERMINATION

Estimation of the toxicity concentration was determined based on a dose-response curve producing half maximal inhibitory concentration (IC_{50}) (concentration affecting the maximum photosynthetic rate (P_{max}) response by half). To assess the thresholds of metal toxicity, I exposed *T. weissflogii* cultures to a range of Cu, Zn, and Pb concentrations and monitored the P_{max} over the period of 48-hrs. For example, Cu concentrations of 17 μM and below did not lead to any deviation from the control and therefore did not exhibit a toxic effect on the maximum photosynthetic rate within 48-hrs (Fig. 3.1 and 3.2 E and F). Inhibition of P_{max} occurred under Cu concentrations above 17 μM. The selected concentration serves two functions: first, it represents measured doses observed in the aquatic environment and secondly, it elicits an adverse response to the maximum photosynthetic rate 48-hrs, which is roughly the average lifetime of the cells in the population (the reciprocal cell division rate). Based on these observations and requirements, 25μM was chosen as the appropriate concentration of Cu for detailed examination of the stress development. This same process was carried out for Pb and Zn. The metal concentrations selected were 25, 50, and 450 μM for Cu, Zn, and Pb respectively. Due to precipitation, the Pb concentration was maintained at the soluble concentration of 450 μM by re-adding Pb daily. Thus, I was only able to estimate the IC_{50} of Pb as greater than 450 μM.

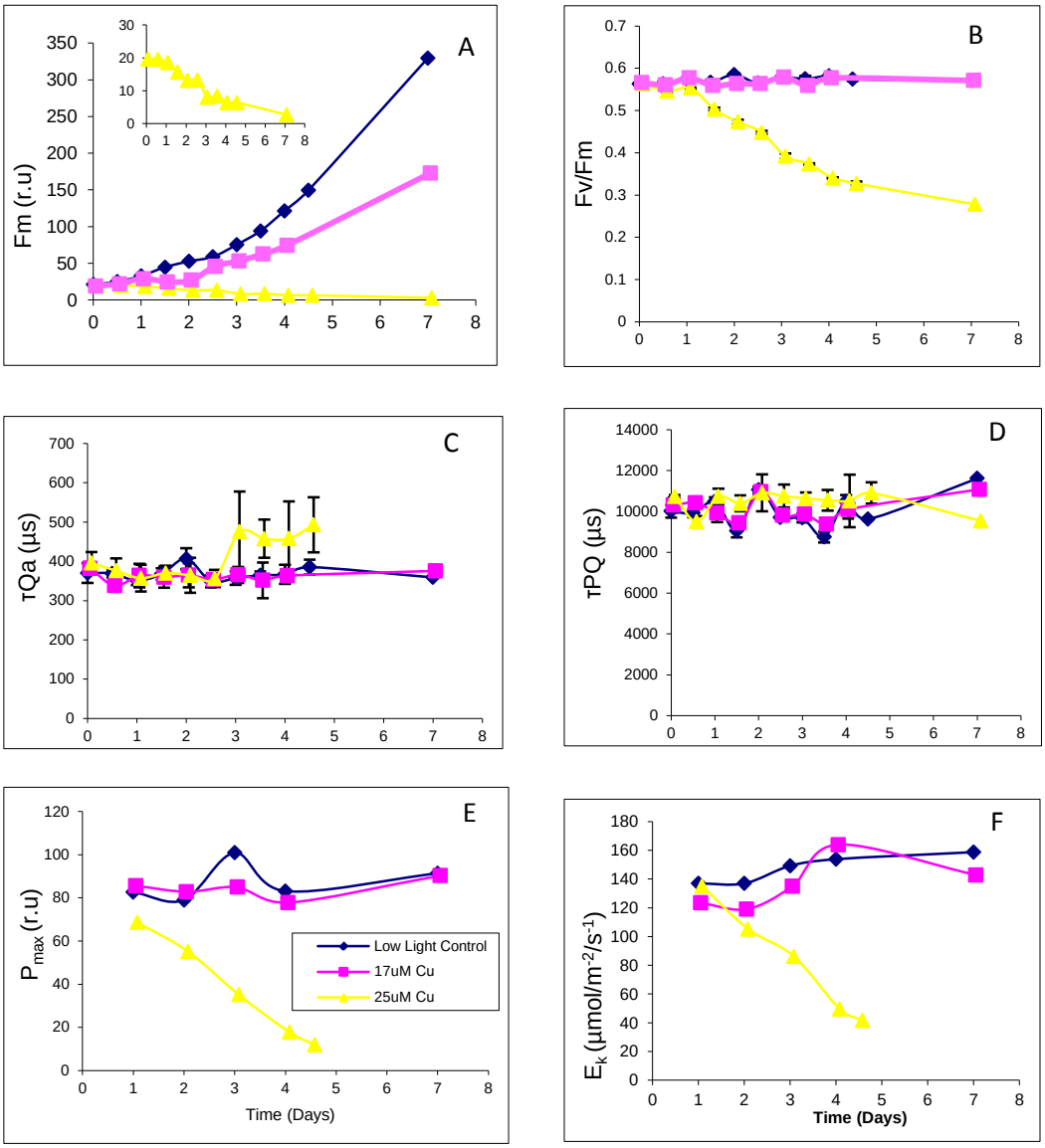

Fig. 3.1 The onset and duration of Cu-induced effects to photochemical processes over four days under low light growth irradiance. The effects to the secondary photosynthetic reactions are noted in graphs E and F. Measurements of the secondary photosynthetic reactions occurred 30 minutes after dosing with the metal solution. The small insert graph inside graph A shows the pronounced effect of 25 μM Cu on cell division which mirrors the maximum photosynthetic rate (Pmax) and light saturation coefficient (E_k). Temporal evolution of the photosynthetic parameters under 0, 17, and 25μM of Cu low light conditions. These parameters include: (a) biomass, (b) quantum efficiency of photochemistry in PSII, (c) rate of electron transport on PSII acceptor side, (d) rate of electron transport between PSII and PSI, (e) maximum photosynthetic rate (P_{max}) and (f) light saturation coefficient (E_k) for *T. weissflogii.* Cells grown under 25 μM of Cu showed visible result to growth, Q_A re-oxidation, photochemical efficiency of PSII, and secondary photosynthetic reactions.

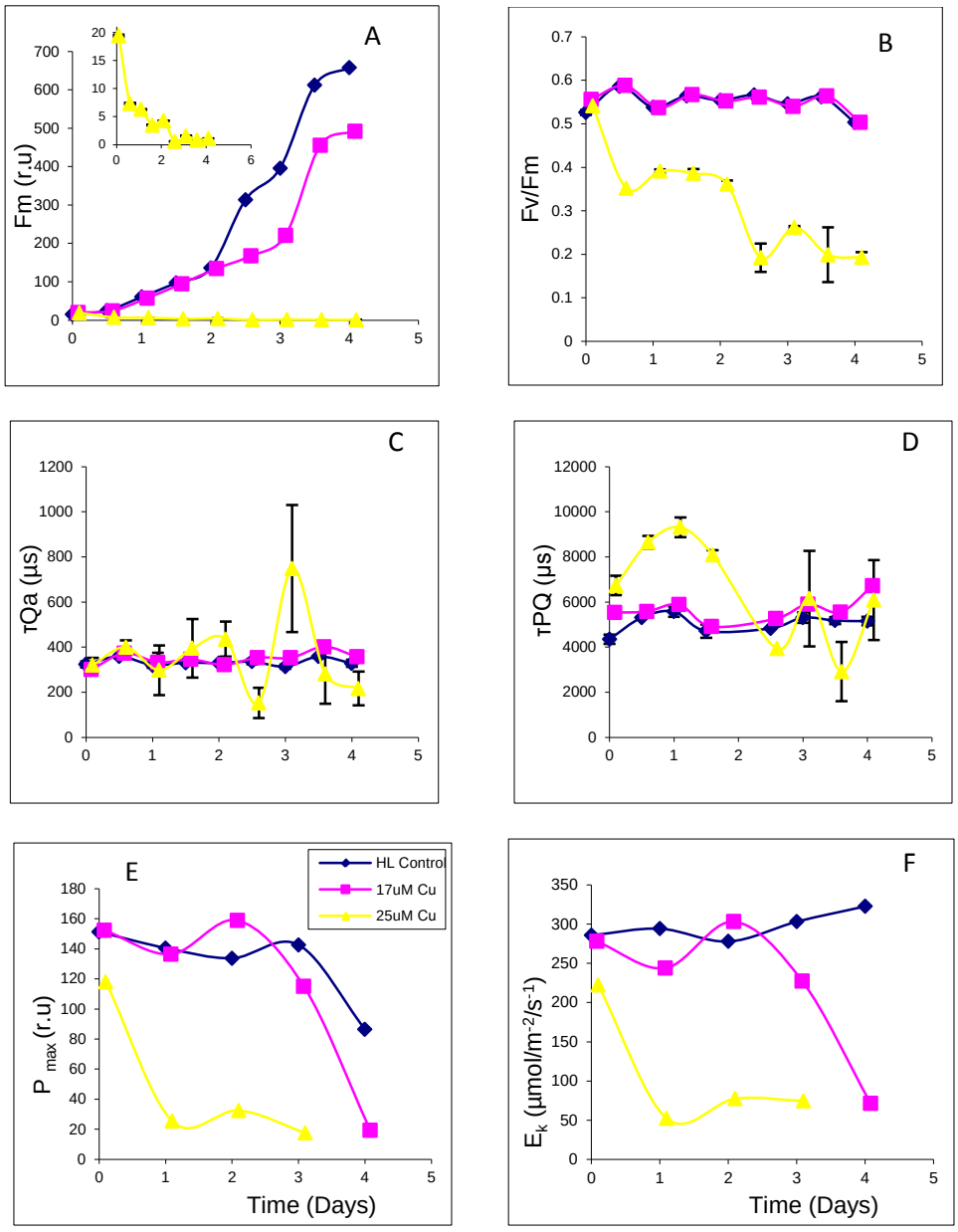

Fig. 3.2 The onset and duration of Cu-induced effects to photochemical processes over four days under high light growth irradiance. The effects to the secondary photosynthetic reactions noted in graphs E and F. Measurements of the secondary photosynthetic parameters occurred within two minutes after dosing cultures with the metal solution. The small insert graph inside graph A shows the pronounced effect of 25 µM Cu on cell division. Temporal evolution of the photosynthetic parameters under 0, 17, and 25µM of Cu under high light conditions. These parameters include: (a) biomass, (b) quantum efficiency of photochemistry in PSII, (c) rate of electron transport on PSII acceptor side, (d) rate of electron transport between PSII and PSI, (e) maximum photosynthetic rate (P_{max}) and (f) light saturation coefficient (E_k) for *T. weissflogii.* Cells grown under 25 µM of Cu showed visible results to growth, electron transport between PSII and PSI, quantum efficiency of photochemistry in PSII, and secondary photosynthetic reactions; to the growth and secondary photosynthetic reactions under 17 µM of Cu.

The sigmoid dose-response curve was transformed into a straight line using Finney (1971) probit analysis and a half maximal inhibitor concentration, the concentration at which a toxicant produces a response that has reduced by half, was determined and used to carry out the study.

%	0	1	2	3	4	5	6	7	8	9
0	2.60	2.67	2.95	3.12	3.25	3.36	3.45	3.52	3.59	3.66
10	3.72	3.77	3.82	3.87	3.92	3.96	4.01	4.05	4.08	4.12
20	4.16	4.19	4.23	4.26	4.29	4.33	4.36	4.39	4.42	4.45
30	4.48	4.5	4.53	4.56	4.59	4.61	4.64	4.67	4.69	4.72
40	4.75	4.77	4.8	4.82	4.85	4.87	4.9	4.92	4.95	4.97
50	5.00	5.03	5.05	5.08	5.10	5.13	5.15	5.18	5.20	5.23
60	5.25	5.28	5.31	5.33	5.36	5.39	5.41	5.44	5.47	5.50
70	5.52	5.55	5.58	5.61	5.64	5.67	5.71	5.74	5.77	5.81
80	5.84	5.88	5.92	5.95	5.99	6.04	6.08	6.13	6.18	6.23
90	6.28	6.34	6.41	6.48	6.55	6.64	6.75	6.88	7.05	7.33

Table 3.1 Conversion of percent response to probit unit. Look up the corresponding percent response on the outer column and upper row. The inner column/rows correspond to the probit unit. For example, a 18% response corresponds to a probit of 4.08. A probit unit of 5 corresponds to a 50% response (IC_{50}).

3.3.3 ASSAY FOR REACTIVE OXYGEN SPECIES FORMATION

2,7-dichlorofluorescin diacetate (DCFH-DA) is a nonpolar compound that readily crosses the cell membrane. Inside the cell it is de-acetylated or converted into a polar derivative (2',7'-dichlorofluorescin - DCFH) by cellular esterases. DCFH is cellularly bound but nonfluorescent. It is the oxidation of DCFH to 2',7'-dichlorofluorescein (DCF) by intracellular hydrogen peroxide, hydroxyl radical, or peroxyl radical that renders the dye fluorescent. Intracellular oxidative stress was monitored using a Spectra Max M3 at an excitation wavelength of 485 nM and emission wavelength of 528 nM. DCFH-DA was prepared by the method of Eruslanov and Kusmartsev (2010). In brief, a final

concentration of 7 µM DCFH-DA was added to cultures. The solution was incubated at room temperature for 40 minutes before intracellular fluorescence intensity was analyzed. The fluorescent intensity is proportional to the ROS levels within the cell cytosol.

3.3.4 FLUORESCENCE

Chlorophyll a fluorescence and photosynthetic characteristics were measured on *T. weissflogii* using a custom-built FIRe (Gorbunov and Falkowski 2004). After adjusting each culture to ambient light for 20 minutes, 2 mL was pipetted out of each flask and dark adapted for 10 minutes. First, FIRe single turnover flash (STF) protocol was completed. Then the multiple turnover flash (MTF) protocol was completed. The STF protocol consisted of a 100 µs long saturating flash (induction phase) followed by a sequence of week relaxation pulses. The number of pulses in the relaxation sequence was 40 and the total duration of the relaxation phase was 200 ms. Under the STF protocol, the minimal fluorescence level (F_o), the maximum fluorescence level (F_m), the variable fluorescence (Fv = Fm-Fo), the quantum efficiency of photochemistry in PSII (Fv/Fm), and the rates of electron transport on the acceptor side of Photosystem II (i.e., the rates of Q_A re-oxidation) were measured (Gorbunov and Falkowski, 2004). The MTF protocol consisted of a 100 ms long saturating flash followed by a sequence of week relaxation pulses (Fig. 1.2). Since the MTF flash fully reduces the plastoquinone pool and thus saturates the chain of electron carriers between PSII and PSI, the relaxation in fluorescence yield after the MTF reflects the rates of plastoquinone pool re-oxidation, i.e. the rates of electron transport between PSII and PSI. This rate is usually ca. 10 times slower than that of Q_A re-oxidation measured after the STF. Please refer to Fig. 1.2 for the schematic showing kinetic phase of fluorescence induction.

The photosynthetic electron transport rates as a function of irradiance (photosynthesis-versus-irradiance profiles) were retrieved from FIRe fluorescence measurements under varying ambient light. Samples were exposed to 12 increased irradiance levels, ranging from 0 up to 1500 µmol/m^{-2}/s^{-1}, with 50 s interval at each irradiance. The maximum photosynthetic rate was calculated for every light level as the product PAR* ΔF'/Fm'. PAR is the light intensity that stimulates photosynthesis. ΔF'/Fm' describes the probability which an absorbed light quanta are utilized to push electrons through photosystem II. The photosynthesis-versus- irradiance profiles were fitted with a hyperbolic equation (in Sigma Plot) resulting in the maximum photosynthetic rate (P_{max}) and the light saturation coefficient parameter (E_k).

3.3.5 GROWTH RATE CALCULATION

Increase in F_m over the course of the experiment was used as a proxy of population growth. The reported F_m values were corrected for change in the FIRe detector gain. The measurements were made in triplets. The report values are the averages of the measurements.

3.3.6 MINEQL+ CALCULATIONS

MINEQL+ was used to determine the chemical distribution of Cu, Zn, and Pb species in solution. Majority of the metals were bound to ethylenediaminetetraacetic acid. The aqueous concentrations of Cu, Zn, and Pb were $1.05e^{-17}$, $3.29e^{-16}$, and $4.5e^{-05}$, respectively.

3.3.7 STATISTICAL ANALYSIS

Statistical analyses were performed using Sigma Stat software. One-way analysis of variance with treatment as a factor was applied to detect differences among treatments

(control, Cu, Zn, and Pb). Median inhibition concentrations (IC_{50} as percentage of photochemical efficiency) for the Cu, Zn, and Pb exposures were calculated from induction curves using probit analysis to fit a linear regression.

3.4. RESULTS

3.4.1 COPPER

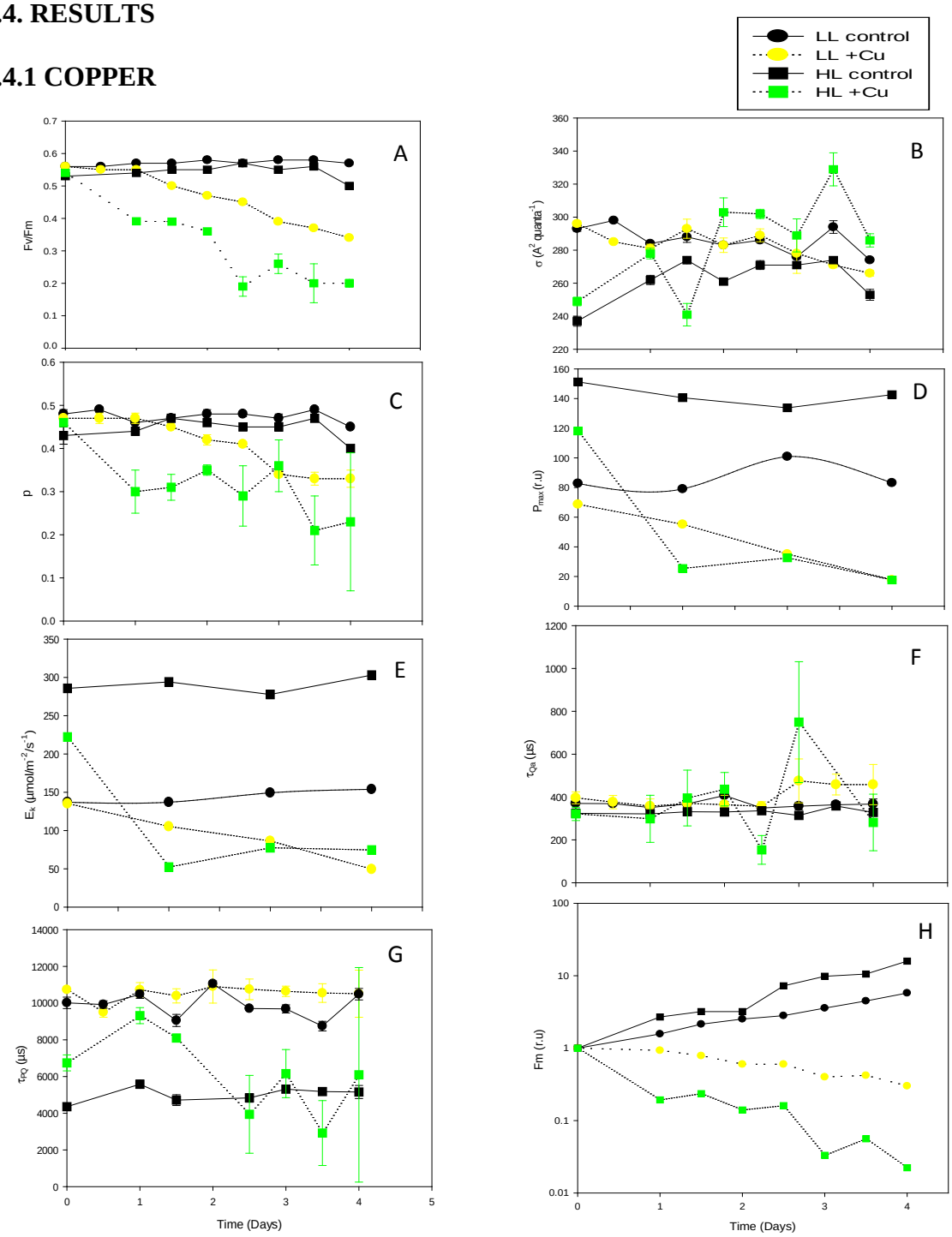

Fig. 3.3 Temporal evolution of the photosynthetic parameters under 25 µM Cu under high and low light growth irradiance exposure. These parameters include: quantum yield of photochemistry – Fv/Fm (a), functional absorption cross-section - σ_{PSII} (b), connectivity factor – p (c), maximum photosynthetic rate - P_{max} (d), the light saturation coefficient - E_k (e), rate of electron transport of PSII acceptor side - τ_{Qa} (f), rate of electron transport between PSII and PSI - τ_{PQ} (g), and maximum fluorescence (h). The proxy for chlorophyll biomass (F_m) was normalized to the first day measurement to remove sample to sample variability. Within minutes after dosing, effects were observed under high light growth irradiance for P_{max}, E_k, and τ_{PQ}. Low light growth irradiance delayed the negative response for 48-hrs.

3.4.2 QUANTUM YIELD OF PHOTOCHEMISTRY OF PSII (FV/FM)

The physiological state of the photosynthetic apparatus was monitored using Fv/Fm. According to the data, the controls were able to efficiently complete photochemistry activity noted by a minimum Fv/Fm value of 0.5. Cu treated cells under high growth irradiance declined 30% every 48-hrs (Fig. 3.3 A). Whereas, Cu treated cells under low light growth irradiance declined 20% every 48-hrs (Fig. 3.3 A). The severity of the decline for cells grown at 25μM of Cu was more pronounced under high compared to low growth conditions.

3.4.3 CONNECTIVITY FACTOR AND FUNCTIONAL ABSORPTION CROSS-SECTION OF PSII

The energy transfer between PSII units in photosynthesis is represented by the connectivity factor. Control connectivity factor did not statistically differ from Cu exposed cells under low growth irradiance ($p > 0.05$). The additional stress from high light growth conditions resulted in Cu treated cell significant decline in its ability to transfer energy between PSII units ($p < 0.05$).

3.4.4 PHOTOSYNTHESIS – IRRADIANCE CURVE (P-I)

The light saturation photosynthetic rate (P_{max}) value diminished 20% within minutes of Cu exposure under high light (Fig. 3.3 D). An impact on P_{max} under low growth light was not observed within minutes of Cu exposure. Beginning at 69 r.u, low light P_{max} declined 80% on day three (Fig. 3.3 D). The other parameter, light saturation coefficient (E_k), lessened 70% on day three under low light (Fig. 3.3 E). As with many other parameters tested, an increase in growth irradiance resulted in a stronger response.

The analysis of high light P_{max} and E_k decreased 90 and 80%, respectively of the control on day three (Figs. 3.3 D & E).

3.4.5 PHOTOSYNTHESIS ELECTRON FLOW.

Conversion of light into chemical energy involves the transfer of electron. Interruptions within the electron flow from Q_A was not observed (Fig. 3.3 F). Cu treated cells grown under high light conditions displayed a longer time to complete the oxidation-reduction reaction of the quinone, PQ, for the first 48-hrs of the experiment (Fig. 3.3 G). After which time, the rate of oxidation-reduction for PQ resumed to a time value similar to the control.

3.4.6 POPULATION GROWTH

The growth rate was measured to observe the effects of the whole organism. *T. weissflogii* did not grow in 25 μM of Cu (Fig. 3.3 H). Mortality rates of 1.00 ± 0.30 d^{-1} and 0.30 ± 0.40 d^{-1} were observed for treated Cu cultures under high and low light conditions, respectively.

3.4.7 ZINC

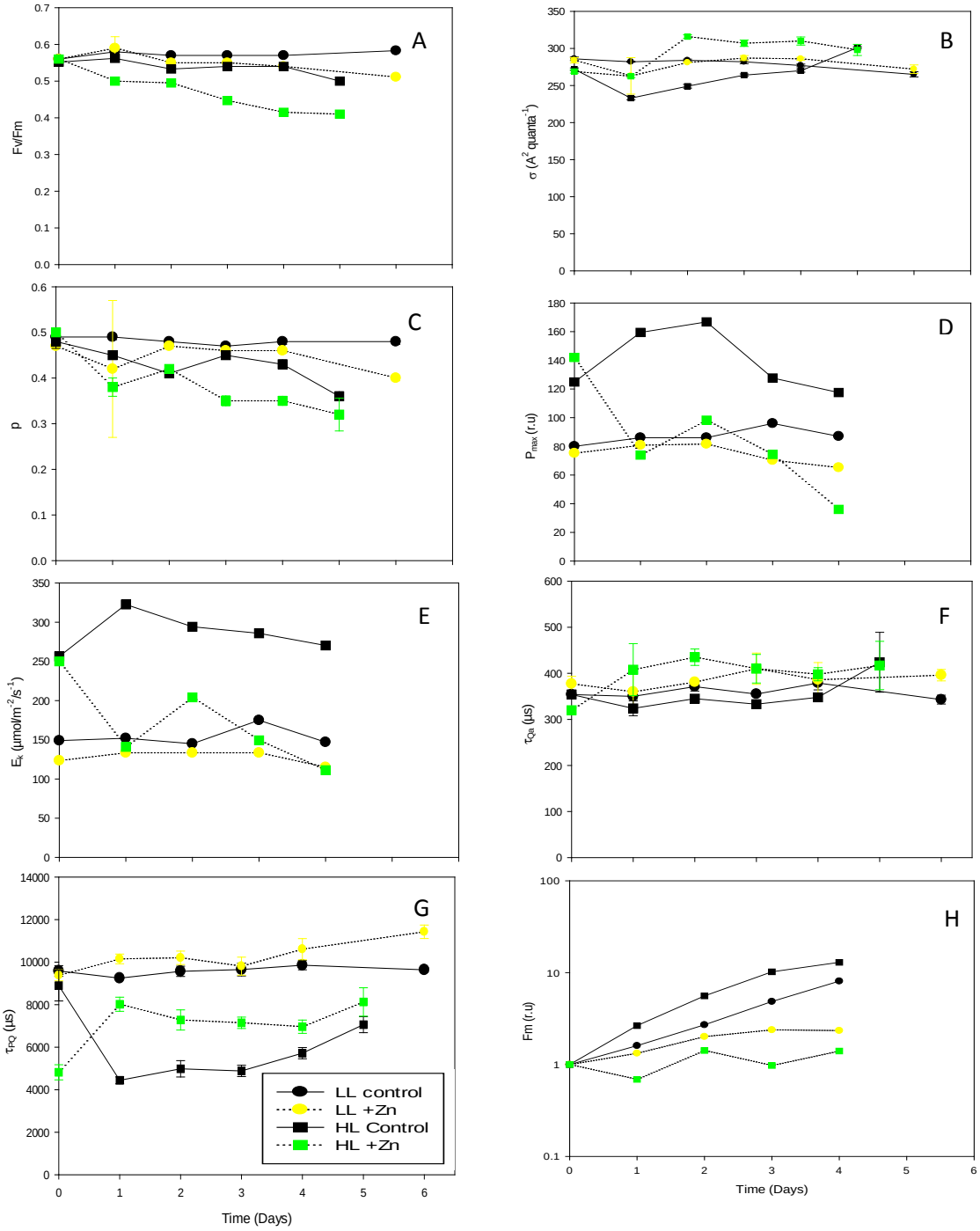

Fig. 3.4 Temporal evolution of the photosynthetic parameters under at 50 µM Zn high and low light growth irradiance. These parameters include: quantum yield of photochemistry – Fv/Fm (a), functional absorption cross-section - σ_{PSII} (b), connectivity factor - p (c), maximum photosynthetic rate - P_{max} (d), the light saturation coefficient - E_k (e), rate of electron transport of PSII acceptor side - τ_{Qa} (f), rate of electron transport between PSII and PSI - τ_{PQ} (g), and maximum fluorescence (f). The proxy for chlorophyll biomass (F_m) was normalized to the first day measurement to remove sample to sample variability. Negative effects under low light growth irradiance was noted after 72-hrs of exposure to Zn in biomass production only. Whereas, high light growth irradiance within 24-hrs in parameters representing growth and secondary photosynthetic reactions.

3.4.8 QUANTUM YIELD OF PHOTOCHEMISTRY OF PSII (FV/FM)

Apparent in this finding, Zn exposure did not severely affect photochemistry. Control and treatment cultures under low light irradiance mirrored each other throughout the experiment (Fig. 3.4 A). Whereas, the treatment cultures under high light conditions showed a decreased probability that photon energy would be used for photosynthesis (Fig. 3.4 A). The alteration in high light growth irradiance Fv/Fm values was not statistically significant ($p > 0.05$). Fv/Fm trends under Zn exposure contrasts the Cu experiment (Fig. 3.3 A). For the Cu experiment, both light conditions yielded a statistically significant difference between controls and treatments.

3.4.9 CONNECTIVITY FACTOR AND FUNCTIONAL ABSORPTION CROSS-SECTION OF PSII

Measured values for the connectivity factor and the functional absorption cross-section of PSII did not differ between control and treated cells under either light condition (Figs. 3.4 C&D).

3.4.10 PHOTOSYNTHESIS – IRRADIANCE CURVE (P-I)

High light growth irradiance setting yielded P_{max} and E_k values which were reduced by half of its initial reading within the first day of the experiment. Zn exposed cell had a similar P_{max} and E_k as the control under low light growth settings at the start of the experiment. Then the P-I parameters declined 20% (E_k) and 30% (P_{max}) after 72-hrs (Figs. 3.4 D&E). Also after 72-hrs, high light growth irradiance rendered a decrease in P_{max} and E_k of 40% and 50% respectively (Figs. 3.4 D&E). In contrast to Cu, Zn exposure under low growth irradiance did not vary throughout the experiment.

3.4.11 PHOTOSYNTHESIS ELECTRON TRANSPORT RATE

The re-oxidation time constants of Qa and PQ did not differ from the controls under either growth irradiance (Figs. 3.4 F&G).

3.4.12 POPULATION GROWTH

Zn exposure slowed the cell division rate. The degree to which this rate was slowed was more pronounced under high light (Fig. 3.4 H).

3.4.13 LEAD

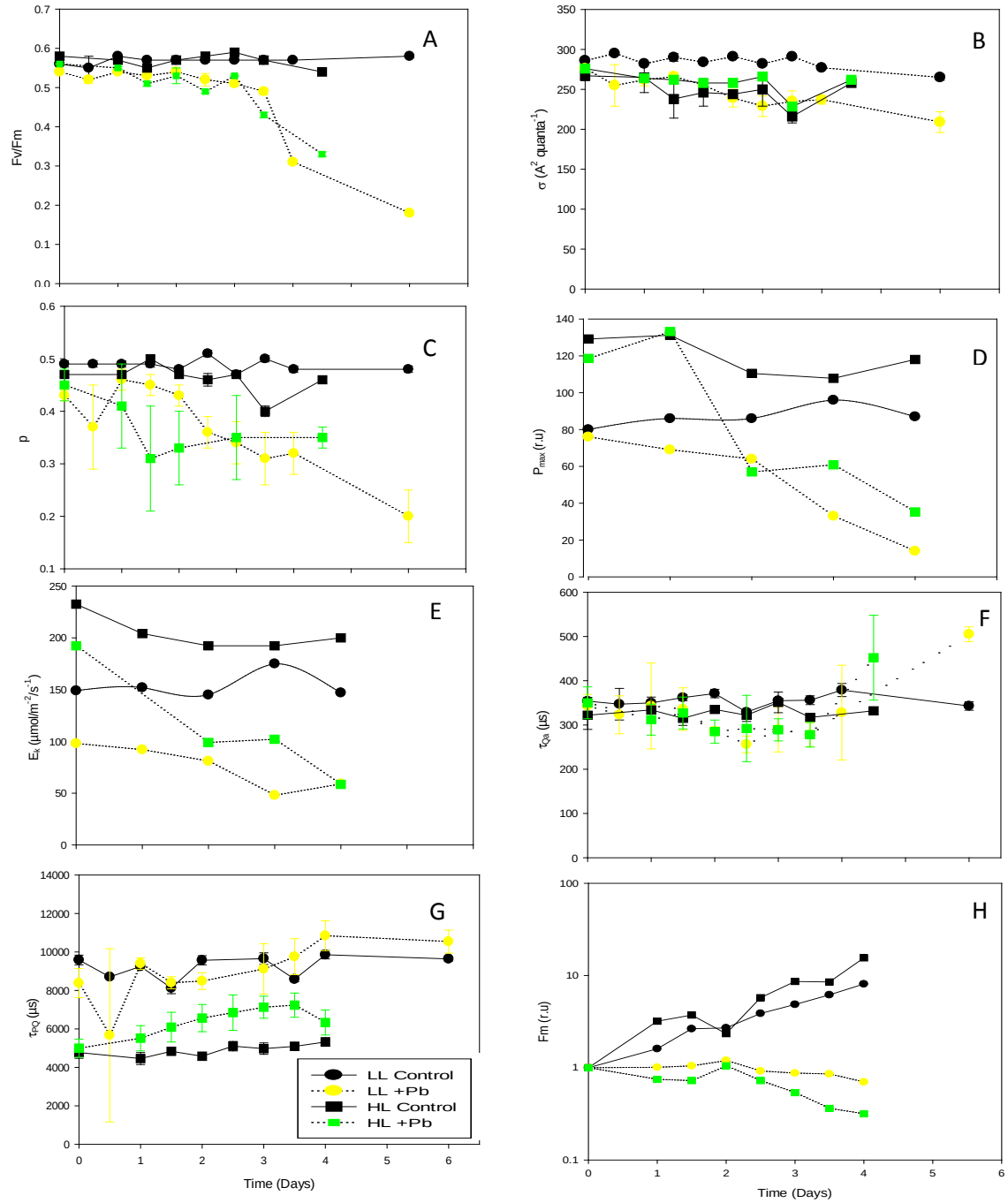

Fig. 3.5 Temporal evolution of the photosynthetic parameters under550 µM Pb high and low light growth irradiance. These parameters include: quantum yield of photochemistry – Fv/Fm (a), functional absorption cross-section - σ_{PSII} (b), connectivity factor – p (c), maximum photosynthetic rate - P_{max} (d), the light saturation coefficient – E_k (e), rate of electron transport of PSII acceptor side – τ_{Qa} (f), rate of electron transport between PSII and PSI – τ_{PQ} (g), and maximum fluorescence (f). The proxy for chlorophyll biomass (F_m) was normalized to the first day measurement to remove sample to sample variability. Effects of Pb on E_k were observed in minutes under both growth irradiances. Notable effects to growth, energy transfer, and Fv/Fm occurred days after the effect to the secondary photosynthetic parameters.

3.4.14 QUANTUM YIELD OF PHOTOCHEMISTRY OF PSII (FV/FM)

Expression of Fv/Fm response to Pb treatment is shown in Fig. 3.5A. 72-hr exposure to Pb under high and low light settings did not induce a stress response. However, exposure to Pb beyond 72-hr was required for *T. weissflogii* to express a restriction in its quantum yield of photochemistry of PSII.

3.4.15 CONNECTIVITY FACTOR AND FUNCTIONAL ABSORPTION CROSS-SECTION OF PSII

There was no difference between any treatments and controls tested for the functional absorption cross-section of PSII parameter (Fig. 3.5 B). The connectivity factor in Pb treated cells transferred energy between PSII units 40% and 30% less than the controls under high and low growth light conditions by day four (Fig. 3.5 C).

3.4.16 PHOTOSYNTHESIS – IRRADIANCE CURVE (P-I)

Effects to the secondary photosynthetic reactions were confirmed by alterations of P-I curve parameters P_{max} and E_k. Our results indicate that both parameters were reduced in both light conditions in response to Pb treatment (Figs. 3.5 D&E). From the initial ready, P_{max} and E_k declined 80% and 60% respectively under both light regimes.

3.4.17 PHOTOSYNTHESIS ELECTRON TRANSPORT RATE

After four days, a decline of 10 and 25% was observed for Q_A re-oxidation time constant for Pb exposed cells in low and high light growth environments, respectively (Fig. 3.5 F). Statistical analysis revealed no significant difference between the re-oxidation times of PQ between the controls and treatments under either growth irradiance ($p > 0.05$) (Fig. 3.5 G).

3.4.18 POPULATION GROWTH

An exposure period of 96-hr to Pb yielded significant changes in population numbers. Until day two, Pb treated cultures under both light regimes maintained a constant population size. Beyond 48-hr, cells under both growth irradiances started to lose its viability noted by a mortality rate of $0.10 \pm 0.30\ d^{-1}$ and $0.10 \pm 0.309\ d^{-1}$ for high and low light, respectively (Fig. 3.5 H). Cultures exposed to Pb had more viable cells than Cu treated cultures noted by the lower mortality rate in Pb experiments.

3.4.19 REACTIVE OXYGEN SPECIES (ROS)

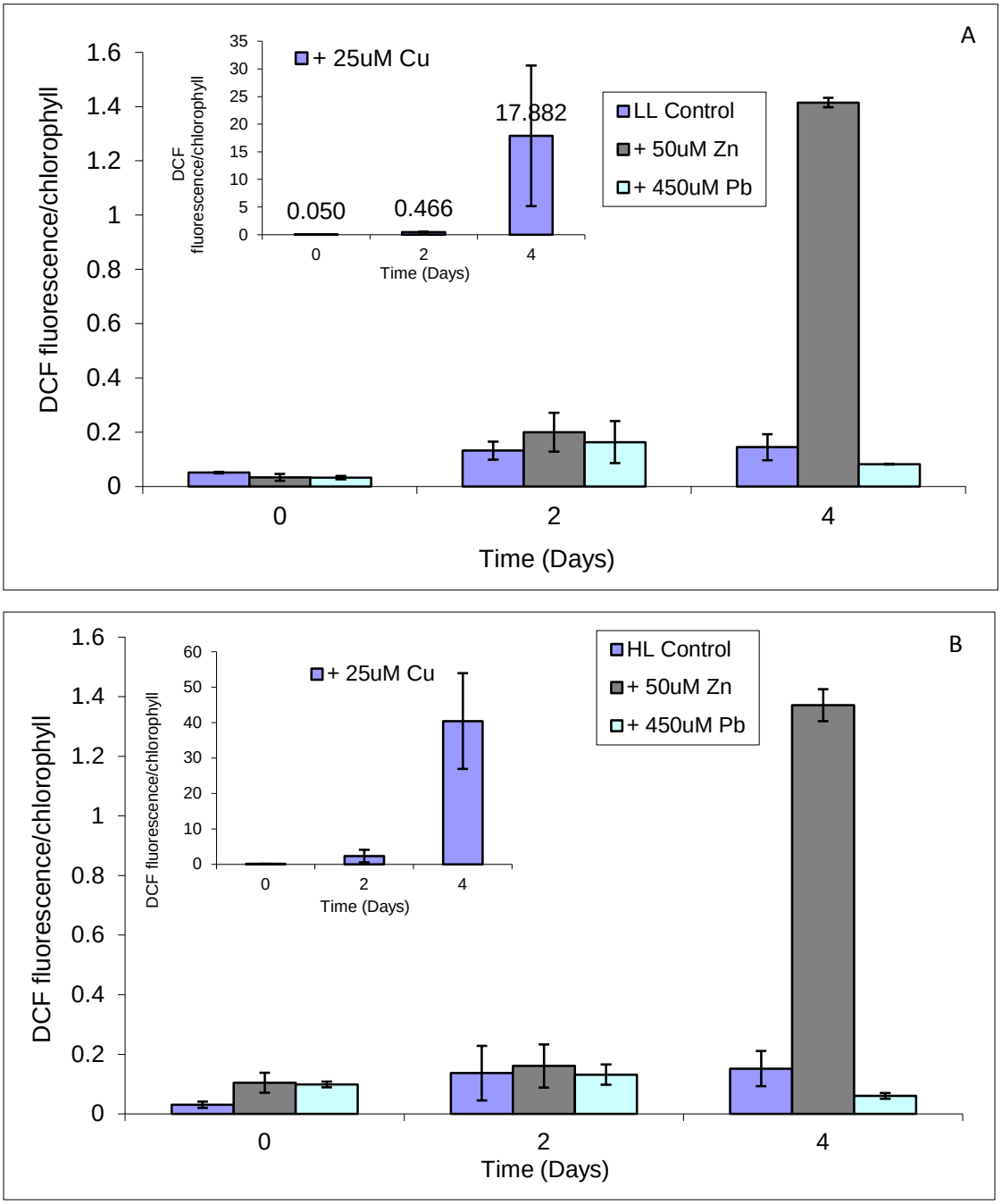

Fig. 3.6 DCF fluorescence normalized to chlorophyll showing the generation of intracellular reactive oxygen species under Cu, Zn, and Pb low (A) and high (B) growth irradiances exposure. Values are reported as fluorescence after 30 minutes, 48-hr, and 96-hr of exposure. Control and Pb cultures had values that remained below 0.20 DCF fluorescence/chlorophyll. There was a gradual increase in both Zn and Cu treated cultures over the experimental timeframe.

The ROS signal intensity for the three metals tested are shown in Fig. 3.6. Algal cells treated with Pb showed minimal generation of ROS. The DCF fluorescence units were similar between the control and Pb treated cultures throughout the experiment period. Cultures exposed to Cu continuously increased ROS production over time (Figs. 3.6 A&B). No difference between ROS production in cultures exposed to Zn was noted in the high or low growth irradiance until the last day of the experiment. Growth irradiances did have an effect on ROS production in cultures exposed to Cu.

3.5 DISCUSSION

Secondary photosynthetic reactions are those which include processes occurring after the flow of electron through photosystem I. The most notable secondary photosynthetic reaction is the Calvin cycle. While this study did not directly measure the amount of carbon fixed, there are tool which serves as a proxy. One of these tools is the photosynthetic-irradiance (P-I) curve. The activity of the main enzyme in the Calvin cycle, Rubisco, directly relates to the photosynthetic capacity and is represented in the P-I curve as the P_{max} (Cho et al., 1984; Fischer et al., 1989). Analyses of physiological functions related to the primary and secondary photosynthetic reactions are typically analyzed separately. This study analyzed these reactions concurrently to determine which reaction was the primary target of metal toxicity.

3.5.1 COPPER

The toxicity of excess Cu on the primary and secondary photosynthetic reactions was demonstrated. These effects were more severe than for the other metals tested in this study and for Sn (Chapter 2).

Light Intensity	P_{max}	E_k	Fv/Fm	Electron transport rate between photosystems	PSII acceptor side electron transport	Growth rate
Low light	1st ++	3rd +	4th +++	No effect	No effect	2nd
High light	1st +	1st +	2nd +++	1st	No effect	2nd

Table 3.2: Divergence timeline for each measured physiological parameter under Cu exposure. The statistical significance is notated at + marks. + indicates a $p < 0.05$, ++ is a $p < 0.01$, and +++ is a $p < 0.001$. P-values greater than 0.05 are not reported.

Although some parameters were affected to different degrees, the timeframe of inhibition varied and is depicted in Table 3.2. P_{max} and E_k parameters under high growth

irradiance had the same degree of inhibition after 24-hrs of exposure to Cu. The degree of inhibition of τPQ was half the observed value for P_{max}/E_k after 24-hrs of exposure to Cu grown in high irradiance. Therefore, the secondary photosynthetic parameters were more sensitive than the electron transport rate between the photosystems grown under high irradiance. An initial change in the re-oxidation time constant of PQ was not mentioned in Table 3.2 but had an immediate response under high growth irradiance. Pmax and Ek appeared to be the most sensitive parameter under low growth irradiance. The time between observed effects to the secondary photosynthetic parameters and any primary photosynthetic parameter was 24-hrs.

Although light is a substrate needed for photochemical energy conversion, in excess it damages the D1 protein of the reaction center and produces excess ROS (Yamamoto et al., 2008; Tyystjari, 2008; Barber and Andersson, 1992). Reported consequences of ROS production include interaction with sulfhydryl group, disturbance to chlorophyll biosynthesis, increase in F_o, membrane degradation, and cleavage of the large subunit of Rubisco (Shakya et al., 2008; Chettri et al., 1998; Ralph and Burchett, 1998; Luo et al., 2002; Eckardt and Pell, 1995; Roberts et al., 2003; Rao et al., 1989; Jacob and Lawlor, 1992). One reaction that induces ROS production and inhibits the cellular defense to oxidative damage under Cu exposure is the Fenton reaction (Shanmuganatha et al., 2004; Knauert and Knauer, 2008; Nishiyama et al., 2001). A cellular defense to ROS production under high irradiance is to alter the electron flow through the photosystem. If the amount of energy converted decreases, it is assumed that the amount of ROS produced to interact with cellular processes decreases. Up until 48-hrs after dosing with Cu, an alteration in the electron flow between the photosystems was

recorded and corresponded to low ROS production under high growth irradiance (Figs. 3.3 G & 3.6). Once the electron flow through the photosystem reached a value comparable to the control, detectable ROS rose (Figs. 3.3 G & 3.6). ROS production at 96-hr in high growth irradiance Cu exposed cultures was twice that observed at low irradiance. This demonstrates a synergistic relationship between growth irradiance and Cu. The consequences of ROS accumulation reduced the energy transfer between PSII units and maximum rate at which dark reactions proceeded (Fig. 3.3 C, D, & E). Cu-induced loss of quantum yield of PSII may have results from ROS damage to theD1.

Excess cellular Cu is chelated and one detoxification process is through the complex formed with glutathione (Freedman et al., 1989). Resistance to Cu toxicity is dependent upon the glutathione levels (Freedman et al., 1989; Irihimovitch and Shapira, 2000). The level of reduced glutathione protects and regulates the translation of Rubisco large subunit (Cohen et al., 2005; Sedigheh et al., 2011; Feller et al., 2008). An increase in growth irradiance did not increase the resistance of *T. weissflogii* to Cu, which contradicts Nielsen and Nielson (2010). P_{max} and E_k exhibited an immediate effect upon exposure to Cu for cells adapted to high light growth irradiance. The initial effect to P_{max} and E_k is attributed to the Cu ion followed by a combined effect with ROS. Whereas, low light adapted data suggest co-inhibition of primary and secondary photosynthetic reactions. This was demonstrated by the initial stress effect being observed in P_{max} and Fv/Fm at same time (Figs. 3.3 A&D). When the light intensity approaches 1000 µmol/ m^{-2}/s^{-1} about 25% of the absorbed quantum is used and excess ROS is produced (review by Long et al., 1994).

Growth and photosynthesis are not always coupled. Comparison of growth and Fv/Fm can be used to infer if these reactions were uncoupled during trace metal stress to preserve the photosynthetic efficiency. Therefore, Fv/Fm was used as an indicator of stress and related to the metabolic disruption.

3.5.2 ZINC

T. weissflogii had a higher tolerance to Zn stress than the other metals tested in this study. Zn is commonly observed to induce the least amount of stress on measured responses compared to other metals (Stiborova et al., 1988; Shakya et al., 2008; Plekhanov and Chemeris, 2003). Parameters representing the primary photosynthetic reactions (Fv/Fm, p, τ_{PQ}, τ_{QA}, σ_{PSII}) had no significant effect under Zn exposure ($p > 0.05$), which was similar to the information obtained in the Sn (Chapter 2) study and noted in Table 3.3. Studies reporting alterations in the primary photosynthetic reaction parameters used Zn concentrations an order of magnitude higher than what was used in this study (Vaillant et al., 2005; Plekhanov and Chemeris, 2003; van Assche and Clijster, 1986b). Zinc concentrations greater than 100 µM showed clear effects on the primary photosynthetic reactions such as the electron flow (Hampp et al., 1976).

Light Irradiance	P_{max}	E_k	Fv/Fm	Electron transport rate between photosystems	PSII acceptor side electron transport	Growth rate
Low light	No effect	No effect	No effect	No effect	No effect	1st
High light	1st +	1st ++	3rd	No effect	No effect	2nd

Table 3.3: Divergence timeline for each measured physiological parameter under Zn exposure. The statistical significance is notated at + marks. + indicates a $p < 0.05$, ++ is a $p < 0.01$, and +++ is a $p < 0.001$. P-values greater than 0.05 are not reported.

Only FIRe parameters relating to the secondary photosynthetic reactions and growth were altered with the addition of excess Zn and occurred when cultures were grown under high irradiance. Reduction in the growth irradiance ameliorated the measured Zn effects. A similar conclusion of reducing light to decrease Zn bioaccumulation and negative response was previously reported (Hassler and Wilkinson, 2003). Despite the growth irradiance, Zn exposure limits growth. Biomass reduction is a general response of photosynthetic organisms to excess Zn (Vaillant et al., 2005; Stauber and Florence, 1990).

Unlike Cu, the photoprotective mechanisms were not activated by the addition of Zn. But, Zn exposure still produced ROS. The amount of ROS produced was independent of the growth irradiance (Fig. 3.6). Heavy metals are known to generate ROS (Chaoui et al., 1997). Combining the heavy metal, Zn, with a high growth irradiance should have yielded higher measurable ROS than what was recorded under low growth irradiance. Either Zn participates in a process that increases the scavenging of ROS or the experimental timeframe was insufficient to allow ROS accumulation. For example, it took over 172-hrs for ROS levels to show higher values under high growth irradiance (Weckx and Clijsters, 1997). The conclusion of indirect means yielding the response to the secondary photosynthetic parameters was not gleamed from this study.

3.5.3 LEAD

The following inhibition pattern was determined from measuring various parameters when cultures were exposed to Pb under low growth irradiance: $E_k > P_{max} >$ growth rate > Fv/Fm. The more sensitive parameters under low light growth irradiance are the secondary reactions. The intensity to which Pb ions impaired the photosynthetic

apparatus was between the trends seen for Zn and Cu. The inhibition sequence at a higher irradiance level was the growth rate followed by P_{max} and E_k and then Fv/Fm (Table 3.4).

Light Irradiance	P_{max}	E_k	Fv/Fm	Electron transport rate between photosystems	PSII acceptor side electron transport	Growth rate
Low light	2nd +	1st +++	3rd +++	No effect	No effect	2nd
High light	2nd	2nd ++	3rd +++	No effect	No effect	1st

Table 3.4: Divergence timeline for each measured physiological parameter under Pb exposure. The statistical significance is notated at + marks. + indicates a $p < 0.05$, ++ is a $p < 0.01$, and +++ is a $p < 0.001$. P-values greater than 0.05 are not reported.

This study showed that exposure to Pb involved direct interaction between the metal ion and photochemical processes. The lack of ROS production supports my conclusion that Pb directly interacted with photochemical processes to yield an inhibition in the maximum rate at which the dark reaction proceeds (Fig. 3.6). Furthermore, exposure to Pb under either growth irradiance did not inhibit the photosynthetic electron flow through the photosystem. The redox state of the PQ pool is ultimately influenced by ATP/ADP ratio (Rochaix, 2011). No interruption within the PQ re-oxidation suggests that the diminished carbon fixation rate in this case was not attributed to insufficient ATP nor insufficient reductants produced for the Calvin cycle.

Upon addition of Pb to the cultures, a white precipitate formed. It was suspected that this precipitate was lead phosphate. The production of lead phosphate increased with daily additions of lead sulphate. Thus, acute limitations of phosphorus would induce lead immobilization effecting growth. The strategy to reserve phosphorus yielded the

cell population in stationary phase (Fig. 3.5 E). This observation was independent of the growth irradiance.

3.6 CONCLUSION

This study described the sequence of physical alterations within the photosynthetic apparatus of the marine diatom *Thalassiosira weissflogii* exposed to trace metals. The divergence pattern is illustrated in Tables 3.5 and 3.6 below.

	Metal Exposed Under Low Growth Irradiance			
Parameter	50 µM Zn	25 µM Cu	450 µM Pb	800 µM Sn
P_{max}	NA	1st	2nd	1st
E_k	NA	3rd	1st	1st
Growth	1st	2nd	2nd	2nd
Fv/Fm	NA	4th	3rd	NA

Table 3.5 Summary of the divergence pattern for tested metals under low growth irradiance. The statistical significance is notated at + marks. + indicates a $p < 0.05$, ++ is a $p < 0.01$, and +++ is a $p < 0.001$. P-values greater than 0.05 are not reported.

	Metal Exposed Under High Growth Irradiance			
Parameter	50 µM Zn	25 µM Cu	450 µM Pb	800 µM Sn
P_{max}	1st	1st	2nd	1st
E_k	1st	1st	2nd	1st
Growth	2nd	2nd	1st	2nd
Fv/Fm	3rd	2nd	3rd	3rd

Table 3.6 Summary of the divergence pattern for tested metals under high growth irradiance. The statistical significance is notated at + marks. + indicates a $p < 0.05$, ++ is a $p < 0.01$, and +++ is a $p < 0.001$. P-values greater than 0.05 are not reported.

The metals tested showed considerable differences with respects to their toxicity ranges in *T. weissflogii* yielding unique fluorescence signatures. Cu had largest effects irrespective of the growth irradiance. Every photosynthetic process displayed stress when exposed to excess Cu. Stress to the primary photosynthetic reactions were measured 48-hrs and 96-hrs prior to any other metal tested for high and low growth irradiance, respectively when cells were exposed to Cu. A measurable effect to P_{max} under Cu high growth irradiance was observed 24-hrs prior to the other metals tested. It took Cu treated cultures an additional 48-hrs for effects to be observed under the low growth irradiance. While Pb interacted with multiple reactions within the photosynthetic process, it was the only metal that displayed a measurable stress to E_k under low growth irradiances within minutes of exposure. Alterations to the photosynthetic apparatus grown with excess Zn is dependent on growth irradiance. In this study, Zn effected growth, P_{max}, and E_k under high growth irradiance only.

However, one constant between all metal toxicity was the inhibition to the secondary photosynthetic reactions. The secondary photosynthetic parameters (P_{max} and E_k) were the first and second observed parameters negatively affected by the tested metals. The effect on the secondary photosynthetic parameters could be the result of direct Cu ion interaction with Rubisco. Cu effects were the result of metal ions and ROS production.

CHAPTER 4

4.0 Synergistic toxicity of Texas crude oil and dispersant Corexit 9527 to *Symbiodinium spp.* photosynthetic apparatus

4.1 ABSTRACT

The impacts of oil spills are reduced by dispersants; however, the ecological impact of transferring oil from the water surface into the water column is still debatable. Information pertaining to the dispersant effect on primary producers are lacking. I used the dinoflagellate *Symbiodinium spp* to assess the photosynthetic effect when exposed to 186 µM 4-chlorophenol (reference toxicant), 3.8 ppm Corexit 9527, 98.3% water accommodated fraction (WAF) of Texas crude oil, and 6 % chemically enhanced water accommodated fraction (CEWAF) for five to fourteen days under a static (constant test solution concentration) or dilution (declining test solution concentration) conditions. The energy transfer between photosystem II (PSII) units and secondary photosynthetic reactions appeared to be one of the sensitive parameters. Recovery of the secondary photosynthetic reactions occurred in cells exposed to CEWAF under low growth irradiance. This work provides evidence that there are no long-term subtle physiological effects of exposure to *Symbiodinium spp.* to the primary or secondary photosynthetic reactions under low irradiance.

4.2 INTRODUCTION

Maritime trafficking of crude oils are prone to accidental spills. Oil films are transformed by physical, chemical, photochemical, and biological processes. Existing approaches taken to treat and reduce the impact of oil to aquatic organisms, shorelines, and subtidal areas include: enhancement of oil-degrading microbes, use of boom,

skimmers or sorbent materials, and application of surfactants (Fox, 1989; Pritchard et al. 1992; Chakrabarty, 1985; Rasiah and Voroney, 1993). Dispersants are surfactants containing anionic and nonionic molecules at ratios that render both hydrophilic and hydrophobic properties. The purpose of surfactants is to form aggregates with its hydrophobic tails pointing inward towards the oil to minimize the free energy of the system (Canevari, 1978). The concentration at which aggregation occurs is the critical micelle concentration. These aggregates are termed micelles and are dispersed within the water column.

The majority of dispersant research on the reformulated dispersant has addressed toxicity to macroinvertebrates and fish. The acute toxicity of dispersants Corexit 9500, Corexit 9527, SPC 1000, Nokomis 3-F4, Nokomis 3-AA, ZI-400, and JD 2000 has been established for a wide variety of aquatic organisms (Judson et al., 2010; review by Georges-Ares and Clark, 2000). The 96-hr LC_{50} for Corexit 9527 to several species ranged from 1.6 to >1000 ppm, while the 96-hr LC_{50} for Corexit 9500 to the same subphylum ranged from 3.5 to 354 ppm (Duval et al., 1982; Environment Canada, 1994; Foy, 1982; Gulec et al., 1997; Singer et al., 1991).

Chemical dispersion of oil yields the dissolution of petroleum hydrocarbons, oil droplets encased in surfactant, and dissolved surfactants into the water column (Singer et al., 1998). Dissolved petroleum hydrocarbons accumulate on organic membranes due to its lipophilic nature (Ren et al., 1994). This has proven to increase the bioavailable fraction of polycyclic aromatic hydrocarbon (PAH) by increasing its water solubility (Wolfe et al., 2001; Ramachandran et al. 2004; Heintz et al., 1999; Yamada et al., 2003; Couillard et al., 2005). This enrichment phenomenon was calculated by Anderson et al.

(1974). Their study showed that South Louisiana crude oil aromatic enrichment was a factor of 14.3, Kuwait crude oil was a factor of 125, and Bunker C oil or No. 2 fuel oil was between a factor of 21 to 35.

Enhanced bioavailability of PAH to organisms would yield greater accumulation suggesting that water accommodated fraction (WAF) of crude oil would be less toxic than chemically enhanced water accommodated fraction (CEWAF). The toxicities of crude oil, dispersants, and its mixture yield conflicting data in the literature. Epstein et al. (2000) reported a low oil: sea water ratio of 1: 200 which was not toxic to *Stylophora pistillata* planula larvae but became highly toxic after chemical dispersion. Le Gore et al. (1983) concluded that corexit 9527 was not toxic to Arabian Gulf corals. No difference was observed between dispersant, oil plus dispersant, nor crude oil effects on the seagrass, *Halophila ovalis* (Ralph and Burchett, 1998).

Different WAF and CEWAF test solutions may have different dominant hydrocarbon groups and other methodological variations, which makes comparison of previous data difficult. Additionally, previous studies have investigated the growth, quantum yield of photochemistry of PSII, and oxygen production effects on photosynthetic organisms due to the application of chemical dispersing crude oil independently. Due to the listing criteria of the National Oil and Hazardous Substance Pollution Contingency Plan (NCP), species from different trophic levels are lacking specifically the available information on the toxic effects to algal species. The use of photosynthesis allows for rapid investigation of Corexit on the cell membrane.

This study expands our knowledge of how Corexit 9527, WAF, and CEWAF affect the photosynthetic apparatus. Most studies evaluate short-term affects since

dispersed oil is washed away in the ocean current. The aim of this work was to assess direct long-term effects of Texas crude oil and dispersed crude oil on marine phytoplankton during an oil spill event where the concentration of undispersed and dispersed oil is maintained over days using the model symbiotic organism *Symbiodinium spp*. *Symbiodinum spp.* were exposed to the toxicant at a constant concentration (static) and to a concentration that is diminishing (dilution) over the length of the experiment.

4.3 MATERIALS & METHODS

4.3.1 Test Organism and Growth Conditions

Light fluctuates from limiting to excess levels on a diurnal timescale. The efficiency at which light is harvested changes with light intensity, which can influence the degree of phytotoxicity. Thus, exposure to *Symbiodinum spp.* (CCMP2460) were carried out under constant day length (12-hr/12-hr light/dark photoperiod), constant temperature of 25°C , and constant light intensity (either 70 or 350 µmol/m^{-2}/$s^{-1}$of low or high light, respectively white fluorescent light) in F/2 medium without silica.

4.3.2 Exposure Determination

Estimation of the toxicity concentration utilized within the study was determined based on a dose-response curve. Solution concentrations ranged from 0 and 10% CEWAF, and 0 to 130% WAF (v/v). The exposure duration to evaluate the photosynthetic efficiency (Fv/Fm) was 48-hrs after exposure. The concentration producing half maximal inhibitory concentration (IC_{50}) (concentration yielding a decline in the Fv/Fm response by half) was chosen to continue the experiment. The selected concentration serves two functions: first, it represents measured doses observed in the aquatic environment and secondly, it elicits an adverse response to the quantum yield of

photochemistry of PSII within two or three days, that is roughly the average lifetime of the cells in the population (the reciprocal cell division rate).

WAF (%)	Fv/Fm	Probit	CEWAF (%)	Fv/Fm	Probit	Corexit 9527 (ppm)	Fv/Fm	Probit
0	0.57	0	0	0.51	0	0	0.57	0
0.03	0.57	0	0.05	0.50	2.95	2	0.48	4.01
0.067	0.59	0	.12	0.50	2.67	4	0.27	5.10
0.2	0.58	0	.25	0.47	3.59	10	0.02	6.88
0.33	0.58	0	.42	0.48	3.45	15	0.00	8.09
0.47	0.57	0	.62	0.42	4.08			
0.67	0.49	3.25	1.05	0.43	4.01			
3.3	0.53	3.12	2.32	0.27	4.92			
33.3	0.52	2.67	4.0	0.26	5.00			
66.7	0.47	3.66	9.0	0.22	5.15			
100	0.24	5.05						
133	0.39	4.26						

Table 4.1 Information used to create a dose-response curve predicted from probit model. The responses were estimated from Fv/Fm of a toxicant free culture. From this information we calculated the IC_{50} for WAF as slightly below 100%, IC_{50} for CEWAF was 6%, and the IC_{50} of Corexit 9527 as 12 ppm ± 3%.

The sigmoid dose-response curve was transformed into a straight line using Finney (1971) probit analysis. A plot of the toxicant log concentration versus the probit unit revealed a linear relation, which can be plotted from the information provided in Table 4.1. The IC_{50} determined from this process was used to carry out the study under static (constant test solution concentration) or dilution (declining test solution concentration) conditions. Prior to starting the experiment, *Symbiodinum spp.* was photoacclimated for two weeks to each growth irradiance.

4.3.3 Fluorescence

Chlorophyll a fluorescence and photosynthetic characteristics were measured on *Symbiodinum spp.* using a custom-built FIRe (Gorbunov and Falkowski, 2004). After adjusting each culture to ambient light for 20 minutes, 2 mL was pipetted out of each flask and dark adapted for 10 minutes. First, FIRe single turnover flash (STF) protocol

was completed. Then the multiple turnover flash (MTF) protocol was completed. The STF protocol consisted of a 100 µs long saturating flash (induction phase) followed by a sequence of week relaxation pulses. The number of pulses in the relaxation sequence was 40 and the total duration of the relaxation phase was 200 ms. Under the STF protocol, the minimal fluorescence level (F_o), the maximum fluorescence level (F_m), the variable fluorescence ($Fv = F_m-F_o$), the quantum efficiency of photochemistry in PSII (Fv/Fm ratio), and the rates of electron transport on the acceptor side of Photosystem II (i.e., the rates of Q_A re-oxidation) were measured (Gorbunov and Falkowski, 2004). The MTF protocol consisted of a 100 ms long saturating flash followed by a sequence of week relaxation pulses. Since the MTF flash fully reduces the plastoquinone pool and thus saturates the chain of electron carriers between PSII and PSI, the relaxation in fluorescence yield after the MTF reflects the rates of plastoquinone pool re-oxidation, i.e. the rates of electron transport between PSII and PSI. This rate is usually ca. 10 times slower than that of Q_A re-oxidation measured after the STF. Please refer to Fig. 1.2 for the schematic showing kinetic phase of fluorescence induction.

The photosynthetic electron transport rates as a function of irradiance (photosynthesis-versus-irradiance profiles) were retrieved from FIRe fluorescence measurements under varying ambient light. Samples were exposed to 12 increased irradiance levels, ranging from 0 up to 1500 µmol/m^{-2}/s^{-1}, with 50 s interval at each irradiance. The relative electron rate was calculated for every light level as the product PAR* ΔF'/Fm'. The photosynthesis-versus- irradiance profiles were fitted with a hyperbolic equation (in Sigma Plot) resulting in the maximum photosynthetic rate (P_{max}) and the light saturation coefficient parameter (E_k).

4.3.4 Growth Rate Calculation

Increase in F_m over the course of the experiment was used as a proxy of chlorophyll biomass. The reported F_m values were corrected for change in the FIRe detector gain. The measurements were made in triplets. The report values are the averages of the measurements.

4.3.5 Reference toxicant

To assess the comparability within laboratory experiments and compare the toxicities of the oil dispersant, the reference toxicant 4-chlorophenol was used (Environment Canada, 1990). Measured concentrations ranged from 0 to 300 µm 4-chlorophenol. A concentration close to the calculated IC_{50} for 4-chlorophenol (186 µm) was run simultaneously with all other toxicity tests to determine if there was change *Symbiodinum spp.* sensitivity over time.

4.3.6 Preparation of Corexit 9527, WAF, and CEWAF

The dispersant concentration was prepared on a volume/volume basis. The preparation of the test medium for the swirl test was prepared as described in the Environmental Protection Agency's 62 F15576 Appendix C to 40 CFR part 300.

The preparation of WAF and CEWAF utilized Texas crude oil, filtered seawater, and the addition of Corexit 9527 (CEWAF only). WAF and CEWAF were prepared according to the standardized technique developed by Singer et al (2000) and are briefly described in Table 4.2. More specifically, 4 mL of Texas crude oil was added to 400 mL of water to create WAF. To prepare CEWAF, seawater was brought to the desired vortex percentage then oil (4 mL) and dispersant (400 µL) were added to the vortex center. The

CEWAF concentration was prepared on a volume/volume basis at a ratio of 1:10 (Cark et al., 2001).

	WAF	CEWAF
Water preparation	Filtered natural seawater through a 0.45 µM filter	Filtered natural seawater
Crude Oil	Texas Crude oil, g oil/L water	
Vessel	500-mL aspirator glass bottle with 400-mL of water	
Dispersant	No dispersant	Corexit 9527, (1:10 ratio of dispersant to oil)
Vortex	No vortex	Vortex 20-25% of water depth
Mixing duration	24 hr in the dark	20 hr
Settling duration	No settling time	3-6 hr

Table 4.2 Standardized method for preparing water-accommodate fractions of crude oil (WAF) and dispersed crude oil (CEWAF) Singer et al., 2000

4.3.7 Surface Tension

The micelle behavior of Corexit 9527 was investigated. Surface tension was measured using a Rame Hart Goniometer. Ten milliliters of the dispersant solution was prepared with 0.45 µm filtered seawater and placed in a glass test tube. Solution concentrations ranged from 0.04 to 1.4 ppm. Triplicate measurements were made for the dispersant. The critical micelle concentration (CMC) of the dispersant was estimated, which is defined as the concentration of surfactants above which micelles form and almost all additional surfactants added to the system go to micelles.

4.3.8 Statistical Analysis

Statistical analyses were performed using Sigma Stat software. One-way analysis of variance with treatment as a factor was applied to detect differences among treatments (control, Corexit 9527, 4-chlorophenol, WAF, and CEWAF). Median inhibition concentrations (IC_{50} as percentage of photochemical efficiency) for the Corexit 9527, 4-chlorophenol, WAF, and CEWAF exposures were calculated from induction curves using probit analysis to fit a linear regression.

4.4 RESULTS

4.4.1 Critical Micelle Concentration

The CMC defines the concentration that separate two kinds of thermodynamic behaviors of the surfactant. Below the CMC level, the surface tension fluctuates and favors a hydrophobic domain. Above the CMC level, the surface tension remains relatively constant and the surfactant begins to aggregate. The CMC is determined once the surface tension stops changing. The IC_{50} concentration utilized in the studied was located on the second line where the surface tension was nearly constant (data not shown). This indicates that the surfactant molecules were micelles.

4.4.2 4-chlorophenol

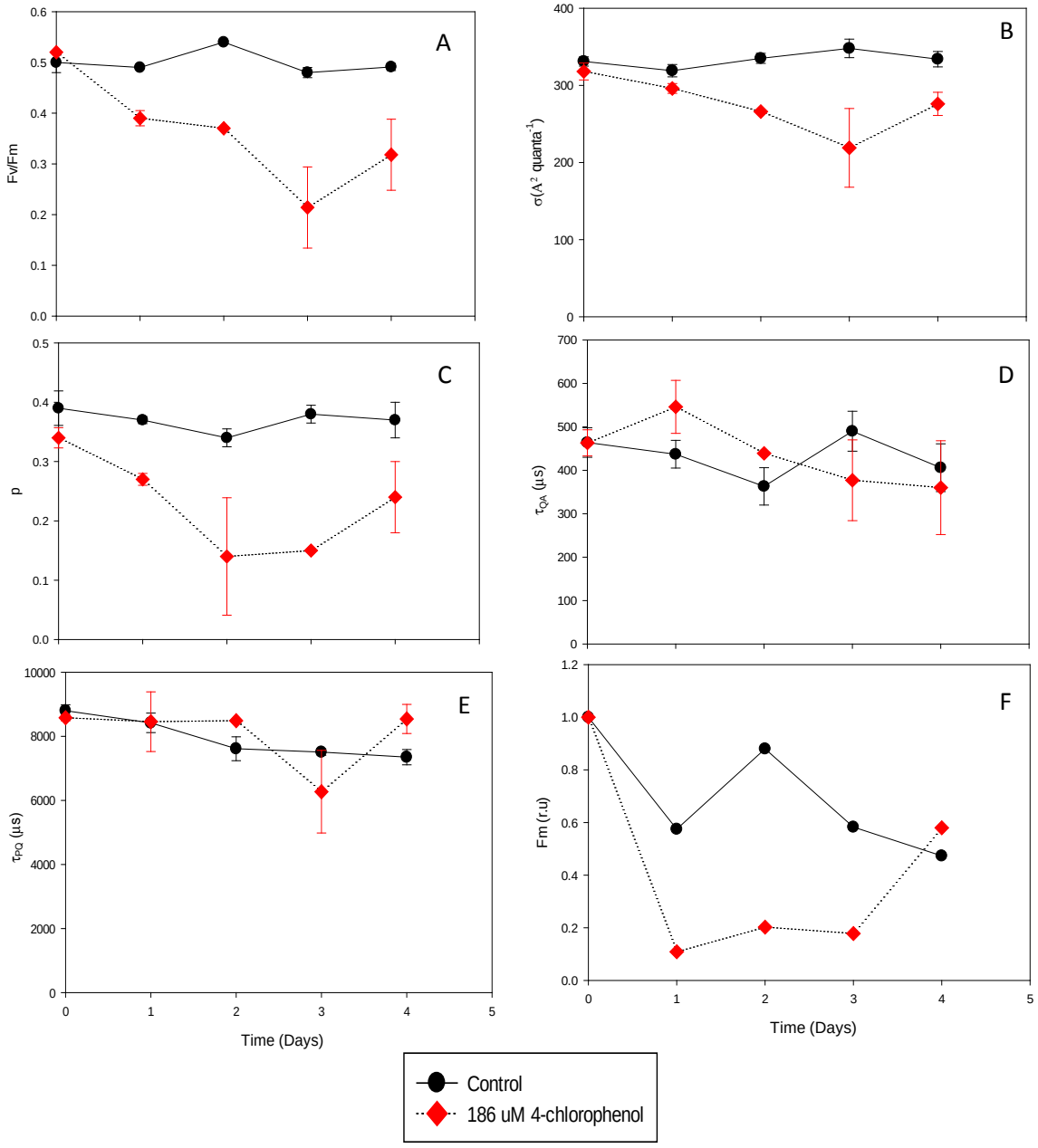

Fig. 4.1 Temporal evolution of the photosynthetic parameter under 186 µM 4-chlorophenolunder high growth irradiance static conditions. These parameters include: quantum yield of photochemistry – Fv/Fm (a), functional absorption cross-section - σ_{PSII} (b), connectivity factor – p (c), rate of electron transport of PSII acceptor side – τ_{Qa} (d), rate of electron transport between PSII and PSI - τ_{PQ} (e), and maximum fluorescence (f). The proxy for chlorophyll biomass (F_m) was normalized to the first day measurement to remove sample to sample variability. Measurable effects were recorded 24-hrs after dosing with the toxicant in parameters representing growth, Fv/Fm, and p. The negative effects were ameliorated after 72-hrs.

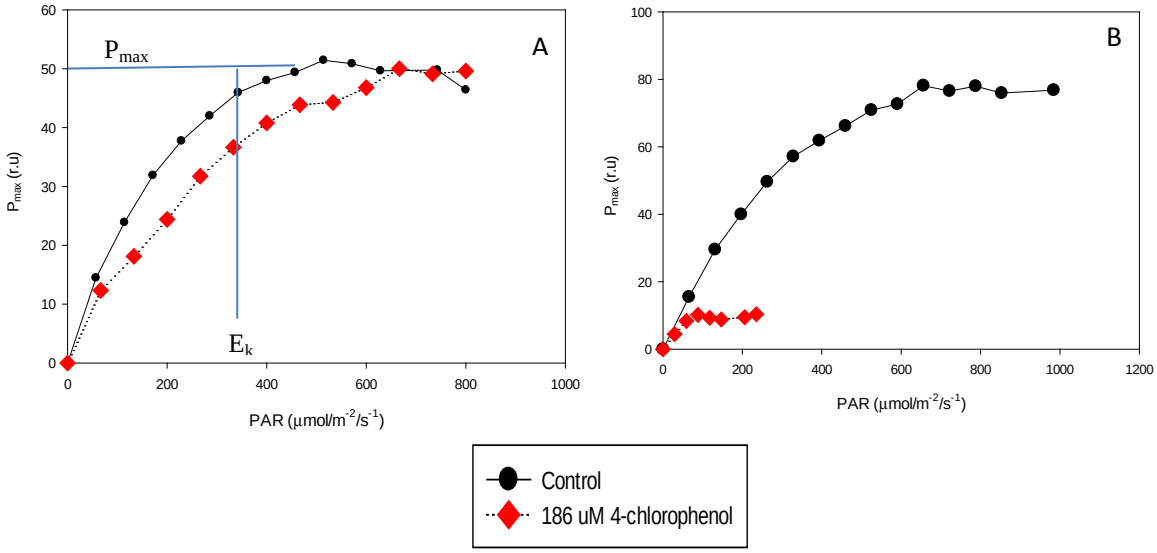

Fig. 4.2 Temporal evolution of the secondary photosynthetic reactions of *Symbiodinum spp.* grown at 186 µM 4-chlorophenol under high growth irradiance static conditions. The photosynthesis – irradiance curve represents P_{max} (maximum photosynthetic rates) and E_k (light saturation coefficient) on day 0 which was measured five minutes after dosing (a), and on day 4 (b). The parameters representing the dark reactions did not yield any effects over the length of the experiment.

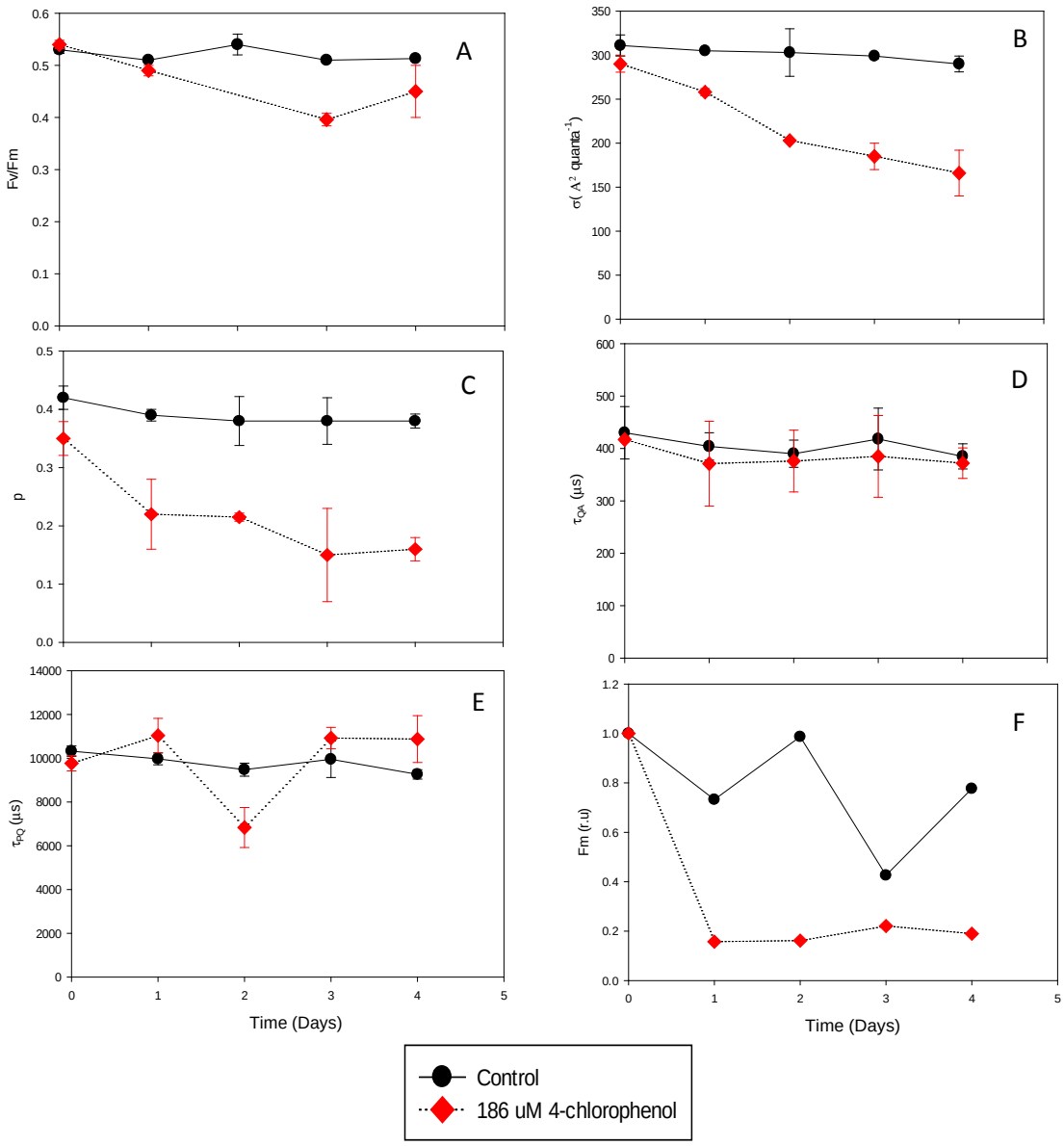

Fig. 4.3 Temporal evolution of the photosynthetic parameter under low growth irradiance static conditions at 186 µM 4-chlorophenol. These parameters include: quantum yield of photochemistry- Fv/Fm (a), functional absorption cross-section- σ_{PSII} (b), connectivity factor – p (c), rate of electron transport of PSII acceptor side - τ_{Qa} (d), rate of electron transport between PSII and PSI - τ_{PQ} (e), and maximum fluorescence (f). The proxy for chlorophyll biomass (F_m) was normalized to the first day measurement to remove sample to sample variability. Measurable effects were recorded 24-hrs after dosing with the toxicant in parameters representing growth, σ_{PSII} and p.

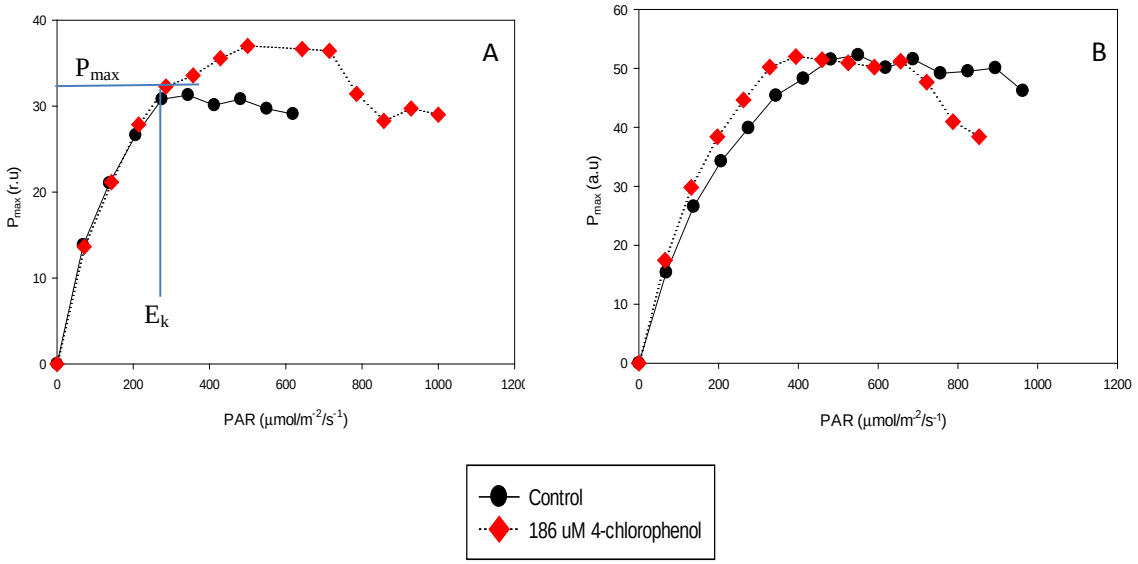

Fig. 4.4 Temporal evolution of the secondary photosynthetic reactions of *Symbiodinum spp.* grown at 186 µM 4-chlorophenol under low growth irradiance static conditions. The photosynthesis – irradiance curve represents P_{max} (maximum photosynthetic rates) and E_k (light saturation coefficient) on day 0 which was measured five minutes after dosing (a), and on day 4 (b). The parameters representing the dark reactions reflect how the maximum photosynthetic rate had lessened over the experiment period under 4-chlorophenol exposure at low irradiance level.

Examination of fluorescence levels representing the primary photosynthetic reaction under high growth irradiance revealed that Fv/Fm, σ_{PSII}, p, and F_m declined 24-hrs after exposure to 4-chlorophenol (Figs. 4.1 A, B, C & F). The greatest deviation between any parameter exposed to 4-chlorophenol and the control was seen in the energy transfer between the PSII units (p) (Fig. 4.1 C). However 96-hrs after exposure to 4-chlorophenol, p began to approach a value comparable to the control (Fig. 4.1 C). Despite this display of recovery, the p-value for the energy transfer between the PSII units was less than .01. Fv/Fm dropped below 0.4 units and remained below this value for the remainder of the experiment (Fig. 4.1 A). Statistically, this divergence in Fv/Fm was statistically significant ($p < 0.05$). As with the quantum yield of PSII, σ_{PSII} started to recover after 72-hrs of exposure (Fig. 4.1 B). The variability of the cell density in control cultures was attributed to the organism's low Reynolds number. This low Reynolds number yields flocculation and an underestimate of the cell number.

4-chlorophenol had no substantial effect on Fv/Fm under low growth irradiance (Fig. 4.3 A). The effects to the functional absorptive cross-section of PSII, connectivity, and growth followed the general trend of high growth irradiance when exposed to 4-chlorophenol (Figs. 4.1 and 4.4 B, C & F). No recovery was observed in any parameter displaying stress. Statistical analysis of the membrane parameters (σ_{PSII} and p) revealed significant depression ($p < 0.05$) within 48-hrs of exposure to 4-chlorophenol (Figs. 4.3 B&C). As time progressed, the impact on σ and p continued until the end of the experiment.

Comparing the impact of growth irradiance on the secondary photosynthetic reactions showed vast differences. Low growth irradiance did not impact the secondary

photosynthetic reactions when cultures were exposed to 4-chlorophenol (Figs. 4.4 A&B). However, a progressive decline in P_{max} and E_k occurred throughout the experiment under high growth irradiance and exposure to 4-chlorophenol (Figs. 4.2 A&B).

4.4.3 Corexit 9527

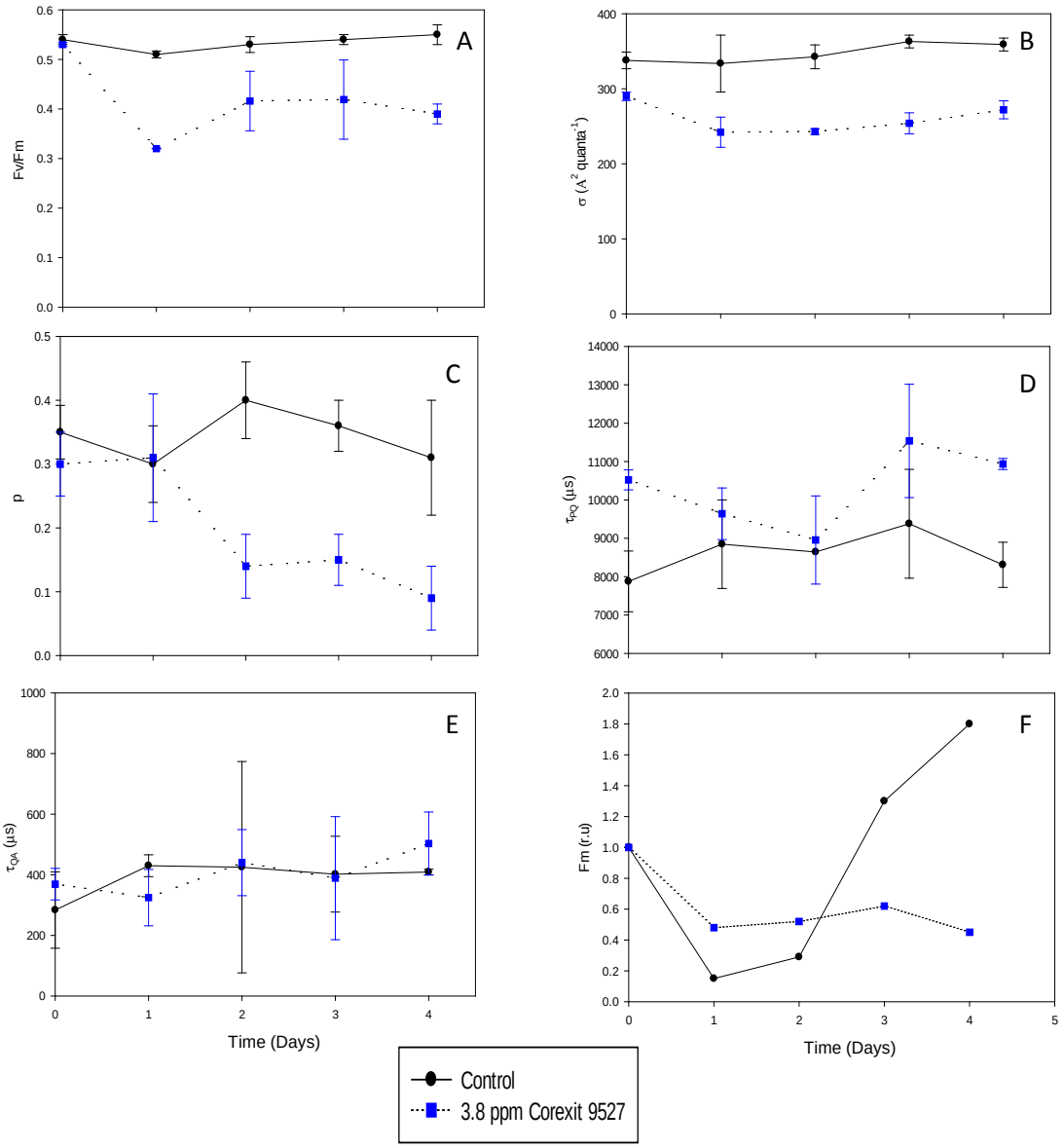

Fig. 4.5 Temporal evolution of the photosynthetic parameters under low growth irradiance static conditions at 3.8 ppm Corexit 9527. These parameters include: quantum yield of photochemistry – Fv/Fm (a), functional absorption cross-section - σ_{PSII} (b), connectivity factor – p (c), rate of electron transport between PSII and PSI - τ_{PQ} (d), rate of electron transport of PSII acceptor side - τ_{Qa} (e), and maximum fluorescence (f). The proxy for chlorophyll biomass (F_m) was normalized to the first day measurement to remove sample to sample variability. Measurable effects were recorded within minutes to the re-oxidation of PQ and 24-hrs after dosing with the toxicant to growth rate and Fv/Fm. The values recorded 48-hrs after exposure to the dispersant p continuously decline until the conclusion of the experiment.

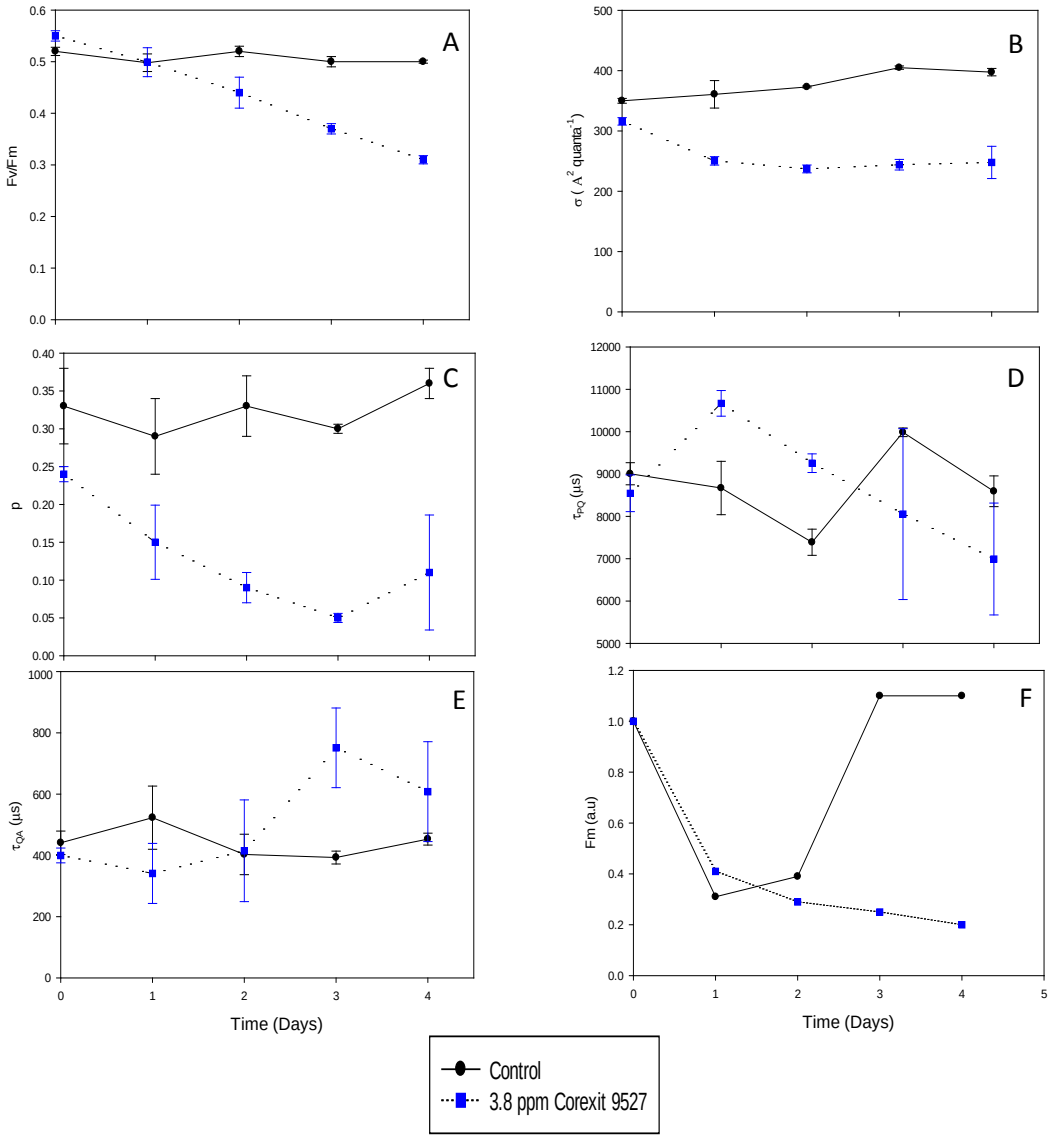

Fig. 4.6 Temporal evolution of the photosynthetic parameters under high growth irradiance static conditions at 3.8 ppm Corexit 9527. These parameters include: quantum yield of photochemistry – Fv/Fm (a), functional absorption cross-section – σ_{PSII} (b), connectivity factor – p (c), rate of electron transport between PSII and PSI – τ_{PQ} (d), rate of electron transport of PSII acceptor side – τ_{Qa} (e), and maximum fluorescence (f). The proxy for chlorophyll biomass (F_m) was normalized to the first day measurement to remove sample to sample variability. Measurable effects were recorded within minutes of exposure to the dispersant on the energy transfer parameter (p), which did not began to recover until the last 24-hrs. It was not until after 72-hr that a negative effect was observed on the Fv/Fm. The growth rate continuously declined throughout the experiment with the greatest decline in rate within the first 24-hrs.

Static Toxicity Test

The results of Corexit 9527 on the photosynthetic parameters reflect changes when the dispersant concentration is maintained throughout the experimental timeframe. Corexit 9527 affected Fv/Fm within 24-hrs under low light and within 72-hrs after exposure under high light irradiance (Fig. 4.5 & 4.6 A). Recovery of Fv/Fm occurred in dispersant cultures exposed to low light growth irradiance after 48-hrs but remained at a value which was still deemed unhealthy. The energy transfer between PSII units was affected under both growth irradiances ($p < 0.05$). Cultures exposed to dispersant under high growth irradiance displayed an immediate effect to the energy transfer between PSII units (4.6 C). A gradual decline was noted for the energy transfer between PSII units under low light conditions. A significant difference ($p < 0.05$) was observed in cultures' σ_{PSII} under both growth irradiances (Fig. 4.5 and 4.6 B). The cell density declined within 24-hrs after exposure to the dispersant but then maintained that cell density for the remainder of the experiment under low light growth irradiance (Fig. 4.5 F). The cell density declined within 24-hrs after exposure to the dispersant under high light growth irradiance but the cell density continued to decline for the duration of the experiment (Fig. 4.6 F). No effect was observed to the electron transport flow through photosystem II under high growth irradiance (Fig. 4.6 D&E).

4.4.4 WAF

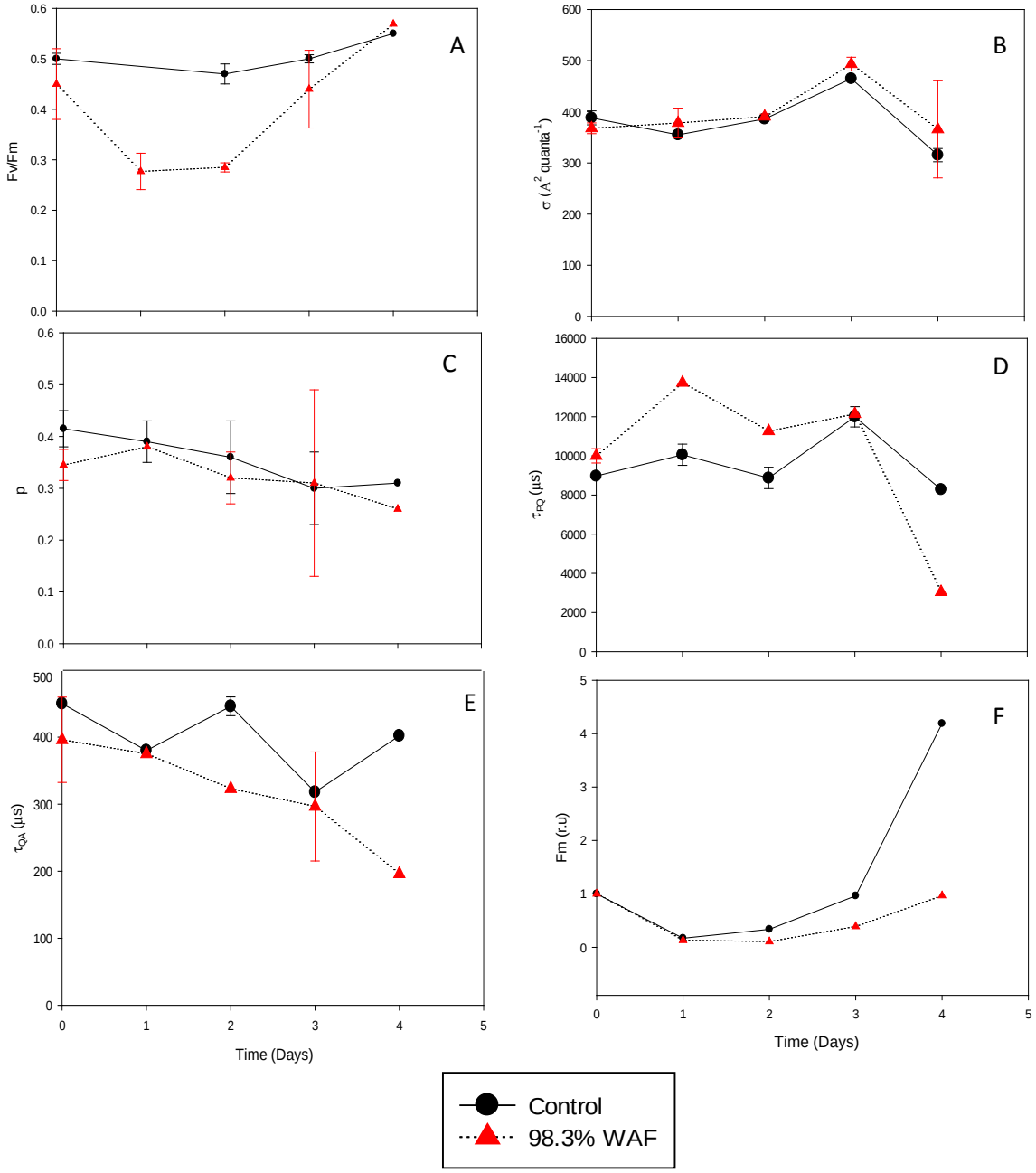

Fig. 4.7 Temporal evolution of the photosynthetic parameters under low growth irradiance static conditions at 98.3% WAF. These parameters include: quantum yield of photochemistry – Fv/Fm (a), functional absorption cross-section – σ_{PSII} (b), connectivity factor – p (c), rate of electron transport between PSII and PSI – τ_{PQ} (d), rate of electron transport of PSII acceptor side – τ_{Qa} (e), and maximum fluorescence (f). The proxy for chlorophyll biomass (F_m) was normalized to the first day measurement to remove sample to sample variability. A measurable effect on Fv/Fm was observed 24-hrs after exposure to WAF but recovered 72-hrs after exposure. 72-hrs after exposure to WAF the re-oxidation of Qa and PQ was affected.

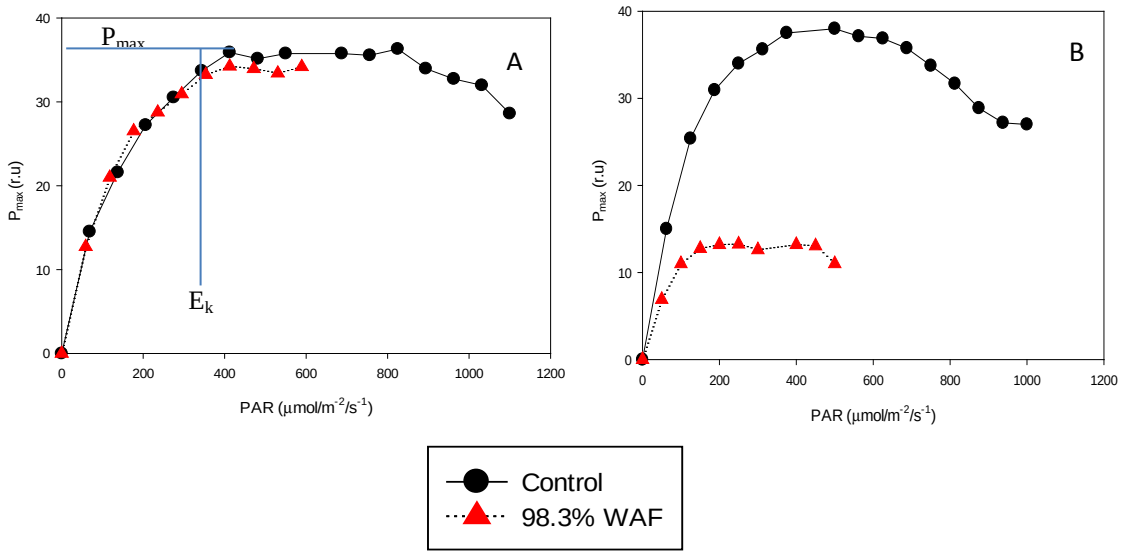

Fig. 4.8 Temporal evolution of the secondary photosynthetic reactions of *Symbiodinum spp.* grown at 98.3% WAF under low growth irradiance static conditions. The photosynthesis – irradiance curve represents P_{max} (maximum photosynthetic rates) and E_k (light saturation coefficient) on day 0 which was measured five minutes after dosing (a), and on day 4 (b). The maximum rate at which the dark reaction proceeds was immediately impacted upon exposure to WAF and remained at that rate for the duration of the experiment.

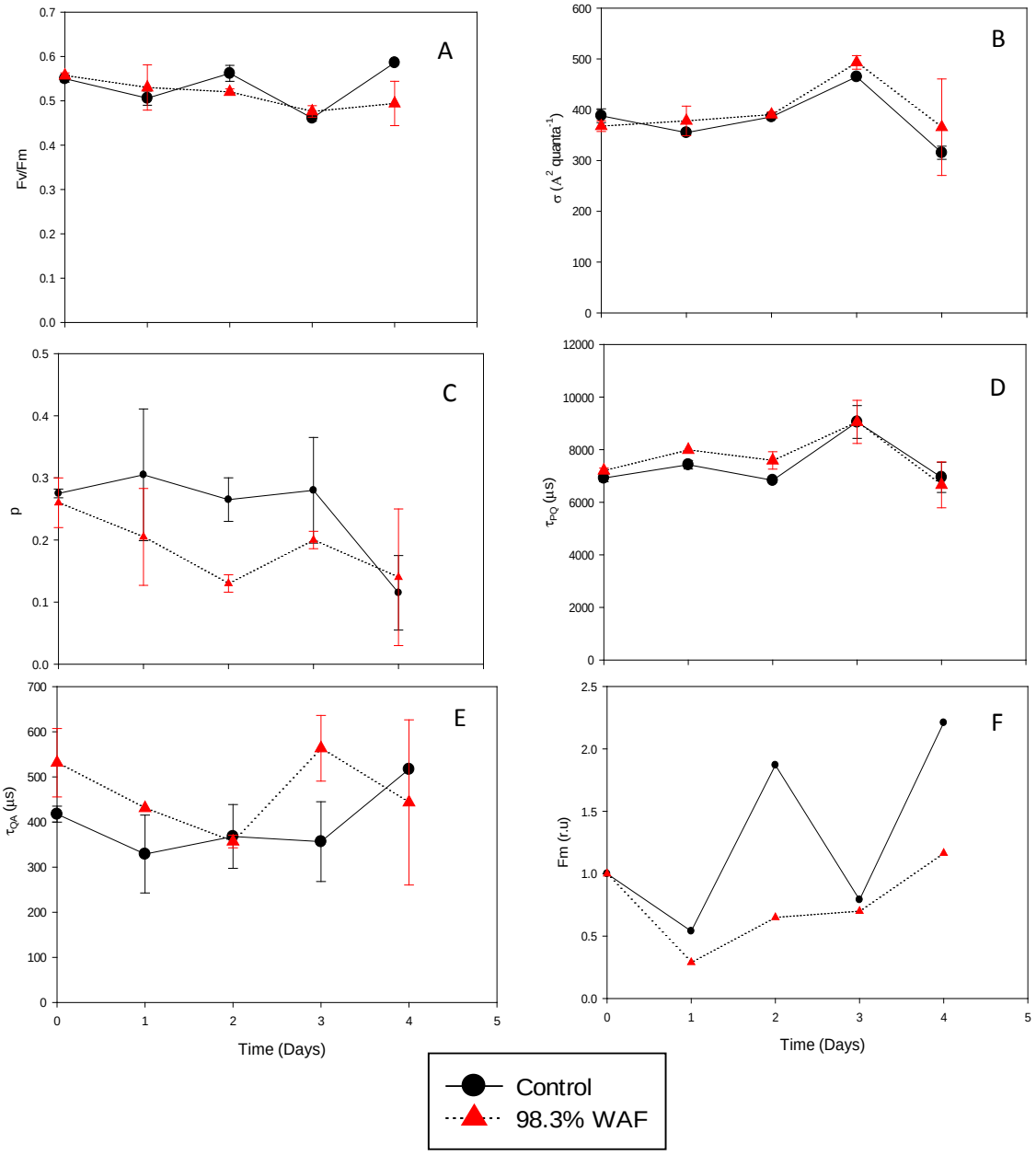

Fig. 4.9 Temporal evolution of the photosynthetic parameters under high growth irradiance static conditions at 98.3% WAF. These parameters include: quantum yield of photochemistry – Fv/Fm (a), functional absorption cross-section – σ_{PSII} (b), connectivity factor – p (c), rate of electron transport between PSII and PSI – τ_{PQ} (d), rate of electron transport of PSII acceptor side – τ_{Qa} (e), and maximum fluorescence (f). The proxy for chlorophyll biomass (F_m) was normalized to the first day measurement to correct for factors other than those being tested in the experiment. No measurable effects were observed except on the growth rate which was not sustained.

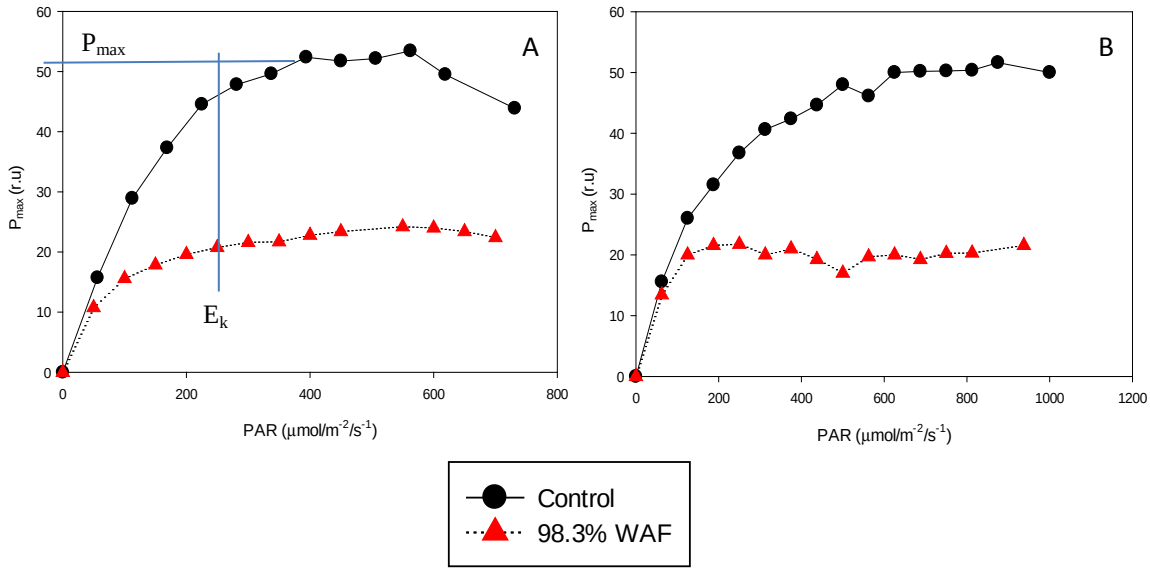

Fig. 4.10 Temporal evolution of the secondary photosynthetic reactions of *Symbiodinium spp.* grown under high growth irradiance static conditions 98.3% WAF. The photosynthesis – irradiance curve represents P_{max} (maximum photosynthetic rates) and E_k (light saturation coefficient) on day 0 which was measured five minutes after dosing (a), and on day 4 (b). The maximum rate at which the dark reaction proceeds gradually declined over the experiment duration. At the conclusion of the experiment, the culture with WAF had a dark reaction that proceeded at a rate that was less than half that of the control.

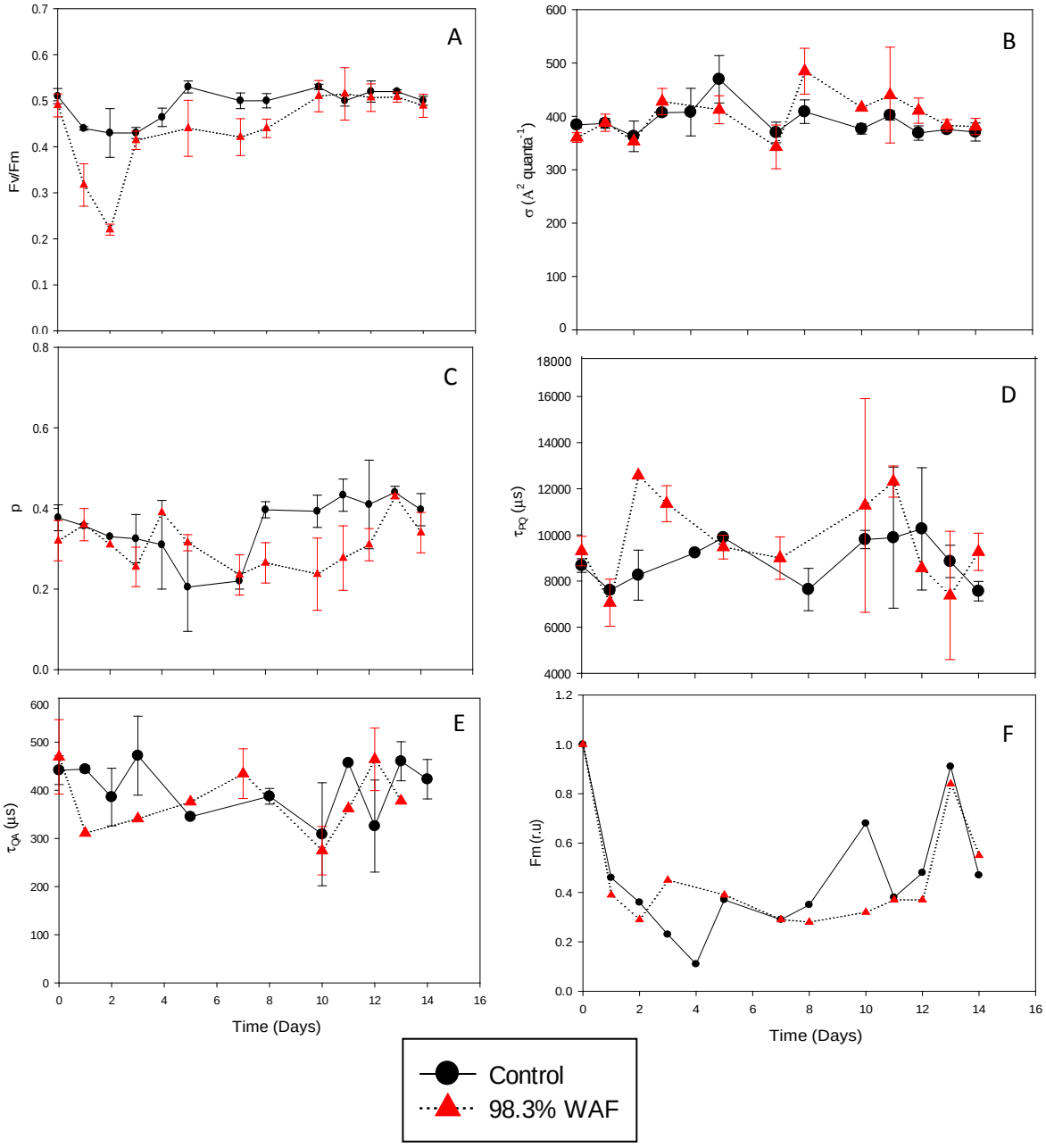

Fig. 4.11 Temporal evolution of the photosynthetic parameters under low growth irradiance dilution conditions at 98.3% WAF. These parameters include: quantum yield of photochemistry – Fv/Fm (a), functional absorption cross-section – σ_{PSII} (b), connectivity factor – p (c), rate of electron transport between PSII and PSI – τ_{PQ} (d), rate of electron transport of PSII acceptor side - τ_{Qa} (e), and maximum fluorescence (f). The proxy for chlorophyll biomass (F_m) was normalized to the first day measurement to correct for factors other than those being tested in the experiment. The only measurable difference between the control and WAF was during 48-hrs after exposure only.

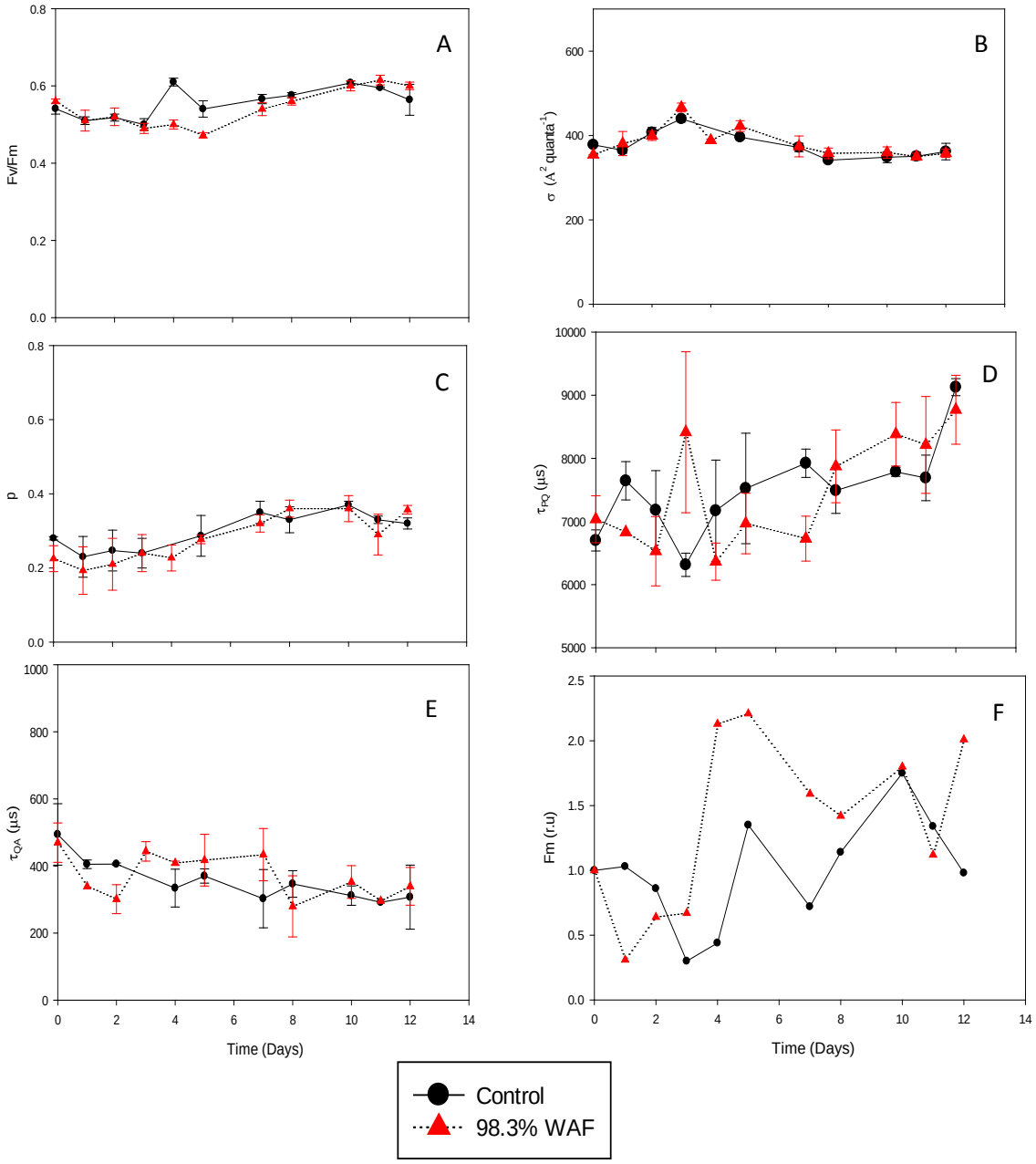

Fig. 4.12 Temporal evolution of the photosynthetic parameters grown under high growth irradiance dilution conditions at 98.3% WAF. These parameters include: quantum yield of photochemistry – Fv/Fm (a), functional absorption cross-section – σ_{PSII} (b), connectivity factor – p (c), rate of electron transport between PSII and PSI – τ_{PQ} (d), rate of electron transport of PSII acceptor side – τ_{Qa} (e), and maximum fluorescence (f). The proxy for chlorophyll biomass (F_m) was normalized to the first day measurement to correct for factors other than those being tested in the experiment.

Static Toxicity Test

Fv/Fm declined within 24-hr after exposure to WAF and maintained a value of 0.3 units until the last 48-hrs of the low growth irradiance experiment (Fig. 4.7 A). A slow steady decline in Qa re-oxidation under low growth irradiance was observed but was not statistically significant ($p > 0.05$) (Fig. 4.7 E).

No statistically significant effects ($p > 0.05$) on the primary photosynthetic reactions were observed under high growth irradiance (Fig. 4.9). A minor difference in the energy transfer between PSII and PSI was observed after 72-hrs of exposure to WAF under high irradiance conditions (Fig. 4.9 D).

Comparing the impact of growth irradiance on the secondary photosynthetic reactions showed vast differences. Low growth irradiance did not impact the secondary photosynthetic reactions immediately when combined with WAF (Figs. 4.8 A&B). However, an immediate impact was observed to P_{max} and E_k under high growth irradiance when combined with WAF (Figs. 4.10 A&B). This effect to P_{max} and E_k under high growth irradiance did not worsen nor recovered during the remaining days of the experiment.

Dilution Toxicity Test

Interestingly, two days of dilution eliminated the stress induced by WAF to the quantum yield of photochemistry of PSII under low growth irradiance (Fig. 4.11 A). All other experimental culture measurements did not vary form the control throughout the experimental timeframe. No stress was induced by WAF under high growth irradiance (Fig. 4.12).

4.4.5 CEWAF

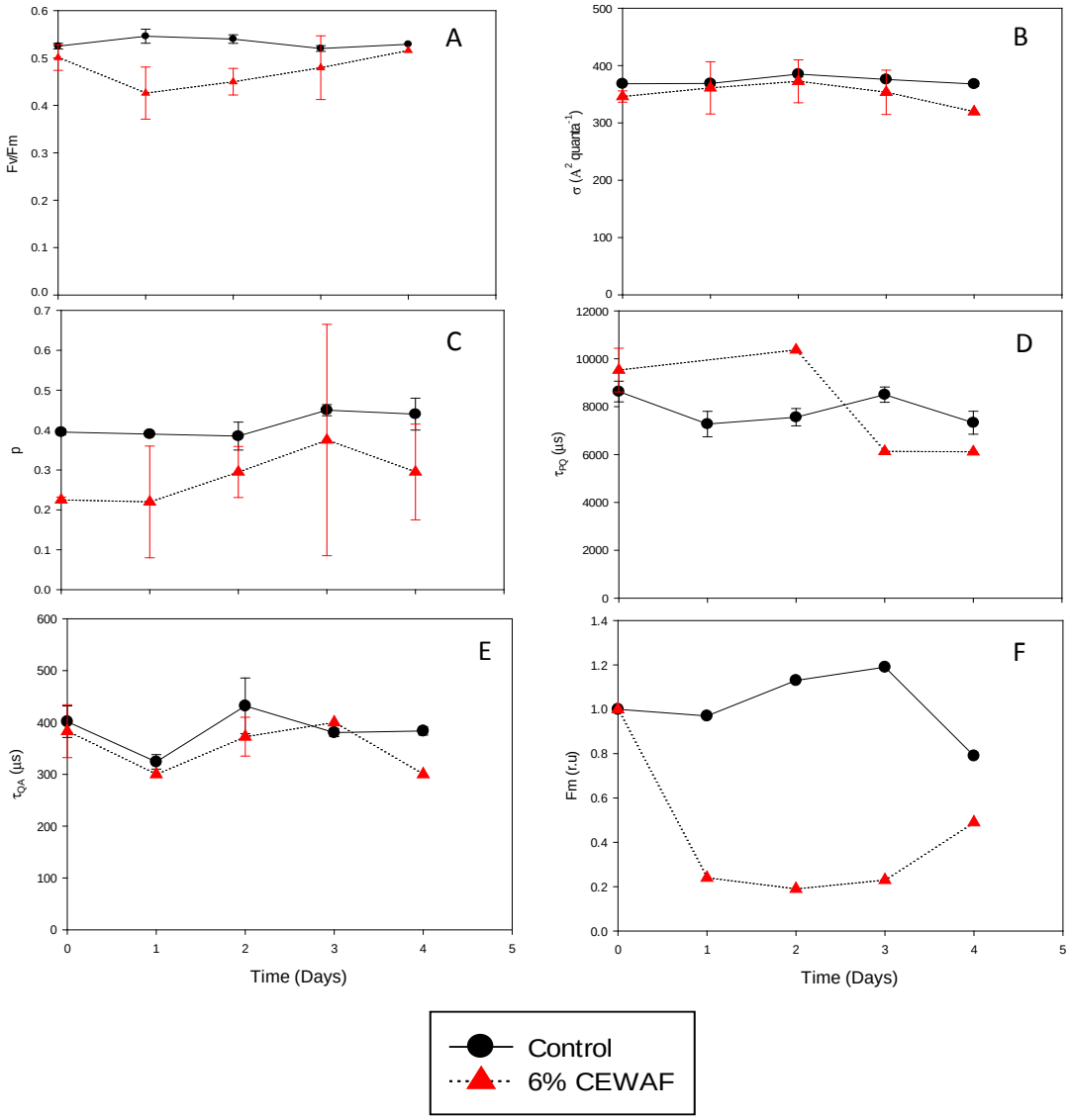

Fig. 4.13 Temporal evolution of the photosynthetic parameters under low growth irradiance static condition at 6% CEWAF. These parameters include: quantum yield of photochemistry – Fv/Fm (a), functional absorption cross-section – σ_{PSII} (b), connectivity factor – p (c), rate of electron transport between PSII and PSI – τ_{PQ} (d), rate of electron transport of PSII acceptor side - τ_{Qa} (e), and maximum fluorescence (f). The proxy for chlorophyll biomass (F_m) was normalized to the first day measurement to correct for factors other than those being tested in the experiment. An immediate effect to the energy transfer between PSII units was observed but was ameliorated by the end of the experiment.

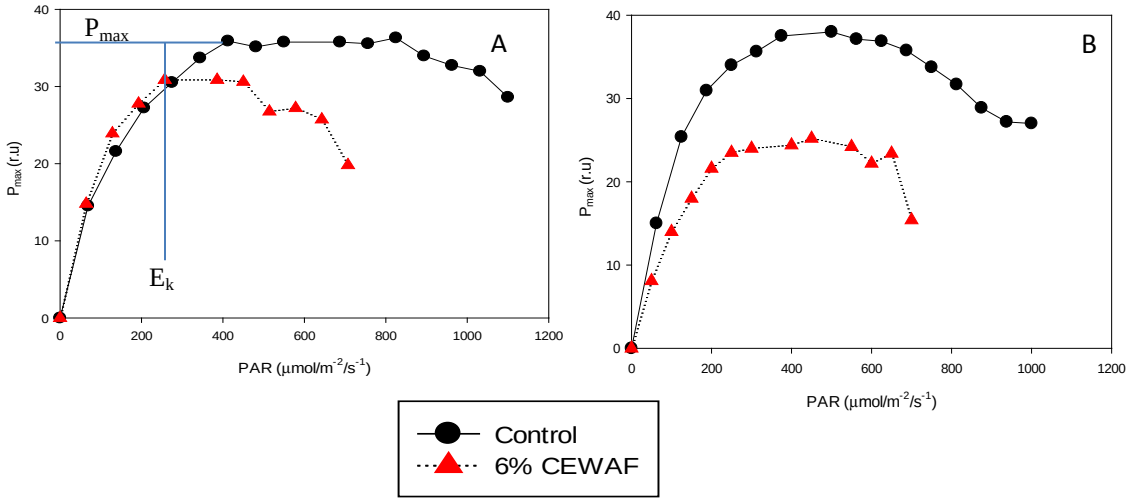

Fig. 4.14 Temporal evolution of the secondary photosynthetic reactions of *Symbiodinium spp.* grown under low growth irradiance static condition at 6% CEWAF The photosynthesis – irradiance curve represents P_{max} (maximum photosynthetic rates) and E_k (light saturation coefficient) on day 0 which was measured five minutes after dosing (a), and on day 4 (b). Within five minutes, the rate at which the dark reactions proceeded was more than half the rate at which the control dark reactions proceeded. This decline in the dark reaction rates did show signs of recovery by the conclusion of the experiment.

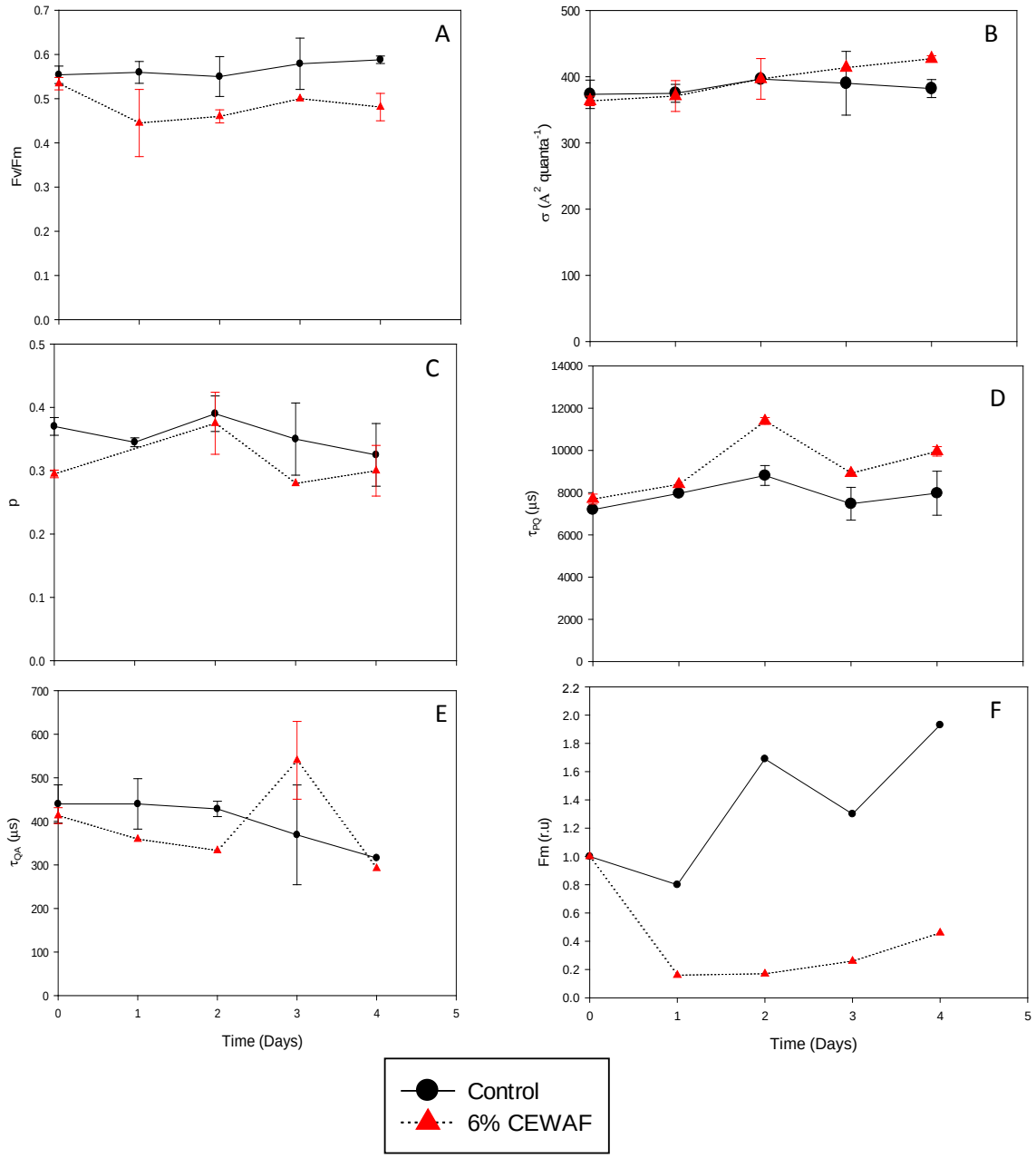

Fig. 4.15 Temporal evolution of the photosynthetic parameters at 6% CEWAF under high growth irradiance static condition. These parameters include: quantum yield of photochemistry – Fv/Fm (a), functional absorption cross-section – σ_{PSII} (b), connectivity factor – p (c), rate of electron transport between PSII and PSI – τ_{PQ} (d), rate of electron transport of PSII acceptor side – τ_{Qa} (e), and maximum fluorescence (f). The proxy for chlorophyll biomass (F_m) was normalized to the first day measurement to correct for factors other than those being tested in the experiment.

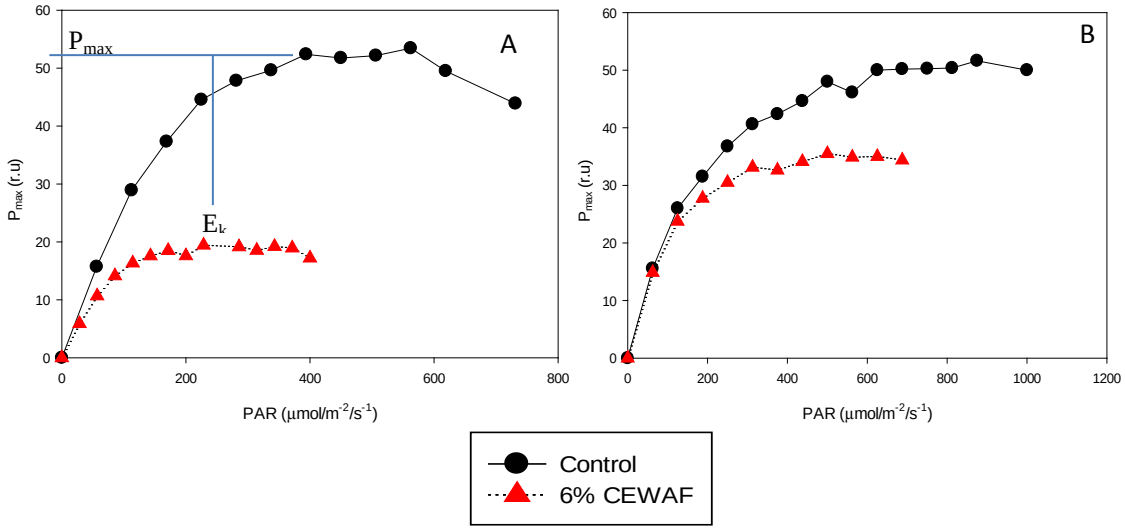

Fig. 4.16 Temporal evolution of the secondary photosynthetic reactions of *Symbiodinium spp.* grown at 6% CEWAF under high growth irradiance static condition. The photosynthesis – irradiance curve represents P_{max} (maximum photosynthetic rates) and E_k (light saturation coefficient) on day 0 which was measured five minutes after dosing (a), and on day 4 (b). The rate at which the dark reaction proceeded gradually declined as the experiment proceeded.

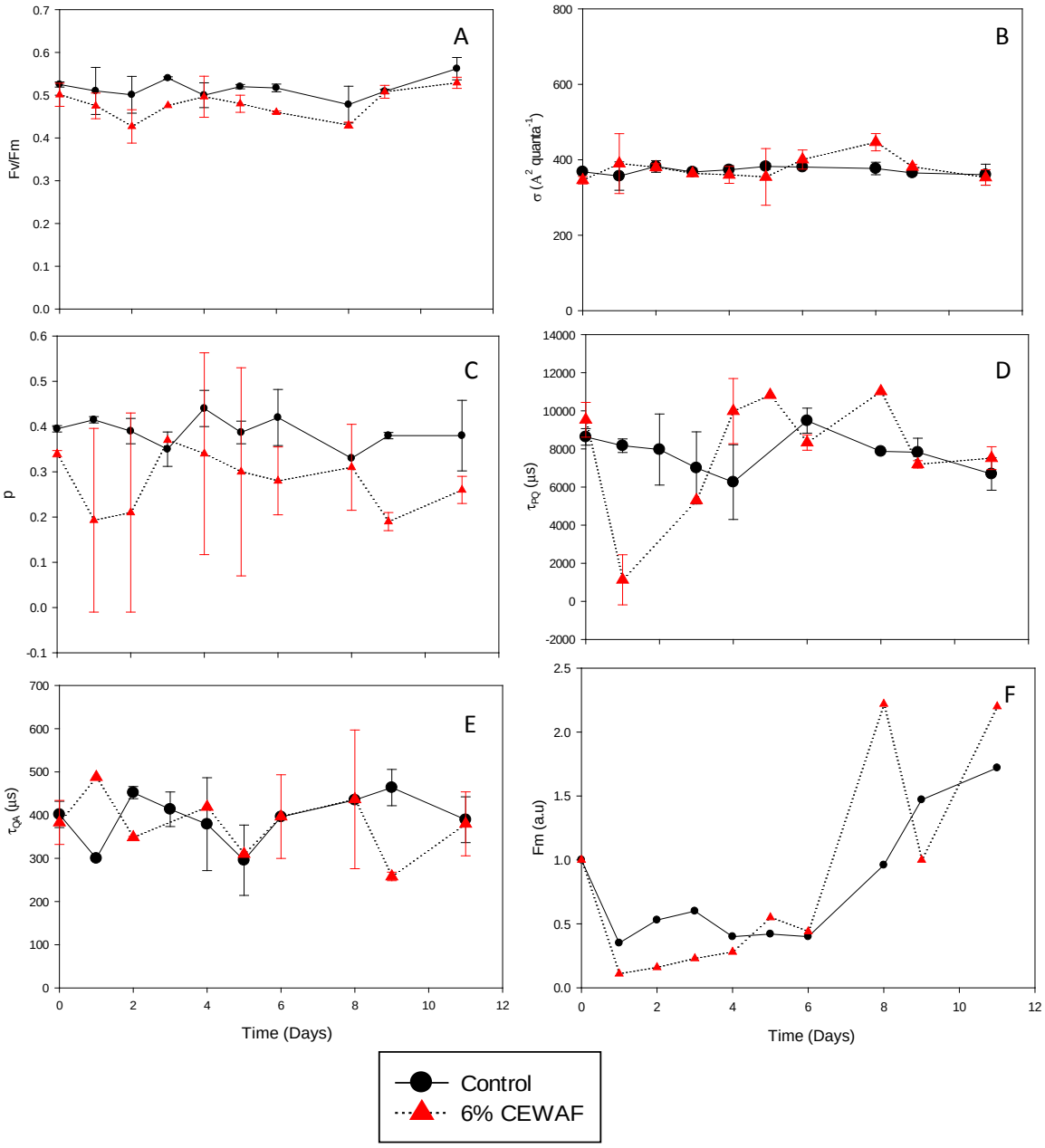

Fig. 4.17 Temporal evolution of the photosynthetic parameters at 6% CEWAF under low growth irradiance dilution condition. These parameters include: quantum yield of photochemistry – Fv/Fm (a), functional absorption cross-section – σ_{PSII} (b), connectivity factor – p (c), rate of electron transport between PSII and PSI – τ_{PQ} (d), rate of electron transport of PSII acceptor side – τ_{Qa} (e), and maximum fluorescence (f). The proxy for chlorophyll biomass (F_m) was normalized to the first day measurement to correct for factors other than those being tested in the experiment. Temporary effects to the energy transfer between PSII units and the re-oxidation of PQ was observed but did recover.

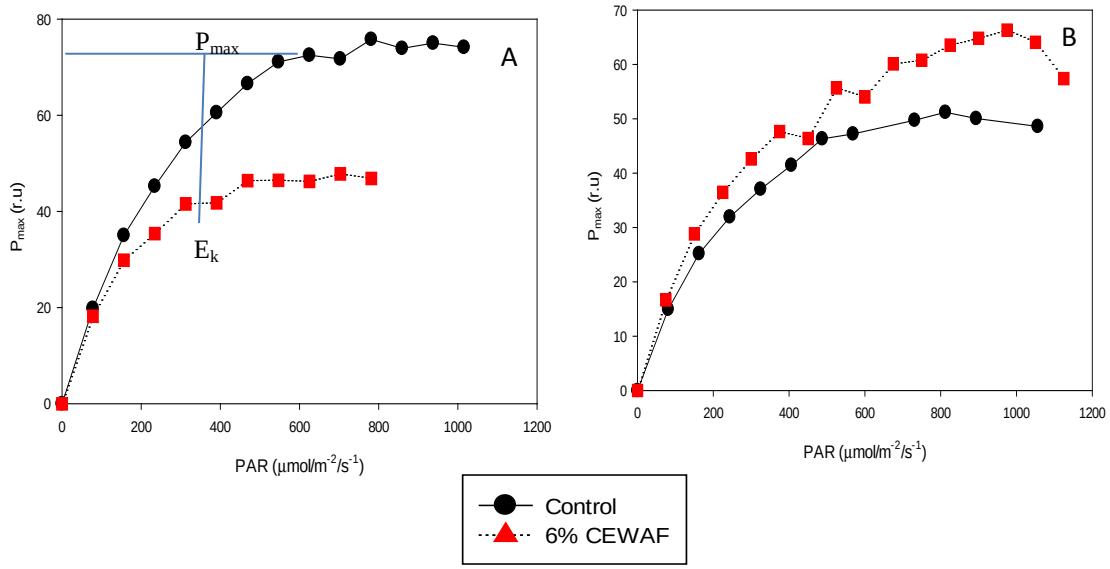

Fig. 4.18 Temporal evolution of the secondary photosynthetic reactions of *Symbiodinium spp.* grown at 6% CEWAF under low growth irradiance dilution condition. The photosynthesis – irradiance represents P_{max} (maximum photosynthetic rates) and E_k (light saturation coefficient) on day 0 which was measured five minutes after dosing (a), and on day 4 (b). Within five minutes of exposure to CEWAF, the rate at which the dark reactions proceed declined approximately 45%. However, the negative effect to the dark reaction rate recovered and exceeded the reaction rate of the control cultures.

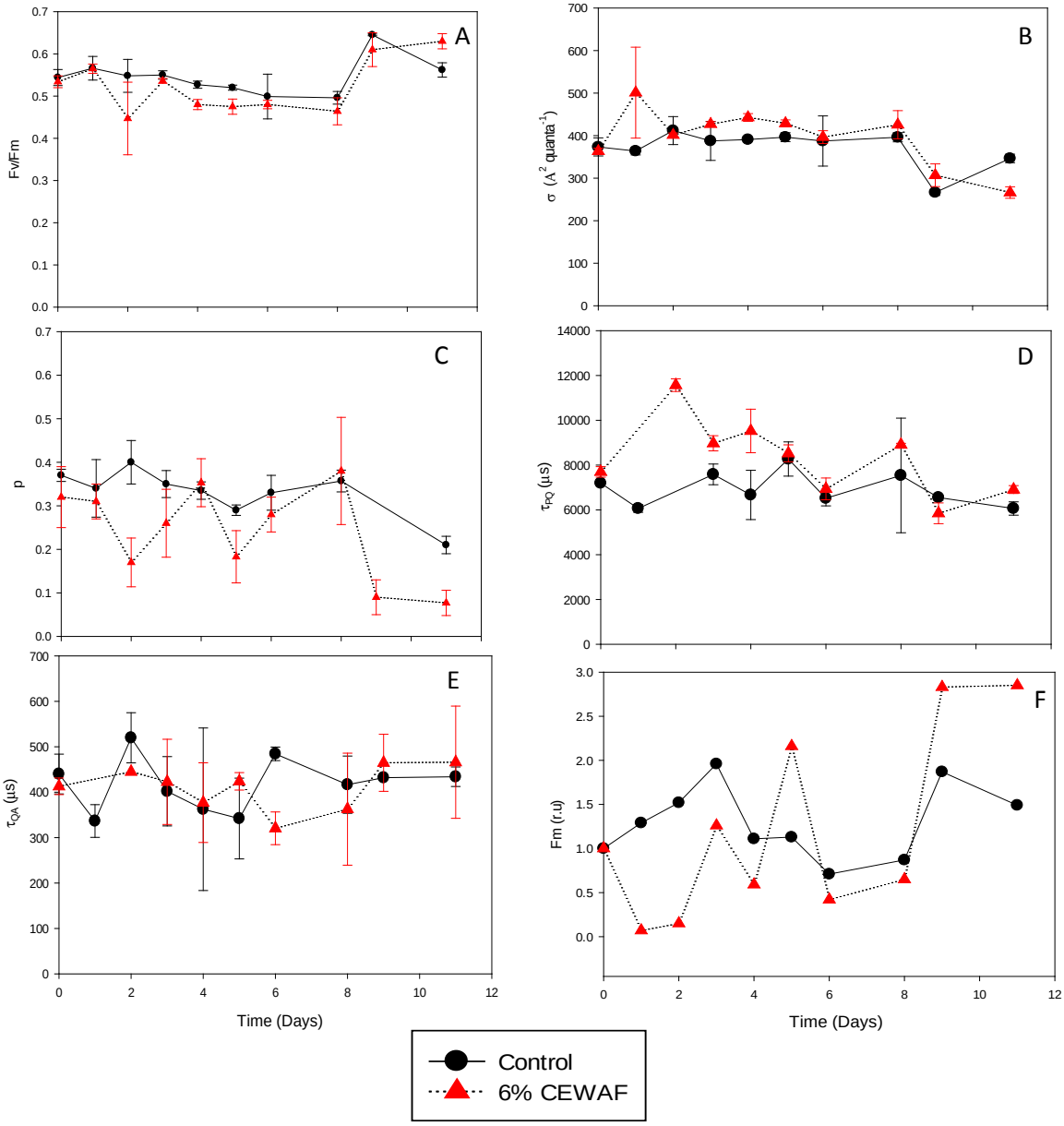

Fig. 4.19 Temporal evolution of the photosynthetic parameters at 6% CEWAF under high growth irradiance dilution condition. These parameters include: quantum yield of photochemistry – Fv/Fm (a), functional absorption cross-section – σ_{PSII} (b), connectivity factor – p (c), rate of electron transport between PSII and PSI – τ_{PQ} (d), rate of electron transport of PSII acceptor side – τ_{Qa} (e), maximum fluorescence (f). The proxy for chlorophyll biomass (F_m) was normalized to the first day measurement to remove sample to sample variability.

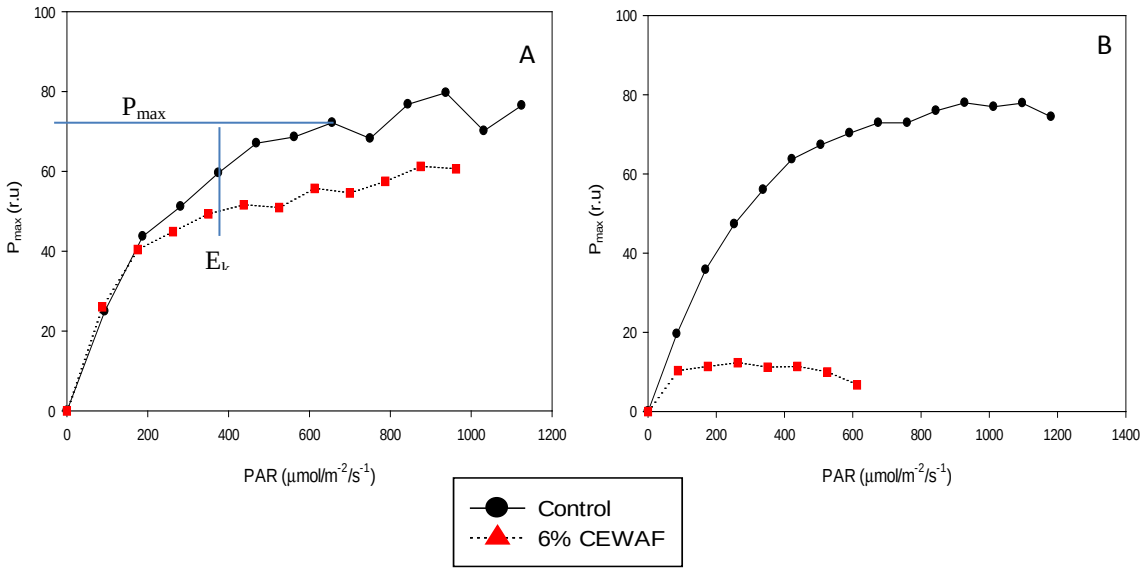

Fig. 4.20 Temporal evolution of the secondary photosynthetic reactions of *Symbiodinium spp.* grown at 6% CEWAF under high growth irradiance dilution condition. The photosynthesis – irradiance curve represents P_{max} (maximum photosynthetic rates) and E_k (light saturation coefficient) on day 0 which was measured five minutes after dosing (a), and on day 4 (b). The rate at which the dark reaction proceeded gradually declined as the exposure time increased.

Static Toxicity Test

CEWAF immediately impacted the energy transfer between PSII units followed by an impact to the cell population under low growth irradiance (Fig.4.13 D). The difference observed between the control and p resulted in a p-value less than 0.05. After the initial change in cell density, the cell population remained at that value for 72-hrs before growth occurred under low growth irradiance in CEWAF solution (Fig. 4.13 F). A slight difference in P_{max} was observed immediately after cultures were exposed to CEWAF under low growth irradiance (Fig. 4.14 A). As time progressed, there was a slow decline P_{max} and E_k in cultures exposed to CEWAF under low growth irradiance (Fig. 4.14 A&B).

CEWAF effected growth under high growth irradiance (4.15 F). The trend for growth was the same under both growth irradiances when cultures were exposed to CEWAF solution. An immediate impact under high growth irradiance was also observed on the P_{max} and E_k parameters when CEWAF solution was added to the cultures (Figs. 4.16 A&B). A slow recovery was noted in the P_{max} and E_k parameters of cultures with CEWAF under high irradiance.

Dilution Toxicity Test

Temporary effects to the re-oxidation of PQ and the energy transfer between PSII units occurred in cultures exposed to CEWAF under low growth irradiance (Fig. 4.18 D). Within 72-hrs of exposure to CEWAF, the effects to the energy transfer between PSII units and the re-oxidation of PQ were eliminated under low growth irradiance. Increasing the growth irradiance yielded negative changes in the growth rate and varying changes in the energy transfer between PSII units (Fig. 4.19 C&F). The remaining

primary photosynthetic parameters in cultures exposed to CEWAF under both irradiances did not show sustained effects during the experimental timeframe. An immediate effect was observed for P_{max} and E_k parameters in cultures exposed to CEWAF under low growth irradiance. But, P_{max} and E_k fully recovered by the end of the experiment under low growth irradiance (Fig. 4.18 A&B). This was different for the secondary photosynthetic reactions exposed to CEWAF under high growth irradiance. In this situation, P_{max} and E_k gradually declined over the course of the experiment (Figs. 4.20 A&B).

4.4.6 BENZENE

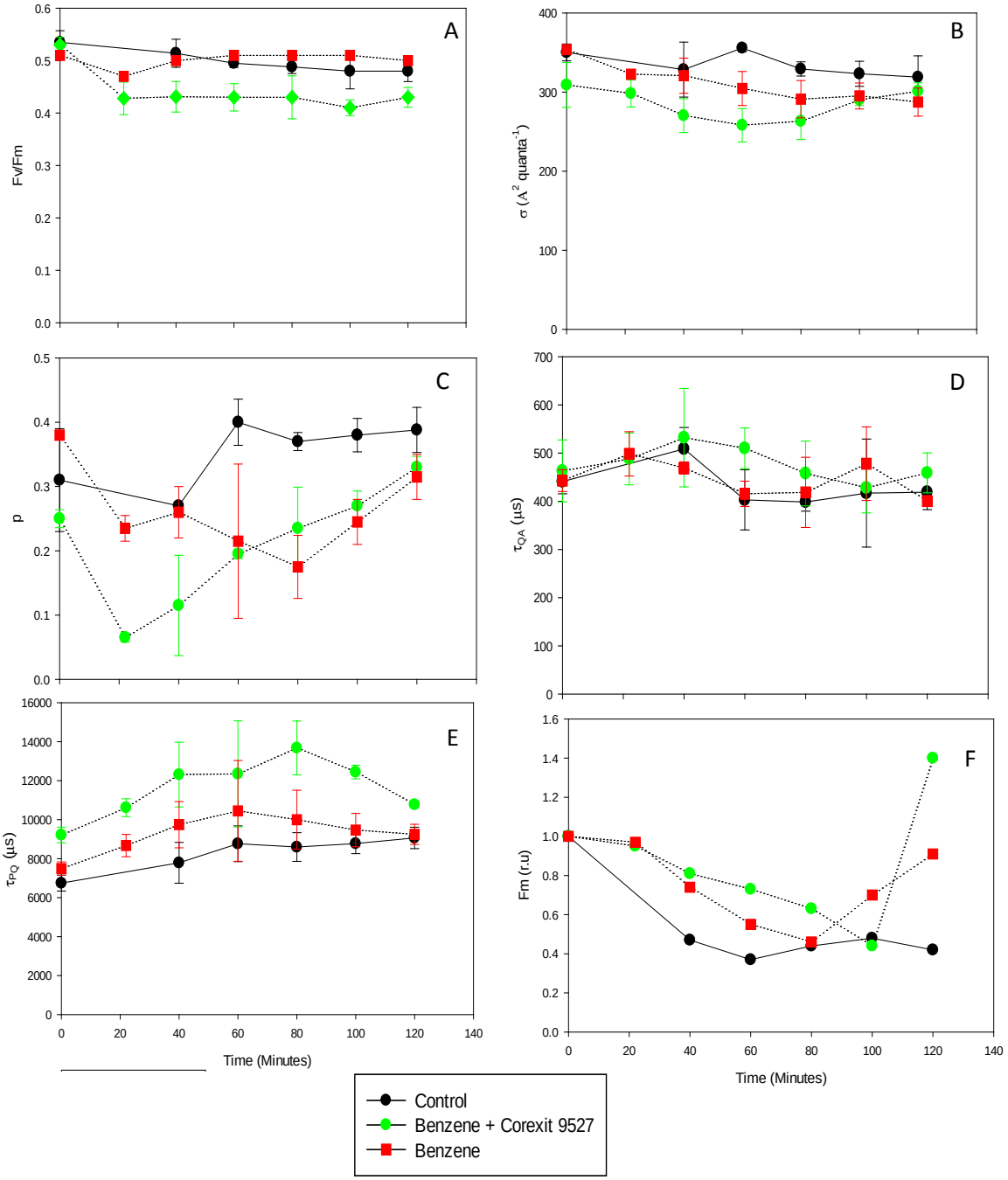

Fig. 4.21 Temporal evolution of the photosynthetic parameters at 19 mM benzene under high growth irradiance dilution condition. These parameters include: quantum yield of photochemistry – Fv/Fm (a), functional absorption cross-section – σ_{PSII} (b), connectivity factor – p (c), rate of electron transport on acceptor side– τ_{Qa} (d), rate of electron transport between PSII and PSI – τ_{PQ} (e), and maximum fluorescence (f). The proxy for chlorophyll biomass (F_m) was normalized to the first day measurement to remove sample to sample variability. The addition of Corexit 9527 enhanced the effects observed under benzene exposure.

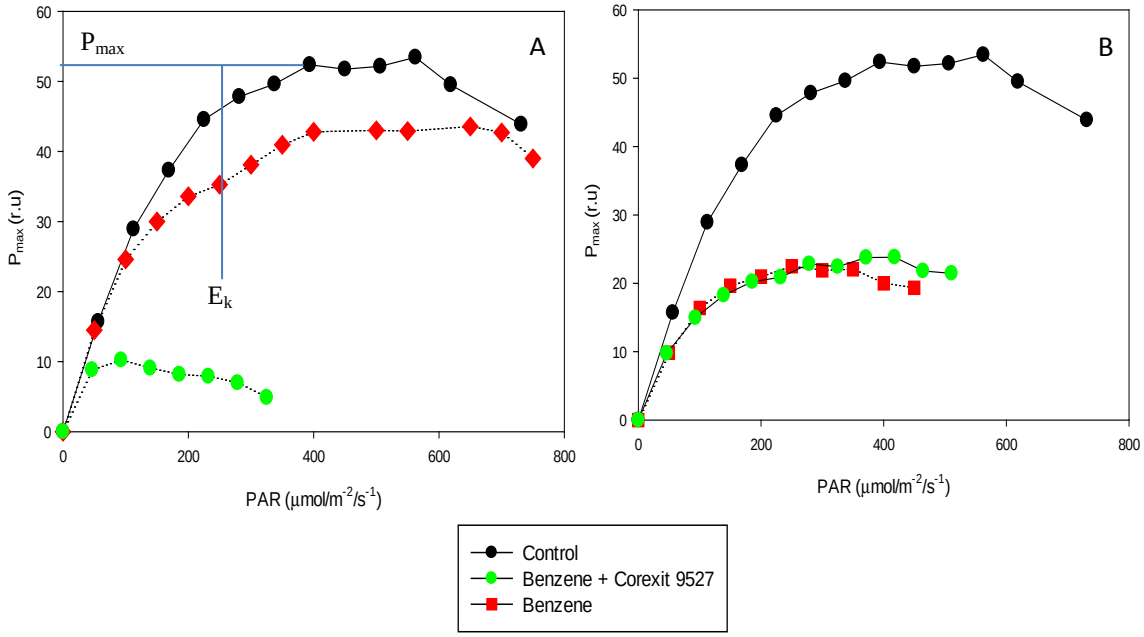

Fig. 4.22 Temporal evolution of the secondary photosynthetic reactions of *Symbiodinium spp.* grown at 19 mM benzene under high growth irradiance dilution condition. The photosynthesis – irradiance curve represents P_{max} (maximum photosynthetic rates) and E_k (light saturation coefficient) on day 0 which was measured five minutes after dosing (a), and on day 4 (b). The rate at which the dark reaction proceeded immediate declines but fully recovered in cells co-exposed with Corexit 9527.

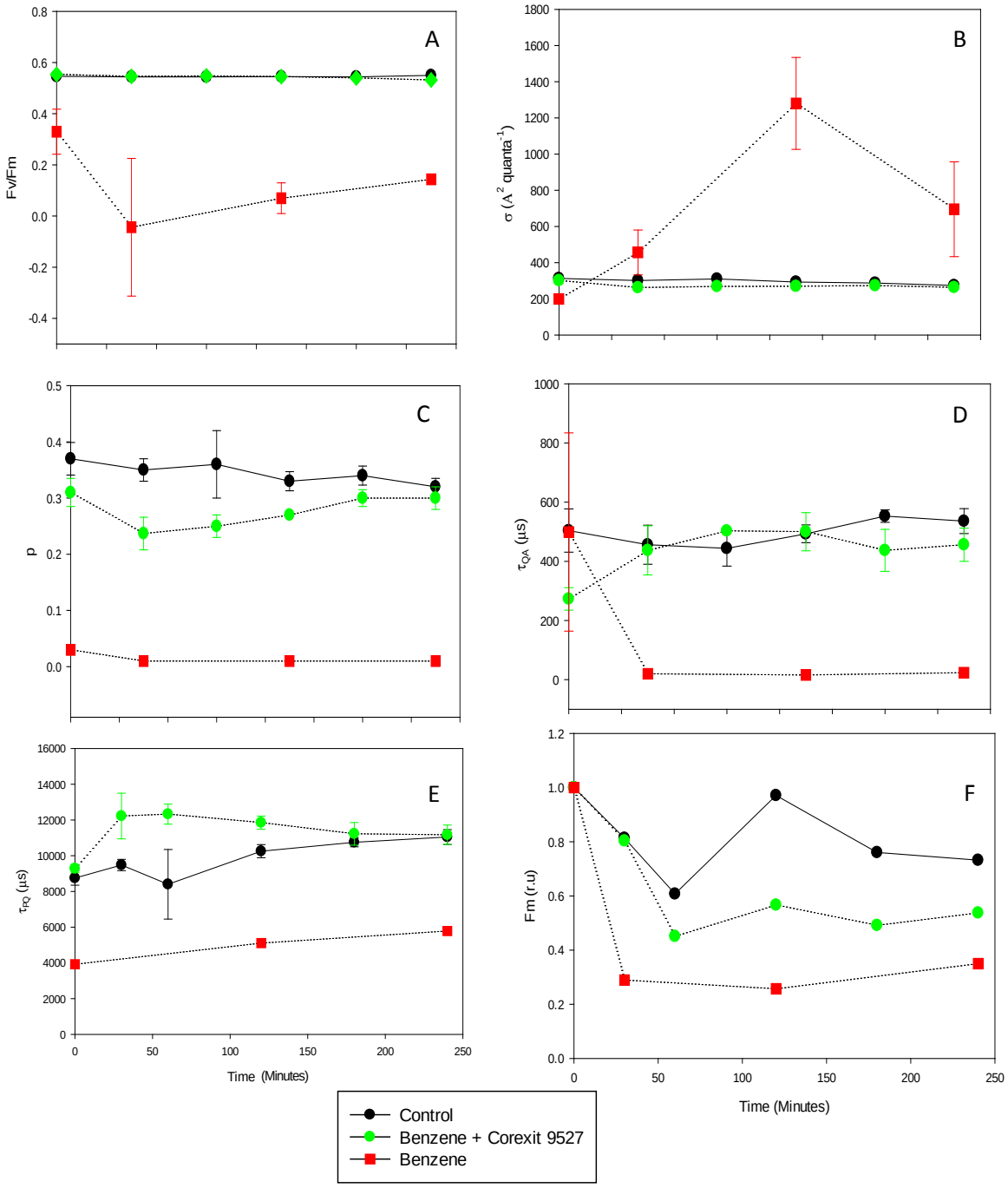

Fig. 4.23 Temporal evolution of the photosynthetic parameters at 19 mM benzene under low growth irradiance dilution condition. These parameters include: quantum yield of photochemistry – Fv/Fm (a), functional absorption cross-section – σ_{PSII} (b), connectivity factor – p (c), rate of electron transport on acceptor side– τ_{Qa} (d), rate of electron transport between PSII and PSI – τ_{PQ} (e), maximum fluorescence (f). The proxy for chlorophyll biomass (F_m) was normalized to the first day measurement to remove sample to sample variability. The effects to the photosynthetic apparatus were improved by the addition of Corexit 9527. Benzene alone stopped the energy transfer between PSII units and had a non-existent photochemical conversion process.

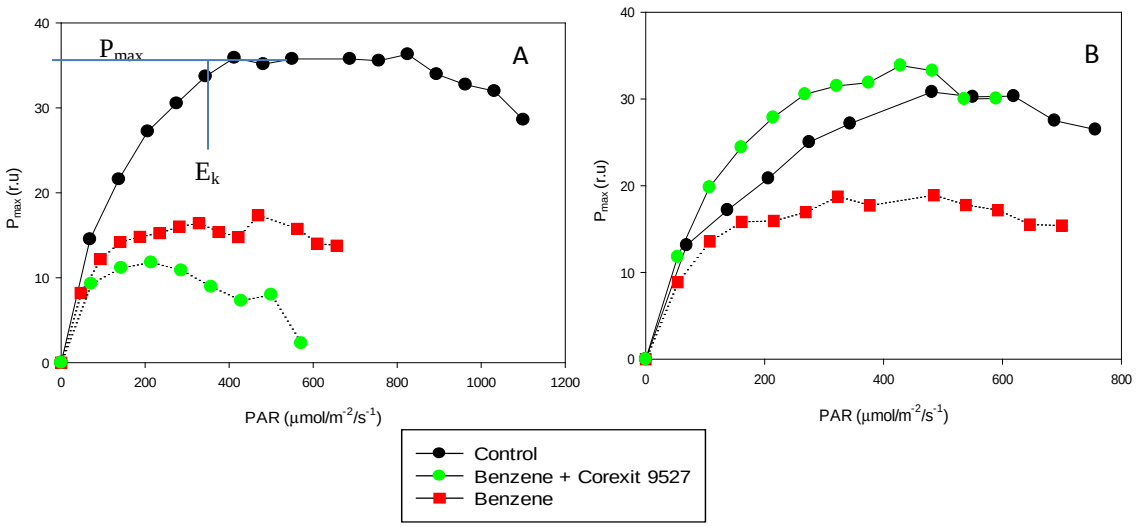

Fig. 4.24 Temporal evolution of the secondary photosynthetic reactions of *Symbiodinium spp.* grown at 19 mM benzene under low growth irradiance dilution condition. The photosynthesis – irradiance curve represents P_{max} (maximum photosynthetic rates) and E_k (light saturation coefficient) on day 0 which was measured five minutes after dosing (a), and on day 4 (b). The rate at which the dark reaction proceeded immediate declines and displays signs of adaptation in cells co-exposed with Corexit 9527. For cultures exposed to benzene alone, there is a gradual decline in P_{max} and E_k.

4.4.7 HEXANE

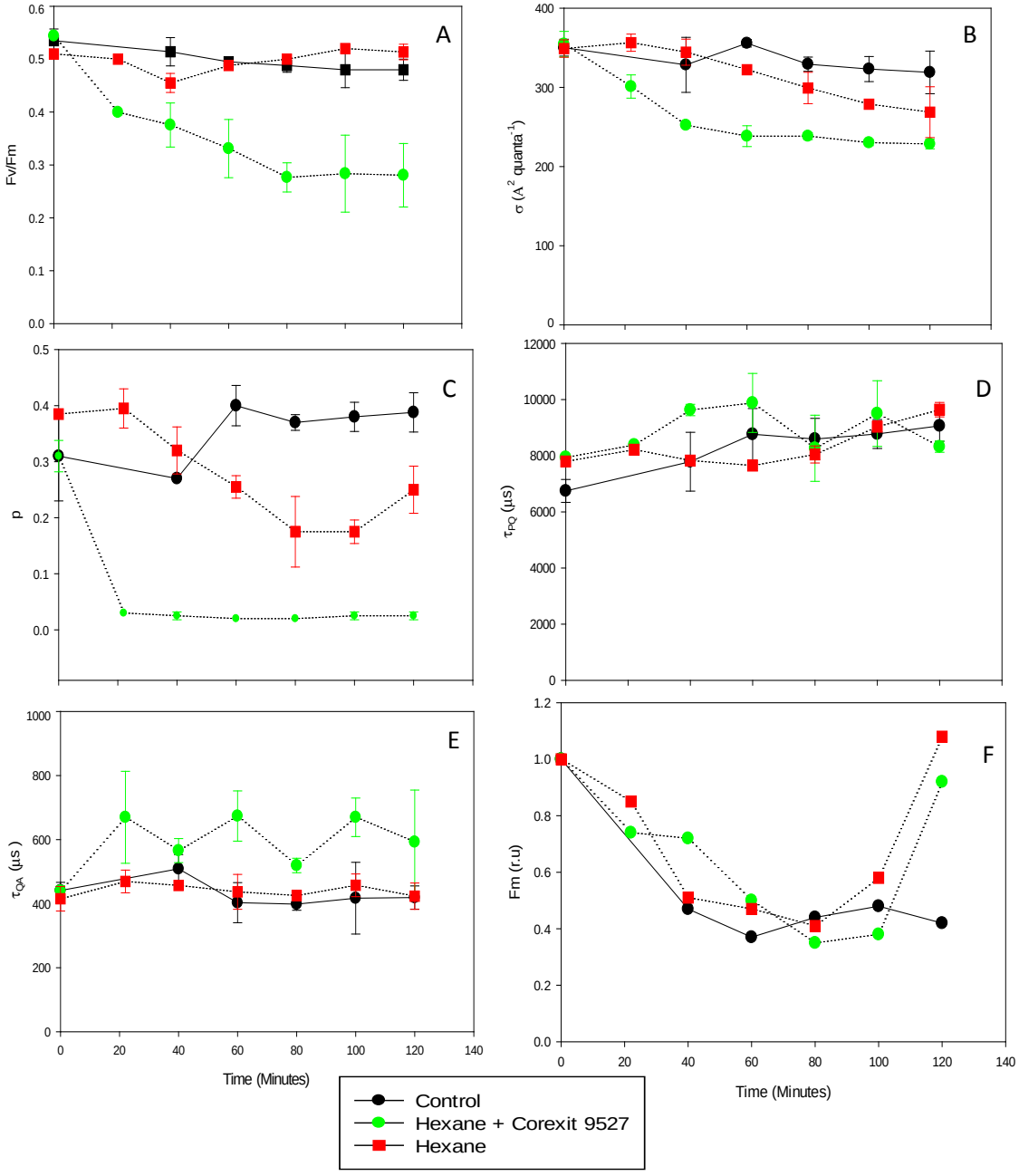

Fig. 4.25 Temporal evolution of the photosynthetic parameters at 66 mM hexane under high growth irradiance dilution condition. These parameters include: quantum yield of photochemistry – Fv/Fm (a), functional absorption cross-section – σ_{PSII} (b), connectivity factor – p (c), rate of electron transport on acceptor side– τ_{Qa} (d), rate of electron transport between PSII and PSI – τ_{PQ} (e), and maximum fluorescence (f). The proxy for chlorophyll biomass (F_m) was normalized to the first day measurement to remove sample to sample variability. A slow but steady decline was observed in cultures exposed to hexane and Corexit 9527. The energy transfer between PSII unit was nonexistent in cultures exposed to hexane and Corexit 9527. Exposure of hexane to the cultures for 90 minutes impaired the energy transfer between PSII units.

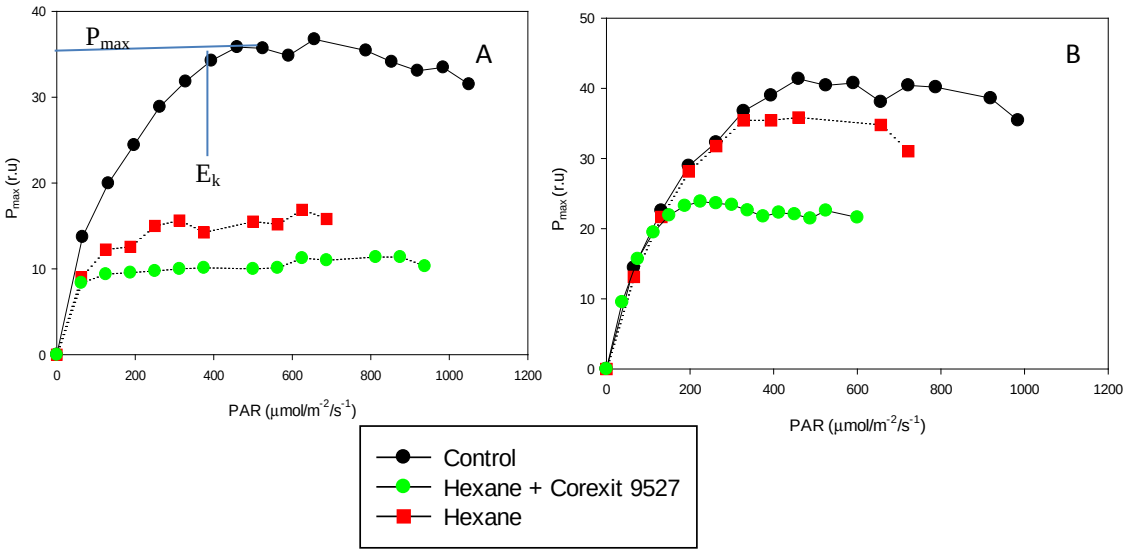

Fig. 4.26 Temporal evolution of the secondary photosynthetic reactions of *Symbiodinium spp.* grown at 66 mM hexane under high growth irradiance dilution condition. The photosynthesis – irradiance curve represents P_{max} (maximum photosynthetic rates) and E_k (light saturation coefficient) on day 0 which was measured five minutes after dosing (a), and on day 4 (b). The rate at which the dark reaction proceeded immediate declines but fully recovered in cells exposed to hexane alone and partially recovered when exposed to hexane and Corexit 9527.

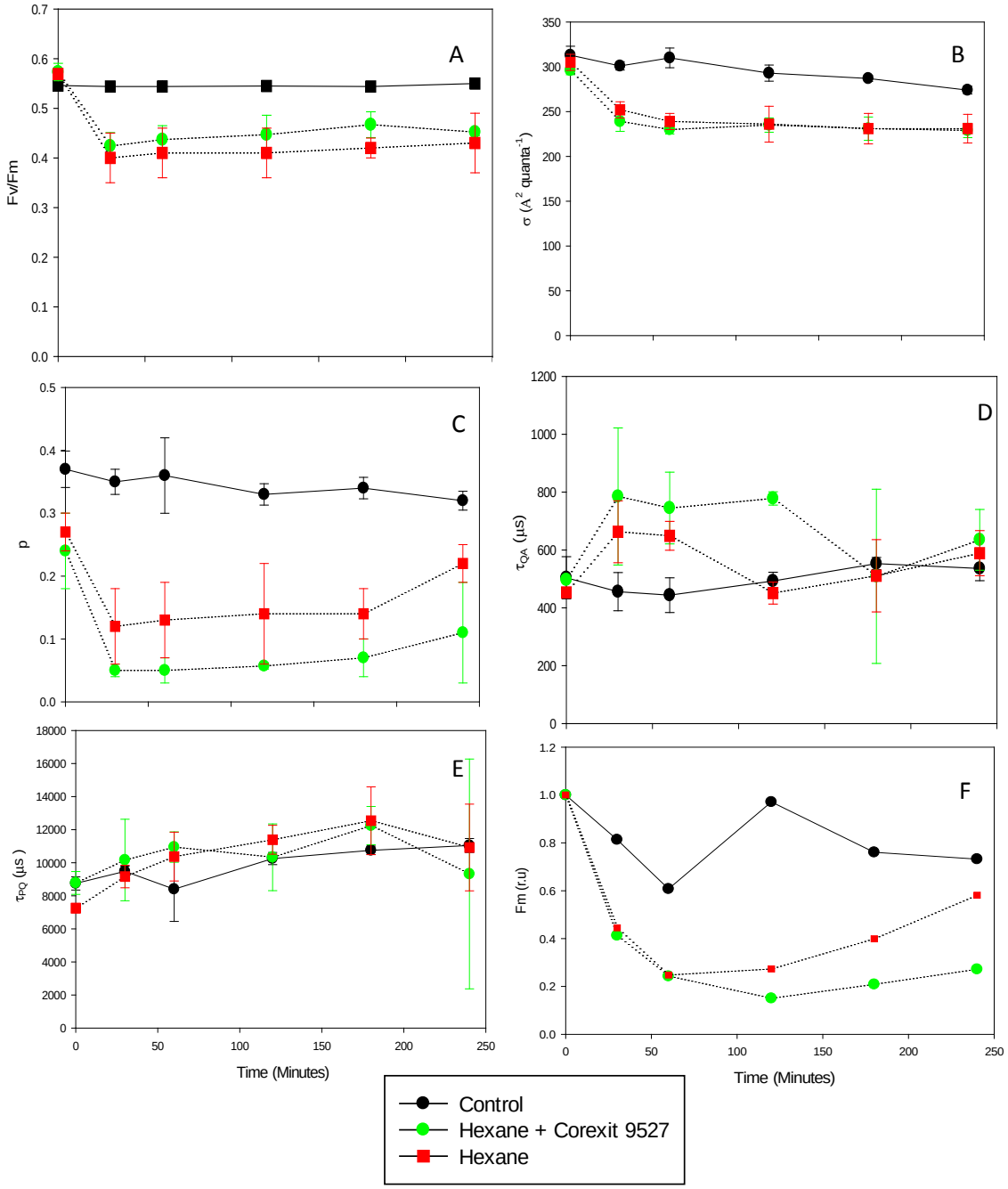

Fig. 4.27 Temporal evolution of the photosynthetic parameters at 66 mM hexane under low growth irradiance dilution condition. These parameters include: quantum yield of photochemistry – Fv/Fm (a), functional absorption cross-section – σ_{PSII} (b), connectivity factor – p (c), rate of electron transport on acceptor side– τ_{Qa} (d), rate of electron transport between PSII and PSI – τ_{PQ} (e), and maximum fluorescence (f). The proxy for chlorophyll biomass (F_m) was normalized to the first day measurement to remove sample to sample variability. Cultures exposed to hexane with and without Corexit 9527 had the same effect to the photosynthetic apparatus. Inhibitions to the growth rates and energy transfer between PSII units were the main effects. Indications of recovered was apparent in cultures exposed to hexane alone.

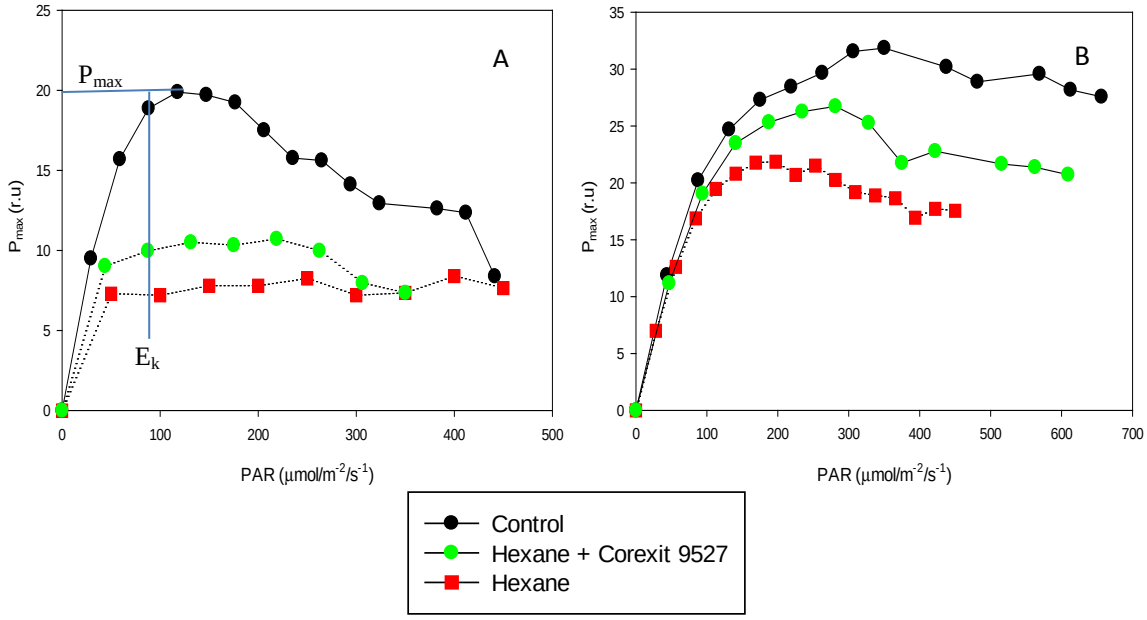

Fig. 4.28 Temporal evolution of the secondary photosynthetic reactions of *Symbiodinium spp.* grown at 66 mM hexane under low growth irradiance dilution condition. The photosynthesis – irradiance curve represents P_{max} (maximum photosynthetic rates) and E_k (light saturation coefficient) on day 0 which was measured five minutes after dosing (a), and on day 4 (b). The rate at which the dark reaction proceeded immediate declines but displayed signs of recovery by the conclusion of the experiment.

High growth irradiance

Because the effects of CEWAF and WAF may be driven by different hydrocarbon groups, we looked at two groups in an attempt to identify which group might better correlate to toxicity. Benzene alone induced a toxic response to the secondary photosynthetic reactions at this growth irradiance. Immediate effects to the secondary photosynthetic parameters were similar under high growth irradiances (Figs. 4.21). Additionally, the addition of corexit 9527 resulted in a change in the energy transfer between PSII units (Fig. 4.21 C). This change gradually recovered and was comparable to the control by the conclusion of the experiment. The response under high growth irradiance resulted in a constant decline the cell's ability to assimilate carbon (Fig. 4.21 F).

The initial impact induced by hexane alone exposure was to the secondary photosynthetic reactions (Fig. 4.25). As the experiment continued, a recovery was seen in Pmax and E_k. A temporary effect in the energy transfer between PSII was observed from 80-100 minutes after the initial exposure to hexane (Fig. 4.25 E). With regards to the primary photosynthetic reactions under exposure to Hexane with corexit 9500, Fv/Fm, the functional cross-section of PSII, and the energy transfer between PSII was observed. The energy transfer between PSII was non-existence throughout the study under hexane high growth irradiance (Fig. 4.25 C). A steady decline in the Fv/Fm was observed until it reached a value of 0.3 units where it maintained this value for the remainder of the study (Fig. 4.25 A).

Low growth irradiance

The effects seen under low growth irradiance was drastically different. Benzene alone affected every measured parameter. The energy transfer between PSII and the re-oxidation of PQ had immediate effects (Fig. 4.23 C). Whereas, the re-oxidation of Q_A, growth, and Fv/Fm maintained a value comparable to the control. Of the stress response observed, no recovery was seen except for the functional absorptive cross-section. The addition of corexit 9527 only changed the growth rate and secondary photosynthetic reactions. Growth retained the same growth rate from 24-hrs until the end of the experiment. The P_{max} and E_k observed at the initial measurement was the same measurement observed at the end of the experiment. When benzene was combined with corexit 9527, the immediate effect on the secondary photosynthetic reaction was also observed (Fig. 4.23). In contrast to benzene alone, the addition of corexit 9527 yielded a recovery of P_{max}.

For the primary photosynthetic reactions, hexane and hexane with corexit 9527 mirrored one another. Minor reductions in Fv/Fm, the functional absorptive cross-section, and the re-oxidation of Q_A were observed. A value around 0.4 for Fv/Fm and 250 A^2 $quanta^{-1}$ was maintained for the Fv/Fm and σ_{PSII} parameter respectively throughout the study. The energy transfer between PSII units operated at a 90% and 70% deficiency when compared to the control for hexane with corexit 9527 and hexane alone, respectively (Fig. 4.25 C). As with the primary photosynthetic reactions, the changes within the secondary photosynthetic reactions were identical for hexane and hexane with corexit 9527. An immediate was observed for P_{max} and E_k under both exposure conditions (Fig. 4.26). By the conclusion of the experiment, both experimental

conditions had begun to recover. Hexane with corexit 9527 had recovered more than hexane alone.

4.5 DISCUSSION

Petroleum is a complex mixture of various chemical compounds. My research revealed that petroleum poisoning was characterized by short-term (hrs) and long-term (dys) impairment to the photosynthetic apparatus. Short-term responses of hydrocarbons included alterations to the energy transfer between PSII units (p), growth rates (Fm), electron flow through the photosystem (τ_{PQ} and τ_{Qa}), functional absorptive cross-section ($\sigma_{PSII)}$, light saturation coefficient (E_k), maximum photosynthetic rate (P_{max}), and the photochemical efficiency of PSII (Fv/Fm) (Figs 4.21 – 4.28). Petroleum exposure resulted in rapid effects on the lipid membrane parameters (p and σ_{PSII}) followed by slower penetration into the photochemical complex. The toxicity of WAF to the primary photosynthetic processes was limited to the initial 48-hr period of exposure under low growth irradiance (Fig. 4.8).

Adding dispersant to WAF, benzene, and hexane caused higher concentrations of hydrocarbons to remain in the aqueous phase which was indicated by the enhanced effects on the photosynthetic apparatus (Figs 4.21 – 4.28). Marked differences between WAF and CEWAF were attributed to the dispersant toxicity. The response of the dispersant was similar to the effects observed in cultures exposed to CEWAF. The most notable effects caused by dispersant exposure were to the energy transfer between PSII units, Fv/Fm, and the functional cross-section of PSII (Figs. 4.6 & 4.7). The exacerbated response noted when Corexit 9527 was added to any culture yielded a response that was greater than a synergistic effect. This is comparable with previous research were the dispersed oil was more toxic. A 10-fold increase in toxicity in shrimp was seen when

WSF was chemically dispersed (Fisher and Foss, 1993). Dispersed crude oil accumulated in the thylakoid membrane (Howard et al., 1989 and Wolfe et al., 1998)).

The interaction of the toxicant with the thylakoid membrane (p and σ_{PSII}) occurred when WAF was chemically dispersed or when cultures were exposed to Corexit 9527 alone. In addition to providing hydrocarbons access through the cellular membrane, dispersed oil or dispersant repressed cell division. Higher growth rates under high growth irradiance might reflect a decline in toxicity due to the volatilization of components within crude oil. The response of the photosynthetic apparatus to increased bioavailable hexane was to stop the energy transfer between PSII units. This response was lethal indicating that the concentration of hexane within the water column exceeded the acute toxicity threshold for that parameter. But, the addition of Corexit 9527 to benzene displayed responses that were sublethal and at the toxicity threshold. While dispersants exaggerated the effects of WAF, CEWAF exposed cultures exhibited adaptability to reactions of the primary photosynthetic process within 48-hr of exposure. This adaptation was not observed for CEWAF secondary photosynthetic processes under high growth irradiance. CEWAF experienced a recovery in all stressed parameters; whereas, WAF only displayed recovery in Fv/Fm. The effect on Fv/Fm could result from a direct interaction of petroleum compounds.

In terms of the mode of toxicity, light intensity is a factor that influences the mechanism of action. Under low growth irradiance, there appears to be a co-inhibition of the secondary and primary photosynthetic reactions. Higher growth irradiance affected the secondary photosynthetic reactions immediately. No significant treatment effects

were observed on P_{max} using the seagrass Halophila ovalis, which highlights the difference between primary producers (Durako et al., 1993).

The maximum rate of dark reaction is reflected in the rate measured under continuous light. Its slope determines the light capturing efficiency. Prior to light saturation, the P-I cure is light limited and photochemical quenching dominates. The information here within explains the differences observed between cells grown under high irradiance versus low irradiance. Cells grown under high irradiance were indicated by a low slope while cells grown under low irradiance had high slope. These observations were also noted in the results by Rosenqvist et al. (2001), and Cruz and Serodio (2008). The differences are due to the development of the chloroplast under that light irradiance. The development of the chloroplast under high irradiance is characterized by low amounts of thylakoids per chloroplast section, low stacking degree, more exposed chloroplast membranes, and higher rates of net CO_2 assimilation (Alves et al., 2002: Lichtenthaler and Burkart, 1999; Ritz et al., 2000). Thus, the slope was lower for high irradiance adapted cells since the light harvesting capacity was reduced.

During the initial days of an oil spill, it would appear that the light cycle through each day would promote efficiency in either photochemical process or carbon fixation. The light source in this study did not include ultraviolet radiation. It has been shown that PAH within WAF undergo photomodification or photosensization (Ren et al., 1994; Boese et al., 1997; Arfsten, 1996; Pelletier et al., 1997). Thus, the effects observed in this study would underestimate the true impact in the field. While WAF was prepared as prescribed in the literature, it is unlikely that oil spills would come to equilibrium prior to eliciting toxic effect as the WAF did in this experiment.

4.6 CONCLUSION

Results in this study highlighted how benzene, hexane, the water soluble fraction of crude oil (WAF), and chemically enhanced water accommodated fraction (CEWAF) of crude oil target the primary and secondary photosynthetic reactions of the symbiotic marine alga *Symbiodinium spp.*. Effects observed when cells were exposed to hexane or hexane with corexit had the same trend under low growth irradiance. With the addition of corexit to hexane cultures, Fv/Fm and σ_{PSII} were negatively impacted along with the secondary photosynthetic parameters under low growth irradiance. Whereas, Fv/Fm and σ_{PSII} were not impacted under hexane grown under high growth irradiance. The broadest impact was to benzene under low growth irradiance. This impact was lessened with the addition of corexit resulting in inhibition to P_{max} and E_k only. Under higher growth irradiance, the addition of benzene or benzene with corexit resulted in the same trend.

When WAF was diluted, no effects to any primary photosynthetic reaction were observed. However under static conditions, the secondary photosynthetic reactions were observed under both growth irradiances. Only high growth conditions displayed an impact to the connectivity parameter. The addition of corexit to WAF did not lessen the impact to the parameters affected when cultures were exposed to WAF alone. Under low growth irradiance connectivity, P_{max} and E_k were common parameters affected when CEWAF was test in static or dilution conditions.

The ability of *Symbiodinum spp.* secondary photosynthetic reactions to recover after exposure to hexane, benzene, and CEWAF suggests a reversible inhibition or a different mechanism of action related to growth irradiance. The secondary photosynthetic reactions recovered under either growth irradiance when exposed to

hexane or hexane with corexit. The addition of corexit to cultures exposed to hexane did not lessen the effects when cultures were exposed to hexane alone. With the addition of Corexit 9527 to cultures exposed to benzene and high growth irradiance, the secondary photosynthetic reactions recovered. The growth irradiance which was conducive for recovery under CEWAF exposure was the low growth irradiance.

The influence of Corexit was limited to observances on the primary photosynthetic reactions. Under both light irradiances, Fv/Fm, the connectivity, and σ_{PSII} were affected. The order in which each parameter was affected differed. The connectivity was the primary target under high growth irradiance. While, Fv/Fm was the primary target under high growth irradiance.

The table below re-constructs the sequence of events in order of which parameters diverged from the control.

	Corexit	WAF Static	CEWAF Static	Hexane	Hexane + Corexit	Benzene	Benzene + Corexit
Fv/Fm	3^{rd}				3^{rd} +		3^{rd} +
σ_{PSII}	2^{nd} +++				3^{rd} +		3^{rd} +++
p	1^{st} +++	2^{nd}	2^{nd} +	2^{nd}	2^{nd}	2^{nd} +	2^{nd} ++
τ_{QA}							
τ_{PQ}						2^{nd}	2^{nd} +++
Growth rate	2^{nd}						
P_{max}		1^{st}	1^{st}	1^{st}	1^{st}	1^{st}	1^{st}
E_k		1^{st}	1^{st}	1^{st}	1^{st}	1^{st}	1^{st}

Table 4.3 Divergence timeline for each measure physiological parameters under high growth irradiance. No sustained effects were observed under declined experiments at this growth irradiance. The statistical significance is notated at + marks. + indicates a $p < 0.05$, ++ is a $p < 0.01$, and +++ is a $p < 0.001$. P-values greater than 0.05 are not reported.

	Corexit	CEWAF Static	CEWAF Decline	Hexane	Hexane + Corexit	Benzene	Benzene + Corexit
Fv/Fm	1st +	3rd +	2nd ++			2nd	3rd ++
σ_{PSII}	3rd +++				3rd +	3rd	
p	2nd +	1st ++	3rd +++	2nd +++	2nd ++	1st +++	1st +++
τ_{QA}				3rd	3rd +	2nd	
τ_{PQ}	3rd +					1st +++	1st ++
Growth rate		2nd				2nd	2nd
P_{max}		1st	1st	1st	1st	1st	1st
E_k		1st	1st	1st	1st	1st	1st

Table 4.4 Divergence timeline for each measure physiological parameters under low growth irradiance. No sustained effects were observed under WAF at this growth irradiance. The statistical significance is notated at + marks. + indicates a $p < 0.05$, ++ is a $p < 0.01$, and +++ is a $p < 0.001$. P-values greater than 0.05 are not reported.

5.0 FUTURE WORKS

Molecular applications in ecotoxicology have seen major advances. Approaches such as proteomics can improve our understanding of recovery mechanisms employed by cells and change the outlook to environmental remediation. This study provided information on how environmental conditions influenced the recovery of the photosynthetic reactions when cells were exposed to WAF and CEWAF. By understanding the signaling pathway, we can see if the environmental conditions could be manipulated to promote recovery. Additionally, the issue of the photosynthetic response when WAF and CEWAF are combined under elevated CO_2 and temperature would provide useful information on which dispersant can be used where and possibly spark the interest in developing another generation of dispersants.

Shifting from the molecular techniques, basic scientific questions still revolve around metal toxicity. Other factors such as nutrient limitation and their effects on the toxicity of heavy metals are poorly understood. Two studies should be completed. The first study should re-examine Pb in tandem with phosphorus limited culture. The second study should monitor the Rubisco level fluctuations over diurnal cycles.

REFERENCE

Afkar, E., Ababna, H., and Fathi, A. 2010. Toxicological response of the green alga *Chlorella vulgaris* to some heavy metals. Am J Environ Sci 6: 230-237

Alves, P., Magalhães, A., and Barja, P. 2002. The phenomenon of photoinhibition of photosynthesis and its importance in reforestation. Botanical Rev 68: 193-208

Anderson, D., and Morel, F. 1978. Copper sensitivity of *Gonyaulax tamarensis*. Limno Oceanogr 23: 283-295

Anderson, J., and Andersson, B. 1988. The dynamic photosynthetic membrane and regulation of solar energy conversions. Trends Biochem Sci 13: 351-355

Anderson, J., Chow, W., and Goodchild, D. 1988. Thylakoid membrane organization in sun/shade acclimation. Aust J Plant Physiol 15: 11-26

Anderson, J., Goodchild, D., and Boardman, N. 1973. Composition of the photosystem and chloroplast structure in extreme shade plants. Biochim Biophys Acta 325: 573-585

Anderson, J., Neff, J., Cox, B., Tatem, H., and Hightower, G. 1974. Characteristics of dispersions and water-soluble extracts of crude and refined oils and their toxicity to estuarine crustaceans and fish. Marine Biol 27: 75-88

Arellano, J., Lazaro, J., Lopez-Gorge, J., and Baron, M. 1995. The donor side of PSII as the Cu-inhibitory binding site. Photosynth Res 45: 127-134

Arfsten, D., Schaeffer, D., and Mulveny, D. 1996. The effects of near ultraviolet radiation on the toxic effects of polycyclic aromatic hydrocarbons in animals and plants: A review. Ecotoxicol Environ Saf 33: 1-24

Babin, M., Morel, A., Claustre, H., Bricaud, C., Kolber, Z., and Falkowski, P. 1996. Nitrogen and irradiance-dependent variations of the maximum quantum yield of carbon fixation in eutrophic, mesotrophic, and oligotrophic marine systems. Deep- Sea Res. 43: 1241-1272

Babu, T., Marder, J., Tripuranthakam, S., Dixon, D., and Greenberg, B. 2001. Synergistic effects of a photooxidized polycyclic aromatic hydrocarbon and copper on photosynthesis and plant growth: evidence that in vivo formation of reactive oxygen species is a mechanism of copper toxicity. Environ Toxicol Chem 20: 1351-1358

Barber, J., and Andersson, B. 1992. Too much of a good thing: light can be bad for photosynthesis. Trends Biochm Sci 17: 61-66

Bately, G. “The distribution and fate of tributyltin in the marine environment” *Tributyltin: a Case Study of an Environmental Contaminant* Ed. De Mora, S.J., 1996. Print

Baumann, H., Morrison, L., and Stengel, D. 2009. Metal accumulation and toxicity measured by PAM—Chlorophyll fluorescence in seven species of marine macroalgae. Ecotox Env Saf 72:1063-1075

Behrenfeld, M.J., Prasil, O., Kolber, Z., Babin, M., and Falkowski, P. 1998. Compensatory changes in Photosystem II electron turnover rates protect photosynthesis from photoinhibition. Photosynth Res 58:259-268

Boardman, N. 1977. Comparative photosynthesis of sun and shade plants. Annu Rev Plant Physiol 28: 355-377

Boese, B., Lamberson, J., Swartz, R., and Ozretich, R. 1997. Photoinduced toxicity of fluoranthene to seven marine benthic crustaceans. Arch Environ Contam Toxicol 32: 389-393

Bonnet, M., Camares, O., and Veisseire, P. 2000. Effects of zinc and influence of *Acremonium lolii* on growth parameters, chlorophyll a fluorescence and antioxidant enzyme activities of ryegrass (*Lolium perenne* L. cv Apollo). J Exp Bot 51: 945-953

Borkow, G., and Gabbay, J. 2005. Copper as a biocidal tool. Curr Med Chem 12: 2163-2175

Branquinho, C., Brown, D., Máguas, C., and Catarino, F. 1997. Lead (Pb) uptake and its effects on membrane integrity and chlorophyll fluorescence in different lichen species. Environ Experi Bot 37:95-105

Bruland, K., and Lohan, M. “The control of trace metals in seawater.” *The Oceans and Marine Geochemistry*. Ed. Harry Elderfield, H.D. Holland, and K.K. Turekian, 2004. Print

Burda, K., Kruk, J., Radunz, A., Schmid, G., and Strzalka, K. 2002. Stimulation and inhibition of oxygen evolution in photosystem II by copper (II) ions. Z Naturforsch 57c: 853-857

Burzynski, M. 1987. The influence of lead and cadmium on the absorption and distribution of potassium, calcium, magnesium and iron in cucumber seedlings. Acta Physiol Plant 9: 229-238

Canevari, G. 1978. Some observations on the mechanism and chemistry aspects of chemical dispersion. L. McCarthy, G. Lindblom, H. Walter (Eds.), Chemical Dispersants for the Control of Oil Spills, Am. Soc. Testing and Materials, Philadelphia (1978), pp. 2–5

Caspi, V., Droppa, M., Horvath, G., Malkin, S., Marder, J., and Raskin, V. 1999. The effect of copper on chlorophyll organization during greening of barley leaves. Photosynth Res 62: 165-174

Cedeno-Maldonado, A., and Swader, J. 1972. The cupric ion as an inhibitor of photosynthetic electron transport in isolated chloroplasts. Plant Physiol 50: 698-701

Chakrabarty, A. 1985. Genetically-manipulated microorganisms and their products in the oil service industries. Trends Biotech 3: 32-38

Chaloub, R., de Magalhaes, C., and Dos Santos, C. 2005. Early toxic effects of zinc on PSII of *Synechocystis Aquatilis* F. Aquatilis (Cyaophycae). J Phycol 41: 1162-1168

Chauoi, A., Mazhousi, S., Ghorbal, M., and Elferjani, E. 1997. Cadmium and zinc induction of lipid peroxidation an defects on antioxidant enzyme activities in bean (*Phaseolus vulgaris* L.). Plant Sci 127: 139-147

Chettri, M., Cook, C., Vardaka, E., Sawidis, R., and Lanaras, T. 1998. The effect of Cu, Zn, and Pb on the chlorophyll content of the lichens Cladonia convolute and Cladonia rangiformis. Environ Exp Bot 39: 1-10

Cho, H., Mancino, L., and Blankenship, R. 1984. Light saturation curves and quantum yields in reaction centers from photosynthetic bacteria. Biophys J 45: 455-461

Chu, Z., and Anderson, J. 1984. Modulations of the light-harvesting assemblies of a shade plant, *Alocasia macrorrhiza*. Photobiochem Photobiophys 8: 1-10

Clark, J., Bragin, G., Febbo, E., and Letinski, D. Toxicity of physically and chemically dispersed oils under continuous and environmentally realistic exposure conditions: applicability to dispersant use decisions in spill response planning. American Petroleum Institute (Ed.) Proceedings, 2001 International Oil Spill Conference pp. 1249-1255

Clendenning, K. 1959. The effects of waste discharge on kelp: fuel oil. Univ of CA Inst. Mar Res 59: 4-12

Clijsters H., and van Assche, F. 1985. Inhibition of photosynthesis by heavy metals. Photosynth Res 7: 31-40

Cohen, I., Knopf, J., Irihimovitch, V., and Shapira, M. 2005. A proposed mechanism for the inhibitory effcts of oxidative stress on Rubisco assembly and its subunit expression. Plant Physiol 137: 738-746

Cook, C. and Knap, A. 1983. Effects of crude oil and chemical dispersant on photosynthesis in the brain coral *Diploria strigosa*. Mar Biol 78: 21-27

Committee on Effectiveness of Oil Spill Dispersants, Marine Board, National Research Council. *Using Oil Spill Dispersants on the Sea*. Washington, D.C.: National Academy Press, 1989. Print

Couillard, C., Lee, K., Legare, B., and King, T. 2005. Effect of dispersant on the composition of the water-accommodated fraction of crude oil and its toxicity to larval marine fish. Environ Toxicol Chem 24: 1496-1504

Cruz, S., and Serodio, J. 2008. Relationship of rapid light curves of variable fluorescence to photoacclimation and non-photochemical quenching in a benthic diatom. Aquat Bot 88: 256-264

Drazkiewicz, M. 1994. Chlorophyll-occurrence, functions, mechanism of action, effects of internal and external factors. Photosynthetica 30: 321-331

Droppa, M., Terry, N., and Horvath, G. 1984.Variation in photosynthetic pigments and plastoquinone contents in sugar beet chloroplasts with changes in leaf copper content. Plant Physiol 74: 717-720

Durako, M., Kenworthy, W., Fatemy, S., Valavi ,H., and Thayer, G. 1993. Assessment of the toxicity of Kuwait crude oil on the photosynthesis and respiration of seagrasses of the Northern Gulf. Mar Pollut Bull 27: 223–227

Duval, W., Harwood, L., and Fink, R. 1982. The sublethal effects of dispersed oil on an estuarine isopod. Technology Development Report, EPS-4-EC-82-1. Environment Canada

Duxbury, C., Dixon, D., and Greenberg, B. 1997. Effects of simulated solar radiation on thebioaccumulation of polycyclic aromatic hydrocarbons by the duckweed *Lemna gibba*. Environ Toxicol Chem 16: 1739-1748

Eckardt, N., and Pell, E. 1995. Oxidative modification of Rubisco from potato foliage in response to ozone. Plant Physiol Biochem 33: 273–282

Environment Canada. Environmental Protection Series Guidance Document on Control of Toxicity Test Precision Using Reference Toxicants Report EPS 1/RM/12. Environment Canada, 1990.

Environment Canada. Laboratory aquatic toxicity data for Corexit 9500. File 4808-13-1. Environment Canada, 1994

Environmental Protection Agency, Office of inspector general. revision needed to national contengency plan based on deepwater horizon oil spill. Report No. 11-P-0534, 2011. Print

Epstein, N., Bak, R., and Rinkevich, B. 2000. Toxicity of third generation dispersants and dispersed egyptian crude oil on Red Sea coral larvae. Mar Poll Bull 40: 497-503

Eruslanov, E., and Kusmartsev, S. "Identification of ROS using oxidized DCFDA and flow-cytometry". *Advanced Protocols in Oxidative Stress II, Methods in Molecular Biology.* Vol. 594. New York: Humana Press, 2010. Print.

Falkowski, P., and Kolber, Z. 1995. Variations in chlorophyll fluorescence yields in phytoplankton in the worlds oceans. Aust J Plant Physiol 22: 341-355

Falkowski, P., and Raven, J. Aquatic Photosynthesis. Princeton: Princeton University Press, 2007. Print

Feller, U., Anders, I., Demirevska, K. 2008. Degradation of rubisco and other chloroplast proteins under abiotic stress. Gen Appl Plant Physiol 34: 5–18

Finney, D. Probit Analysis. Cambridge: University Press, 1971. Print

Fisher, T., Schurtz-Swirski, R., Gepstein, S., and Dubinsky, Z. 1989. Changes in the levels of Ribulose-1,5-bisphosphate carboxylase/oxygenase (Rubisco) in *Tetraedron minimum* (Chlorophyta) during light and shade adaptation. Plant Cell Physiol 30: 221-228

Fisher, W., and Foss, S. 1993. A simple test for toxicity of number 2 fuel oil and oil dispersants to embryos of grass shrimp, *Palaemonetes pugio*. Mar Pollu Bull 26: 385-391

Fox, J. 1989. Native microbes role in Alaskan clean-up. Bio Tech 7: 852

Foy, M. 1982. Acute lethal toxicity of Prudhoe Bay Crude oil and Corexit 9527 to Arctic marine fish and invertebrates. Technology Development Report, EPS 4-EC-82-3, Environment Canada

Freedman, J., Ciriolo, M., and Peisach, J. 1989. The role of glutathione in copper metabolism and toxicity. J Biol Chem 264: 5598-5605

Gadd, G. 2000. Microbial interactions with tributyltin compounds: detoxification, accumulation, and environmental fate. Sci Total Environ 258: 119-127

Garcia-Ferris, C., and Moreno, J. 1994. Oxidative modification and breakdown of ribulose-1,5-bisphosphate carboxylase/oxygenase induced in *Euglena gracilis* nitrogen starvation. Planta 193: 208-215

George-Ares, A., and Clark, J. 2000. Aquatic toxicity of two Corexit dispersants. Chemosphere 40: 897-906

Goodchild, D., Bjorkman, O., and Pyliotis, N.A. 1972. Chloroplast ultrastructure, leaf anatomy and soluble protein in rainforest species. Carnegie Inst. Wash. Year Book 71: 102-107

Godbold, D., and Kettner, C. 1991. Lead influences root growth and mineral nutrition of *Picea abies* seedlings. J Plant Physiol 139: 95-99

Gorbunov, M., and Falkowski, P. "Fluorescence induction and relaxation (FIRe) technique and instrumentation for monitoring photosynthetic processes and primary production in aquatic ecosystems." Photosynthesis: Fundamental Aspects to Global Perspectives, Proceedings of the 13th International Congress of Photosynthesis. Ed. van der Est, A., Bruce, D. Montreal: Allen Press, 2004

Gordillo, F., Jiménez, C., Chavarría, J., and Niell,F. 2001. Photosynthetic acclimation to photon irradiance and its relation to chlorophyll fluorescence and carbon assimilation in the halotolerant green alga Dunaliella viridis. Photosynth Res 68:225-235

Goryshina, T. 1980. Structural and functional features of the leaf assimilatory apparatus in plants of a forest-steppe oakwood. Acta Ecol Ecol Plant 1: 47-54

Gulec, I., and Holdway, D. 1997. Toxicity of dispersant, oil, and dispersed oil to two marine organisms. 1997 International Oil Spill Conference 1010- 1011

Hampp, R., Beulich, K., and Ziegler, H. 1976. Effects of zinc and cadmium on photosynthetic co_2-fixation and hill activity of isolated spinach chloroplasts. Z Pflanzenphysiol 77: 336-344

Hassler, C., and Wilkinson, K. 2003. Failure of the biotic ligand and free-ion activity models to explain zinc bioaccumulation by *Chlorella kesslerii.* Environ Toxicol Chem 22: 620-626

Heintz, R., Short, J., and Rice, S. 1999. Sensitivity of fish embryos to weathered crude oil: Part II. Increased mortality of pink salmon (*Oncorhynchus gorbuscha)* embryos incubating downstream from weathered *Exxon Valdez* crude oil. Environ Toxicol Chem 18: 494-503

Hoch, M. 2001. Organotin compounds in the environment – an overview. Appl Geochem 16: 719-743

Hoffman, M. 1935. The effects of several summer spray oils on the carbon dioxide assimilation by apple leaves. Proc Amer Soc Hort Sci 32: 104-106

Howard, S., Baker, J., and Hiscock, K. 1989. The effects of oil and dispersants on seagrasses in Milford Haven. B. Dicks (Ed.), Ecological Impacts of the Oil Industry, John Wiley and Sons Ltd, Chichester 61–98

Huang, X., McConkey, B., Babu, T., and Greenberg, B. 1997. Mechanisms of photoinduced toxicity of photomodified anthracene to plants: inhibition of photosynthesis in the aquatic higher plant *Lemna gibba* (duckweed). Environ Toxicol Chem 16: 1707-1715

Irihimovitch, V., and Shapira, M. 2000. Glutathione redox potential modulated by reactive oxygen species regulates translation of Rubisco large subunit in the chloroplast. J Biol Chem 275: 16289-16295

Jacob, J., and Lawlor, D. 1992. Dependence of photosynthesis of sunflower and maize leaves on phosphate supply, ribulose-1,5-bisphosphate carboxylase/oxygenase activity, and ribulose-1,5-bisphosphate pool size. Plant Physiol 98: 801-807

Judson, R., Martin, M., Reif, D., Houck, K., Knudsen, T., Rotroff, D., Xia, M., Sakamuru, S., Huang, R., Shinn, P., Austin, C., Kavlock, R., and Dix, D. 2010. Analysis of eight oil spill dispersants using rapid, in vitro tests for endocrine and other biological activity. Environ Sci Technol 44: 5979-5985

Kannan, K,. and Lee, R.F. 1996. Triphenyltin and its degradation products in foliage and soils from sprayed pecan orchards and in fish from adjacent ponds. Environ Toxicol Chem 15: 1492-1499

Kautsky, H., and Hirsch, A. 1931. Neue versuche zur kohlensäureassimilation. Naturwissenschaften 19: 964-964.

Klimov V., and Krasnovsky, A. 1981. Pheophytin as the primary electron acceptor in photosystem 2 reaction centers. Photosynthetica 15: 592–609

Klug, A,. and Rhodes, D. 1987. 'Zinc fingers': a novel protein motif for nucleic acid recognition. Trends Biochem Sci 12: 464-469

Klughammer, C., Heimann, S., and Schreiber, U. 1998. Inhibition of cytochrome b563-oxidation by triorganotins in spinach chloroplasts. Photosynth Res 56: 117-130

Knauert, S., and Knauer, K. 2008. The role of reactive oxygen species in copper toxicity to two freshwater green algae. J Phycol 44: 311-319

Kolber, Z., and Falkowski, P. 1993. Use of active fluorescence to estimate phytoplankton photosynthesis 'in situ.' Limno Oceanogr 38: 1646-1665

Krugh, B., and Miles, D. 1996. Monitoring the effects of five "nonherbidicial" pesticide chemicals on terrestrial plants using chlorophyll fluorescence. Environ Toxicol Chem 15: 495-500

Krupa, Z., and Baszynski, T. 1995.Some aspects of heavy metal toxicity towards photosynthetic apparatus- direct and indirect effects on light and dark reactions. Acta Physiol Plant 17: 177-190

Kupper, H., Kupper F., and Spiller, M. 1998. In situ detection of heavy metal substituted chlorophylls in water plants. Photosynth Res 58: 123-133

Lanaras, T., Moustakas, M., Symenoides, L., Diamantoglou, S., and Karataglis, S. 1993. Plant metal content, growth responses and some photosynthetic measurements on field-cultivated growing on ore bodies enriched in Cu. Physiol Plant 88: 307-314

Leong T. and Anderson, J. 1984. Adaptation of the thylakoid membranes of pea chloroplasts to light intensities. II. Regulation of electron transport capacities, electron carriers, coupling factor (CF_1) activity and rates of photosynthesis. Photosynth Res 5: 117-128

Le Gore, R., Marszalek, D., Hofmann, J., and Cuddebakc, J. 1983. A field experiment to assess the impact of chemically dispersed oil on Arabian Gulf corals. Soc Petr Eng SPE 114444: 51-60

Lichtenthaler, H., and Burkart, S. 1999. Photosynthesis and High Light Stress. Bulg J Plant Physiol 25: 3-16

Lichtenthaler, H., Meier, D., and Buschmann, C. 1984. Development of chloroplast at high and low light quanta fluence rates. Israel J Bot 33: 185-194

Lidon, F., and Henriques, F. 1993. Changes in the contents of the photosynthetic electron carriers, RNAse activity and membrane permeability triggered by excess copper in rice. Photosynthetica 28: 99-108

Long, S., Humphries, S., and Falkowski, P. 1994. Photoinhibition of photosynthesis in nature. Annu Rev Plant Physiol Plant Molec Biol 45: 633-662

Luo, S., Ishida, H., Makino, A., and Mae, T. 2002. Fe^{2+}-catalyzed site-specific cleavage of the large subunit of ribulose 1, 5-bisphosphate carboxylase close to the active site. J Biol Chem 277:12382 -12387

Lyngby, J., and Brix, H. 1984. The uptake of heavy metals in eelgrass *Zostera marina* and their effect on growth. Ecol Bull 36: 81-89

Malea, P. 1994. Seasonal variation and local distribution of meals in the seagrass *Halophila stipulacea* Aschers in the Antikyra Gulf, Greece. Environ Pollut 85: 77-85

Mallakin, A., Babu, T., Dixon, D., and Greenberg, B. 2002. Sites of toxicity of specific photooxidation products of anthracene to higher plants: inhibition of photosynthetic activity and electron transport in *Lemna gibba* L. G-3 (duckweed). Environ Tox 17: 462-471

Mallakin, A., Dixon, D., and Greenberg, B. 2000. Pathway of anthracene modification under simulated solar radiation. Chemosphere 40: 1435-1441

Mallick, N. and Mohn, F.H. 2003. Use of chlorophyll fluorescence in metal-stress research: a case study with the green microalga *Scenedesmus*. Ecotox Env Saf 55:64-69

Marwood, C., Smith, R., Solomon, D., Charlton, M., and Greenberg, B. 1999. Intact and photomodified polycyclic aromatic hydrocarbons inhibit photosynthesis in natural assemblages of Lake Eric phytoplankton exposed to solar radiation. Ecotox Environ Safe 44: 322-327

Marwood, C., Solomon, K., and Greenberg, B. 2001. Chlorophyll fluorescence as a bioindicator of effects on growth in aquatic macrophytes from mixtures of polycyclic aromatic hydrocarbons. Environ Toxicol Chem 20: 890-898

Mateos-Naranjo, E., Redondo-Gomez, S., Cambrolle, J., Luque, T., and Figueroa, M. 2008. Growth and photosynthetic responses to zinc stress of an invasive cordgrass, *Spartina densiflora*. Plant Bio 10: 754-762

Mitchell, F., and Holdway, D. 2000. The acute and chronic toxicity of the dispersants Corexit 9527 and 9500, water accommodated fraction (WAF) of crude oil, and dispersant enhanced WAF (DEWAF) to *Hydra viridissima* (green hydra). Wat Res 34: 343-348

Mohanty, N., Vass, I., and Demeter, S. 1989. Copper Toxicity Affects Photosystem II Electron Transport at the Secondary Quinone Acceptor, Q_B. Plant Physiol 90: 175-179

Morishige, D., and Dreyfuss, B. “Light-Harvesting complexes of higher plants.” *Photosynthesis: A Comprehensive Treatise*. Ed. A.S. Raghavendra. New York: Cambridge University Press, 1998. 18-28. Print

Mysliwa-Kurdziel. B., Prasad, M., and Strzalka, K. “Photosynthesis in Heavy Metal Stressed Plants.” *Heavy Metal Stress in Plants from biomolecules to ecosystems*. Ed. M.N.V. Prasad. India: Narosa Publishing House, 2004. 146-180. Print

Nieboer, E., and Richardson, D. 1980. The replacement of the nondescript term 'heavy metal' by a biologically and chemically significant classification of metal ions. Environ Pollut B 1: 3-26

Nielsen, H., and Nielsen, S. 2010. Adaptation to high light irradiances enhances the photosynthetic Cu+2 resistance in Cu+2 tolerant and non-tolerant population of the brown macroalgae *Fucus serratus*. Mar Pollu Bull 60: 710-717

Nishiyama, Y., Yamamoto, H., Allakhverdiev, S., Inaba, M., Yokota , A., and Murata, N. 2001. Oxidative stress inhibits the repair of photodamage to the photosynthetic machinery. EMBO 20: 5587-5594

Olaizola, M., Roche, J., Kolber, Z., and Falkowski, P. 1994. Non-photochemical fluorescence quenching and the diadinoxanthin cycle in a marine diatom. Photosynth Res. 41: 357-370

Ouzounidou, G. 1996. The use of photoacoustic spectroscopy in assessing leaf photosynthesis under copper stress: correlation of energy storage to photosystem II fluorescence parameters and redox change of P-700. Plant Sci 113: 229-237

Pawlik-Skowronska, B., Kaczorowska, R., and Skowronski, T. 1997. The impact of inorganic tin on the planktonic cyanobacterium *Synechocystis aquatilis*: the effect of pH and humic acid. Environ Pollut 97: 65-69

Perez, P., Fernandez, E., and Beiras, R. 2010. Fuel toxicity on *Isochrysis galbana* and a coastal phytoplankton assemblage: growth rates vs. variable fluorescence. Ecotox Environ Safe 73: 254-261

Pelletier, M., Burgess, R., Ho, K., Kuhn, A., McKinney, R., and Ryba, S. 1997. Phototoxicity of individual polycyclic aromatic hydrocarbons and petroleum to marine invertebrate larvae and juveniles. Environ Toxicol Chem 16: 2190-2199

Piehler, M., Winkelmann, V., Twomey, L., Hall, N., Currin, C., and Paerl, H. 2003. Impacts of diesel fuel exposure on the microphytobenthic community of an intertidal sand flat. J Exp Mar Biol Ecol 297: 219-237

Plekhanov, S., and Chemeris, Y. 2003. Early toxic effects of zinc, cobalt, and cadmium on photosynthetic activity of the green alga *Chlorella pyrenoidosa* Chick S-39. Biol Bull 30: 506-511

Prasad, M., Malec, P., Waloszek, A., Bojko, M. and Strzalka, K. 2001. Physiological responses of *Lemna trisulca L.* (Duckweed) to cadmium and copper bioaccumulation. Plant Sci 161: 881-889

Prassad, D., and Prassad, A. 1987. Altered δ-aminolaevulinic acid metabolism by lead and mercury in germinating seedlings of Bajra (*Pennisetum typhoidem*). J Plant Physiol 127: 241-249

Pritchard, P., Mueller, J., Rogers, J., Kremer, F., and Glaser, J. 1992. Oil spill bioremediation; experiences lessons, and results from the *Exxon Valdez* oil spill in Alaska. Biodegradation 3:3 15-335

Quevauviller, P., Bruchet, A., and Donard, O. 1991. Leaching of organotin compounds from poly(vinyl chloride) (PVC) material. Appl Organomet Chem 5: 125-129

Quigg, A., Finkel, Z., Irwin, A., and Rosenthal, Y. 2003. The evolutionary inheritance of elemental stoichiometry in marine phytoplankton. Nature 425: 291-294

Ralph, P., and Burchett, M. 1998. Impact of petrochemicals on the photosynthesis of *Halophila ovalis* using chlorophyll fluorescence. Mar Pollut Bull 36: 429-436

Ramachandran, S., Hodson, P., Khan, C., and Lee, K. 2004. Oil dispersant increases PAH uptake by fish exposed to crude oil. Ecotox Environ Safety 59: 300-308

Rasiah, V. and Voroney, R. 1993. Assessment of selected surfactants for enhancing C mineralization of an oily waste. Water Air Soil Pollut 71: 347-355

Rashid, P., and Mukherji, S. 1991. Changes in catalase and ascorbic oxidase activities in response to lead nitrate treatments in mungbean. Ind J Plant Physiol 34: 143-146

Rao, M., Fredeen, A., and Terry, N. 1989. Leaf phosphate status, photosynthesis and carbon partitioning in sugar beet. Plant Physiol 90: 820-826

Rao, B., Tyryshkin, A., Roberts, A., Bowman, M., and Kramer, D. 2000. Inhibitory copper binding site on the spinach cytochrome b6f complex: implications for Qo site catalysis. Biochem 39: 3285-3296

Rashid,A., Camm, E., and Ekramoddoullah, K. 1994. Molecular mechanism of action of Pb and Zn^{2+} on water oxidizing complex of photosystem II. FEBS Lett 350: 296-298

Rashid, A., Bernier, M., Pazdernick, L., and Carpentier, R. 1991. Interaction of Zn^{2+} with the donor side of Photosystem II. Photosynth Res 30: 123-130

Rebechini, H., and Hanzely, L. 1974. Lead-induced ultrastructural changes in chloroplasts of the hydrophyte *Ceratophyllum demersum*. Z. Pflanzenphysiol 73:3 77-386

Ren, L., Huang, X., McConkey, B., Dixon, D., and Greenberg, B. 1994. Photoinduced Toxicity of Three Polycyclic Aromatic Hydrocarbons (Fluoranthene, Pyrene, and

Naphthalene) to the Duckweed *Lemna gibba* L. G-3. Ecotox Environ Saf 28: 160-171

Riehl, L., and Wedding, R. 1959. Effects of naphthenic and paraffinic petroleum composition at a comparable molecular weight or viscosity on photosynthesis of Eureka lemon leaves. J Econ Entomol 52: 883-884

Ritz, M., Thomas, J.C., Spilar, A., and Etienne, A.L. 2000. Kinetics of Photoacclimation in Response to a Shift to High Light of the Red Alga *Rhodella violacea* Adapted to Low Irradiance. Plant Physiol 123: 1415-1426

Roberts, I., Murray, P., Caputo, C., Passeron, S., and Barneix, A. 2003. Purification and characterization of a subtilisin like serine protease induced during the senescence of wheat leaves. Physiol Plant 118:483–490.

Rochaix, J. 2011. Reprint of: regulation of photosynthetic electron transport. Biochimica Biophysica Acta 1807: 878-886

Rosenqvist, E. 2001. Light acclimation maintains the redox state of the PS II electron acceptor Q_a within a narrow range over a broad range of light intensities. Photosynth Res 70: 299-310

Sagardoy, R., Morales, F., Lopez-Milan, A., Abadia, A., and Abadia, J. 2009. Effects of zinc toxicity on sugar beet (*Beta vulgaris* L.) plants grown in hydroponics. Plant Bio 11: 339-350

Sedigheh, H., Mortazavian, M., Norouzian, D., Atyabi, M., Akbarzadeh, A., Hasanpoor, K., and Ghorbani, M. 2011. Oxidative stress and leaf senescence. BMC Res Not 4: 477-486

Shakya, K., Chettri, M., and Sawidis, T. 2008. Impact of heavy metals (Copper, Zinc, and Lead) on the chlorophyll content of some mosses. Arch Environ Contam Toxicol 54: 412-421

Shanmuganatha, A., Avery, S., Willetts, S., and Houghton, J. 2004. Copper-induced oxidative stress in *Saccharomyces cerevisiae* targets enzymes of the glycolytic pathway. FEBS Lett 556: 253-259

Sharkey, T. “Photosynthetic carbon reduction.” *Photosynthesis: A Comprehensive Treatise*. Ed. A.S. Raghavendra. New York: Cambridge University Press, 1998. 111-122. Print

Shioi, Y., Tamai, H., and Sasa, T. 1978. Effects of copper on the photosynthetic electron transport systems in spinach chloroplasts. Plant Cell Physiol. 19: 203-209

Simanzhenkov, V., and Idem, R. Crude Oil Chemistry. New York: CRC Press, 2003. Print

Singer, M., Aurand, D., Bragin, G., Clark, J., Coelho, G., Sowby, M., and Tjeerdema, R. 2000. Standardization of the preparation and quantitation of water-accommodated fractions of petroleum for toxicity testing. Marine Pollut Bull 40: 1007-1016

Singer, M., George, S., Lee, I., Jacobson, S., Weetman, L., Blondina, G., Tjeerdema, R., Aurand, D., and Sowby, M. 1998. Effects of Dispersant Treatment on the Acute Aquatic Toxicity of Petroleum Hydrocarbons. Arch Environ Contam Toxicol 34: 177-187

Singer, M., Smalheer, D., Tjeerdema, R., and Martin, M. 1991. Effects of spiked exposure to an oil dispersant on the early life stages of four marine species. Environ Tox Chem 10: 1367-1374

Simpson, D., and Von Wettstein, D. 1989. The structure and function of the thylakoid membrane. Carlsberg Res Commun 54: 55-65

Stauber, J., and Florence, T. 1985. Interactions of copper and manganese: A mechanism by which manganese alleviates copper toxicity to the marine diatom, *Nitzschia closterium* (Ehrenberg) W. Smith. Aquat Toxicol 7: 241-254

Stauber, J., and Florence, T. 1990. Mechanism of toxicity of zinc to the marine diatom *Nimcbia claslerium.* Mar Biol 105: 519-524

Stefanov, K., Seizova, K., Popoya, I., Petkov, V., Kimenov, G., and Popov, S. 1995. Effects of lead ions on the phospholipid composition in leaves of *Zea mays* and *Phaseolus vulgaris*. J Plant Physiol 147: 243-246

Stiborova, M., Ditrichova, M., and Benzinova, A. 1988. Mechanism of action of Cu^{++}, Co^{++}, and Zn^{++} on ribulose-1,5-biphosphate carboxylase from barley (*Hordeum vulgare* L.). Photosynthetica 22: 161-167

Stribet, A., and Govindjee. 2011. On the relation between the Kautsky effect (chlorophyll a fluorescence induction) and photosystem II: basics and applications of the OJIP fluorescence transient. J Photochem Photoiol B 104: 236-257

Sunda, W., and Guilard, R. 1976. The relationship between cupric ion activity and the toxicity of copper to phytoplankton. J Mar Res 24: 511-529

Takahashi, S. and Murata, N. 2008. How do environmental stresses accelerate photoinhibition? Trends in Plant Science 13:178-182

Taiz, L., and Zeiger, E. Plant Physiology. Sunderland, MA: Sinauer Associates, 1998. Print

Tyystjarvi, E. 2008. Photoinhibition of photosystem II and photodamage of the oxygen evolving manganese cluster. Coord Chem Rev 252:361-376

Uribe, E., and Stark, B. 1982. Inhibition of photosynthetic energy conversion by cupric ion evidence for Cu^{2+} coupling factor 1 interaction. Plant Physiol 69: 1040-1045

U.S. Congressional Research Service, Oil Spills in US Coastal Waters: Background, Governance, and Issues for Congress (RL33705; April 30, 2010), by Jonathan L. Ramseur. Text in: LexisNexis® Congressional Research Digital Collection

USEPA. 1997. Swirling Flask Dispersant Effectiveness Test, Revised Standard Dispersant Toxcity Test, and Bioremediation Agent Effectiveness Test. 40 CFR Part 300, Appendix C. EPA 62 FR 15576. US Environmental Protection Agency, Washington, DC April 1, 1997

Vallee, B., and Ulmer, D. 1972. Biochemical effects of mercury, cadmium and lead. Annu Rev Biochem 41: 91-128

Valliant, N., Monnet, F., Hitmi, A., Sallanon, H., and Coudret, A. 2005. Comparative study of responses in four Datura species to zinc stress. Chemosphere 59: 1005-1013

vanAssche, F., and Clijsters, H. 1986a. Inhibition of photosynthesis in *Phaseolus vulgaris* by treatment with toxic concentrations of zinc: effect of ribulose-1,5-biphosphae carboxylase/oxygenase. J Plant Physiol 125: 355-360

vanAssche, F., and Clijsters, H. 1986b. Inhibition of photosynthesis by treatment of *Phaseolus vulgaris* with toxic concentrations of zinc: effects on electron transport and photophosphorylation. Physiol Plant 66: 717-721

van Assche, F., and Clijsters, H. 1990. Effects of metal on enzyme activity in plants. Plant Cell Environ 13: 195-206

Vojtechova, M., and Leblova, S. 1991. Uptake of lead and cadmium by maize seedlings and the effect of heavy metals on the activity of phosphoenolpyruvate carboxylase isolated from maize. Biol Plant 33: 386-394

Wahbeh, M. 1984. Levels of zinc, manganese, magnesium, iron and cadmium in three species of seagrasses from Aqaba (Jordan). Aquat Bot 20:179-183

Walker, W., Miller, J., and Hassett, J. 1977. Effect of lead and cadmium upon the calcium, magnesium, potassium and phosphorus concentration in young corn plants. Soil Sci 124: 145-151

Weckx, J., and Clijsters, H. 1997. Zn phytotoxicity induces oxidative stess in primary leaves of *Phaseolus vulgaris*. Plant Physiol Biochem 35: 405-410

Wild, A. 1979. Physiology of photosynthesis in higher plants. The adaptation of photosynthesis to light intensity and light quality. Ber Dtsch Bot Ges 92: 341-364

Wild, A., Hopfner, M., Ruhle, W., and Richter, M. 1986. Changes in the stoichiometry of photosystem II components as a adaptive response to high-light and low-light conditions during growth. Z Naturforsch 41c: 597-603

Wolfe, M., Schlosser, J., Schwartz, G., Singaram, S., Mielbrecht, E., Tjeerdema, R., and Sowby, M. 1998. Influence of dispersants on the bioavailability and trophic transfer of petroleum hydrocarbons to primary levels of a marine food chain. Aqua. Toxicol, 42: 211–227

Wolfe, M., Schwartz, G., Singaram, S., Mielbrecht, E., Tjeerdema, R., and Sowboy, M. 2001. Influence of dispersants on the bioavailability and trophic transfer of petroleum hydrocarbons to larval topsmelt (*Atherinops affinis*). Aquat Toxicol 52: 49-60

Wong, P., Chau, Y., Kramar, O., and Bengert, G. 1982. Structure-toxicity relationship of tin compounds on algae. Can J Fish Aquat Sci 39: 483-488

Wu, X., Hong, F., Liu, C., Su, M., Zheng, L., Gao, F., and Yang, F. 2008. Effects of Pb^{2+} on energy distribution and photochemical activity of spinach chloroplast. Spectrochim Acta Part A 69: 738-742

Yamamoto, Y., Aminaka, R., Yoshioka, M., Khatoon, M., Komayama, K., Takenaka, D., Yamashita, A., Nijo, N., Inagawa, K., Morita, N., Sasaki, T., and Yamamoto, Y. 2008. Quality control of photosystem II: impact of light and heat stresses. Photosynth Res 98: 589-608

Yamada, M., Takada, H., Toyoda, K., Yoshida, A., Shibata, A., Nomura, H., Wada, M., Nishimura, M., Okamoto, K., and Ohmada, K. 2003. Study on the fate of petroleum-derived polycyclic aromatic hydrocarbons (PAH) and the effect of chemical dispersant using an enclosed ecosystem, mesocosm. Mar Pollut Bull 47: 105-113

Yeoh, H., Badger, M., and Watson, L. 1981. Variation in kinetic properties of ribulose-1,5-bisphosphate carboxylase among plants. Plant Physiol 67: 1151-1155

Yruela, I. 2005. Copper in plants. Braz J Plant Physiol 17: 145-156

Yruela, I., Alfonso, M., Ortiz de Zarate, I., Montoya, G., and Picorel, R. 1993a. Precise location of Cu (II)-inhibitory binding site in higher plant and bacterial

photosynthetic reaction centers as probed by light-induced absorption changes. J Biol Chem 268: 1684-1689

Yruela, I., Montoya, G., and Picorel, R. 1993b. The inhibitory mechanism of Cu (II) on the Photosystem II electron transport from higher plants. Photosynth Res 33: 227-233